Master: Mechanical Engineering

Track: Multi-Machine Engineering

Graduation project

Modelling a novel design of soft grippers actuated by smart hydrogel

Author:

J.P. Schoenmakers (4555554)

Supervisors:

Dr. J. Jovanova
Q. Chen

Report number:

2023.MME.8851

September 18, 2023

Contents

1 Preface

This research is conducted as part of the second year for graduation at the Master Mechanical Engineering at the Delft University of Technology. In this report, a research is done on simulating a novel concept by applying thermoresponsive hydrogel particles as actuator in soft grippers. With this novel concept, an extent to the wide area of actuating soft grippers by smart materials is provided. This research is conducted as contribution to the research of the PhD candidate Q. Chen. Thanks are extended to Dr. J. Jovanova and PhD candidate Q. Chen for their professional guidance and valuable support during this research. Special thanks are extended to Q. Chen for his close guidance and the daily meetings.

2 Summary

In the first part of this research, section 3, a background description is provided. Additionally, sub research questions are formulated to answer the main research question: *How to develop a simulation to determine the effect of specific parameters on the bending performance of soft grippers actuated by thermoresponsive hydrogel?*. In section 4 a literature survey is provided, resulting in a research gap. This research gap showed that soft grippers often lack robustness. Additionally, a conclusion is that thermoresponsive smart materials are commonly used as shape memory alloys or pyroelectrics. Therefore, with this research an aim is done for potential addition to the field of smart materials by using thermoresponsive hydrogels as actuators. The methodology is provided in section 5. The novel design is presented. The mathematics behind describing and implementing thermoresponsive material in simulations is provided. The formula for determining relevant parameters is presented in Equation 7 and the formula for describing the behaviour of the material in simulations is presented in Equation 11. A validation between the material behaviour of the simulations presented in this research and the literature is done. Therefore, Figure 78 is provided, which presents the swelling ratio for specific parameter values of this research and literature. Additionally, this research increased the swelling of the material by increasing the temperature difference. Demo structures are as well designed and fabricated as simulated for 4 different geometry's. A similar trend is found between the manufactures demos and the simulations, which is from most to least amount of bending respectively cylinder, sharp, waved and straight. In 7 relevant parameters are provided of a soft gripper. Based on these parameters, a calibration is executed to show that the simulations behave as expected. Additionally, a normalization is carried out for the four relevant researching parameters in this report. These parameters are the length, material, reinforcement and geometry. The results are presented in Figure 110 - Figure 113. From this normalization, 3 levels for the parameters length, material and geometry are considered and 2 levels for the parameter reinforcement to be included in the Design of Experiments. These levels for the Design of Experiments are provided in Table 11. In section 7 the Design of Experiments is carried out. In total, 54 simulations divided in 18 sets are included and presented in Table 12. The results are presented by measuring the bending angle, which are provided in Table 13. The main effect plot in Figure 119 showed that the most effect on the bending angle is performed by the parameter length, followed by geometry. The material has less effect and the reinforcement can be considered to be negligible. The interaction plot of Figure 120 provides the information that most of the interaction occurs between the length and geometry. Additionally, based on the results a potential application as soft gripper is provided. A simulation is presented in Figure 122 - Figure 124 where a soft gripper based on actuation by thermoresponsive hydrogels approaches an object. In section 8 a conclusion and future work are provided. This research showed that the novel design works and has potential for upcoming researches. It is shown that the researched application of reinforcement has a minor influence on the bending performance. On the other hand, the most influence is performed by the length and geometry of the structure. Therefore, the most amount of bending was obtained by the cylinder structure made of Ecoflex 30 with a length of 50 particles without reinforcement. For the upcoming work, experiments have to be carried out to determine the force which can be exerted by the structures.

3 Background

Robotics are getting more and more important over time. At first, robotics was used to replace human jobs which were dull, dirty or dangerous. A common example of applying robotics is by replacing humans with stiff robotic arms in assembly lines. Besides replacing the dull, dirty and dangerous human jobs with robotics to increase efficiency and safety, also the costs will be reduced, as the costs of robotic grippers is decreasing while the manual labour costs increases [1]. Additionally, certain robotic arms outperform human capability. For example, the lifting power of robotic arms can be at 1000 kg [2]. Besides, the accuracy and precision can be repeatable to 10 μm [3]. At last, the acceleration of the robotic arms can be in the order of 15 G [4]. Often, these robotics are made out of rigid parts, such as magnets, copper or steel bearings or include metal engines for actuation [5]. However, as these robotics are very stiff, these are not (very) adaptable.

The definition of soft robotics can be stated as the principles of classical robotics with an increased desire to improve the flexibility and adaptability in specific tasks [6]. However, to improve the flexibility and adaptability, soft materials are used. The material defines important properties of soft grippers as force and speed. The principle of soft grippers is often being soft and to allow stretching [7]. As a result, elastomers are often a suitable material due to the large supply of different types of elastomers. Common characteristics of elastomers are high strain at rupture and low stiffness. However, the disadvantage of elastomers is that often the robustness of the materials is very low. Besides, low stiffness results in less grabbing force. Therefore, forming an adaptable gripper with sufficient stiffness is challenging.

Applications of soft grippers can be in a wide range of fields. As an example, soft grippers are usable for picking fruits and vegetables in the agriculture sector. Besides, at assembly lines or at packaging of fragile products soft grippers are important to prevent damages. Additionally, in the field of medicine are soft grippers relevant, especially in the area of prosthetic. Replacing a hand with a gripper which is as flexible and adaptable as a real hand is the ultimate goal. Researches on applying soft robotics as prostheses includes often smart materials. Smart materials are included as these can be activated by external stimuli to allow plastic deformation and reform back to the initial condition [8].

[5] provides a view on the animal world. For animals, soft materials are dominant. Generally, despite that many animals and humans have a stiff endoskelet, consists the body mainly out of soft materials and liquids. A remarkable aspect is that for adult human males the endoskelet represents approximately 11% of the body mass, while the skeletal muscles represent approximately 42%. As a result, studying the biology for applying soft materials into robotics can provide solutions to form an adaptable soft gripper with sufficient stiffness. Examples of studied animals as octopuses, elephants and starfishes for soft grippers can be found in [9].

All in all, designing soft grippers with sufficient stiffness is a complex and challenging field. Still ongoing researches to solve key challenges are important to result in a more flexible and adaptable working soft gripper [7]. Based on the background, the main goal of this research can be presented as follows:

Develop a simulation to determine the effect of specific parameters on the bending performance of soft grippers actuated by thermoresponsive hydrogel.

To achieve the main goal, a main question can be formulated. The main research question is therefore:

How to develop a simulation to determine the effect of specific parameters on the bending performance of soft grippers actuated by thermoresponsive hydrogel?

Consequently, the main research question can be divided into multiple sub questions. These questions are:

1. What is the state of the art of smart materials and soft grippers?
2. What is the novel design for soft grippers actuated by thermoresponsive hydrogel?

3. How to simulate thermoresponsive hydrogel?

4. What are relevant parameters and what is their effect on the bending performance of soft grippers?

5. How can the novel design be applied as a soft gripper?

To answer all of the sub questions to consequently answer the main research question, the content of this research is presented as following. At first, an extensive literature survey will be executed and presented in section 4. The focus of the literature survey can be divided into smart materials and soft grippers. However, the literature survey on smart materials is narrowed down to two subsections, which are Shape Memory Materials (SMM) and Hydrogels. In section 5, methodology, the novel actuator will be provided. Besides providing the novel actuator, relevant formulas for implementing and the validation of thermoresponsive hydrogel in simulation are presented. At last, a comparison is made between the simulations and manufactured demos to validate the simulations with structure performances. In section 6 potential influential parameters of soft grippers are provided. Additionally, a calibration is presented to show that the simulations perform as expected. Besides, 4 relevant parameters are selected of which the influence on the bending performance will be determined. A normalization is applied on these selected parameters to determine the upper and lower bounds. From the normalization of section 6, a full factorial Design of Experiments is created. From this full factorial design, the influence of each selected parameter is determined. The trend of different parameters is provided, along with a main effects plot and the interaction plots. Additionally, a potential application as working soft gripper with multiple segments is presented. In section 8] a conclusion is provided of the research.

4 Literature survey

In this chapter, an extensive literature survey is done on smart materials and soft grippers. Initially, robotic grippers were simple and consisted out of only rigid parts and joints [10]. Soft grippers are, as their name represents, made out of soft elements. However, this does not mean that the gripper is soft throughout the whole system. An example can be given with a gripper which can be used for shopping products in a supermarket. The gripper must be able to grab hard or heavy objects such as a can of soup, while more fragile products as tomatoes must be handled too. This means that the gripper must be as well adaptable to the product shape as have a high stiffness during specific operations. According to [11] and [12], a difference can be made between hard and soft robotics. Hard robotics excel at for example massive productions functions, while they are hard to control as high precision is required. Hard robotics are very efficient in a constant environment, where no adaptation is required. Therefore, hard robotics have a very low adaptability in uncertain environments. On the other hand, soft grippers are, despite their low rigidity due to using primarily stretchable and flexible materials, more efficient in uncertain environments. These soft grippers provide more efficiency and safety in complex, uncertain environments. In principal, a reaction force must be created by using any type of actuator such that the gripper can deliver work. If there is no actuation i.e. reaction force, than the gripper is to soft and can not handle the object [5]. This chapter is divided into two parts of the literature survey. One part is a literature survey about smart materials, while the second part is about soft grippers.

4.1 Smart materials

Materials with specific ability's are called smart materials. Smart materials are able to change some of their specific properties under certain conditions. For example, the material structure or composition can be changed under external stimuli. Other properties as electrical or mechanical or even their functional respond can also change due to these external stimuli [13]. In Table 1 of [13] some examples are provided of smart materials which can be used as actuators. However, besides using smart materials as actuators, smart materials can also be used as sensors as some examples are provided in table Table 2.

Material class	Stimulus	Response
Piezoelectrics	Electric current	Mechanical strain
Electrostrictors	Electric current	Mechanical strain
Magenetostrictors	Magnetic field	Mechanical strain
Shape memory alloys	Temperature change	Mechanical strain
Electroactive polymers	Electric field	Mechanical strain
Electrorheological fluids	Electric field	Viscosity change
Magnetorheological fluids	Magnetic field	Viscosity change

Table 1: Examples of smart materials as actuator.

Material class	Stimulus	Response
Pyroelectrics	Temperature change	Electric polarization
Piezoelectrics	Mechanical strain	Electric polarization
Electrostrictors	Mechanical strain	Electric polarization
Magnetostrictors	Mechanical strain	Change in magnetic field
Electroactive polymers	Mechanical strain	Electric polarization
Electroluminescent	Electric field	Light emission
Photoluminescent	Incident light	Light emission
Electrochromic	Electric field	Color change

Table 2: Examples of smart materials as sensor.

Each of the provided smart materials has their own advantages and disadvantages dependent on the type of application. In the research of [14], it is stated that most of the used smart materials for robotic hands are electroactive polymers (EAP) and shape memory alloys (SMA). However, this report has the focus on a novel design based on hydrogel actuation of soft grippers and EAP's can be applied as hydrogel. Therefore, a distinguish is made in this chapter for relevant smart materials between SMMs and hydrogels, followed by soft grippers and application of smart materials in soft grippers.

4.1.1 Shape memory materials

A category which is relevant for soft robotic grippers is shape memory materials. These materials have a specific property, which is the shape memory. The shape memory property can be actuated by a stimuli, which is often the temperature [7]. Representative materials for this application are shape memory polymers(SMPs) and SMAs.

The principles of as well SMPs as SMAs are comparable, but differ somewhat. SMPs are in the cool state i.e. at low temperature below the transition temperature in a specific shape. The material is in this state very stiff and does not deform much. However, when the material is heated to the heated state i.e. at a high temperature above the transition temperature, the material is becoming soft and can be deformed by an external force. The material can now be deformed in the required shape. When the material is cooled during this deformation, the material stiffens and the deformed state will remain. When the material is heated again to above the transition temperature, the material softens and reforms itself to the initial undeformed shape, as can be seen in Figure 1 [7].

SMAs are comparable, except for the fact that only one time heating is required. SMPs can change their properties due to a phase change of the material. The phase change occurs due to crystallization-melting or vitrification-glass. While SMPs have to be heated to above the transition temperature for as well reaching a deformed state as reforming back to the initial state, SMAs can be deformed in the cool state and only need a temperature increase to reform back to the initial state. The change in properties is due to a crystallographic change of the alloy, as the phase of the material changes from martensite into austenite during heating, as can be seen in Figure 2 [7].

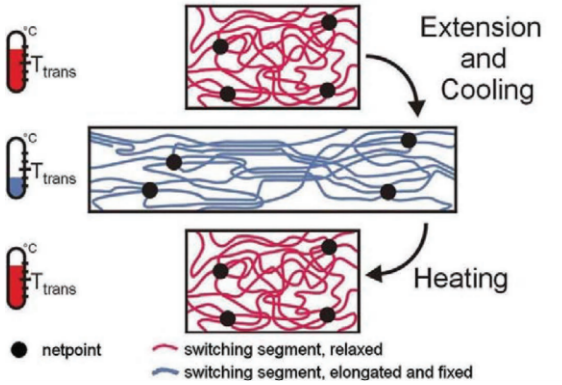

Figure 1: SMPs material behaviour [7].

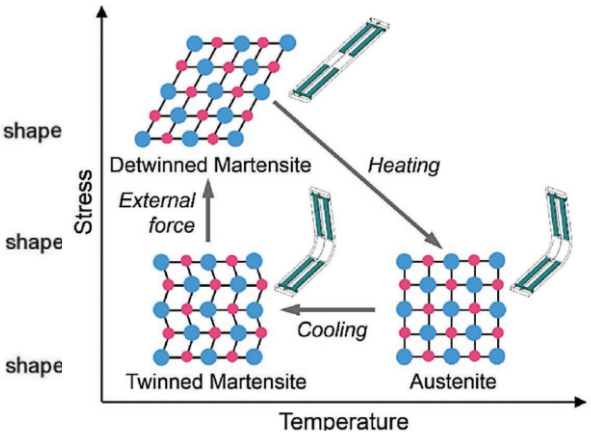

Figure 2: SMAs material behaviour [7].

A significant difference between SMAs and SMPs are the stimuli. SMAs are typically stimulated by temperature, strain and stress [15]. SMPs, on the other hand, can change their properties under stimuli as temperature, pH, electricity, pressure, moisture, light, microwaves, laser heating, solvents and solvent vapors, as can be seen in Figure 3.

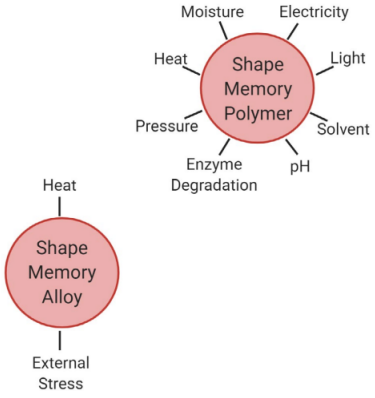

Figure 3: Typical SMP and SMA stimuli [15].

4.1.2 Hydrogel

Hydrogel is a type of polymer network which can change its material properties due to intermolecular interactions with water. As a result, the polymer network can swell. Hydrogels show, in comparison with biological tissue, a higher mechanical compliance. Besides, hydrogels have a high permeability to various molecules and ionic conductivity. Additionally, the biocompatibility of hydrogels is also promising[16].

There are multiple types of hydrogel. The different types of hydrogel can be divided by the stimuli of the material. According to the researches by [16], [7] and [17], hydrogels can be categorized into thermo, chemical, electrical, magnetically, and photo-responsive hydrogels. These 5 category's form the basis of the different main types of hydrogel. However, an additional category can be considered which includes less applied stimuli-responsive materials such as dissolution, humidity and redox states. This categorization is done for all stimuli-responsive hydrogels and is not restricted to application as actuator in soft grippers.

Thermoresponsive hydrogels is the first category. This type of hydrogels are able to change their volume dependent on temperature. According to [18], the phase transition behaviour of thermoresponsive polymers determines the working temperatures of the thermoresponsive hydrogels. There can be made a difference between two types of thermoresponsive hydrogels, which are lower critical solution temperature (LSCT) and upper critical solution temperature (UCST). In Figure 4

of [17] the working principle can be seen. The material on the top of the figure is poly(acrylic acid-co-acrylamide), which is a hydrogel with USCT. At low temperatures (left side), the material shrinks as the water molecules are released. When the temperature increases (right side), the material swells as water molecules will be absorbed. This is the opposite of hydrogels with LSCT, for example as PNIPAM at the bottom in Figure 4. Hydrogels with LSCT will swell at lower temperatures and shrinks at higher temperatures.

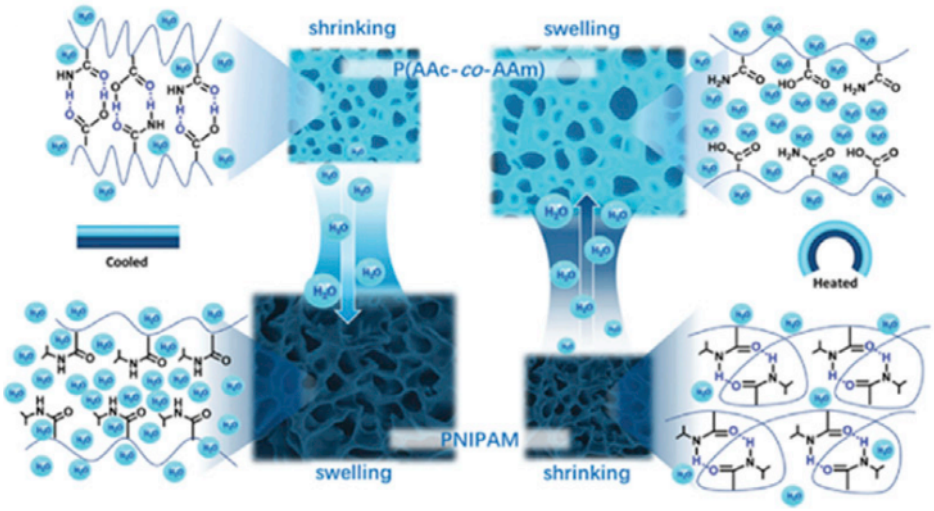

Figure 4: USCT (up) and LSCT (down) material behaviour [17].

Electroresponsive hydrogels can be considered as a group of EAPs which react to electric stimuli by (reversible) deformation i.e. react mechanically [7], [16]. In other words, this smart material can convert electrical input to mechanical movement. Some advantages of EAPs are that they have a high resistance to fracture, are able to dampen vibrations and can withstand high deformation when there is a high force applied [14]. According to [7], two of the most used type of EAPs are dielectric elastomer actuators (DEAs) and ionic polymer-metal composites (IPMCs).

DEAs are actuators which consists out of two electrodes with in between a thin elastomer membrane, as presented in Figure 5. However, for electroresponsive hydrogels instead of using electrodes, ionically conductive hydrogels are used. When a high voltage is applied between the hydrogels, an electrostatic attraction will occur. The elastomer membrane in between the hydrogels will endure a compressing force, resulting in stretching of the membrane, as can be seen in Figure 7.

IPMCs are comparable to DEAs, but instead of using a thin elastomer membrane between two electrodes or hydrogels, IPMCs use a polymer membrane which contains electrolytes. The electrolytes are uniformly distributed in the elastomer when there is no voltage applied. However, when a voltage is applied, the electrolytes (cations and anions) are attracted to the cathode respectively anode. Due to this principle, bending will occur as there arises a differential swelling [19], as can be seen in Figure 6. Despite that IPMCs are not based on hydrogels, this principle can still be applied to hydrogels. This principle for hydrogels is based on electrically induced osmotic pressure [17]. A hydrogel with functional groups with a specific charge and counter ions of the opposite charge are used and placed in a aqueous environment. However, these counter ions are mobile, in comparison to the functional group. Therefore, when an electric field is applied, the counter ions are able to move to the electrode, resulting in a net charge at the electrode. Therefore, ions in the aqueous environment with the same charge as the functional groups will be attracted to this electrode. Therefore, due to ionic gradients an osmotic pressure occurs, resulting in asymmetrically swelling of the hydrogel, as visible in Figure 8.

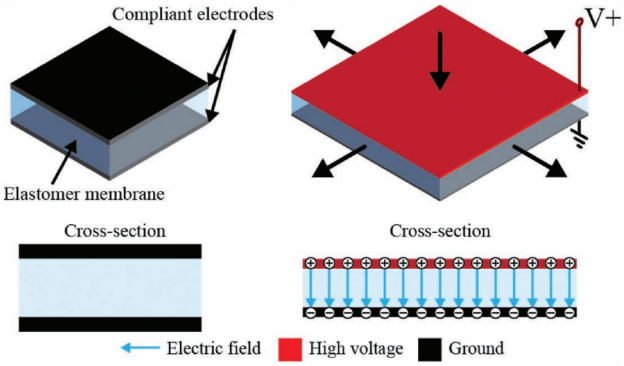

Figure 5: DEA [7].

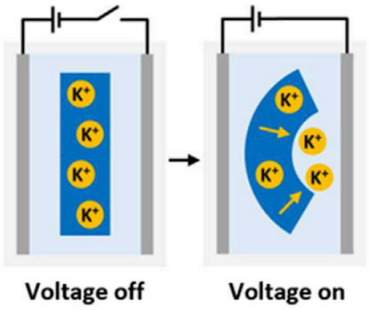

Figure 6: Hydrogel based IPMC [17].

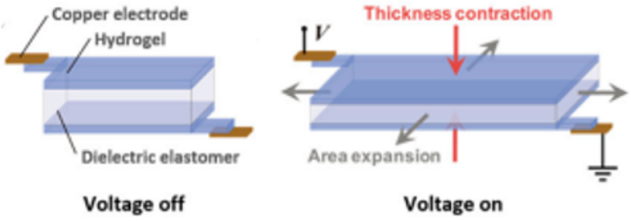

Figure 7: Hydrogel based DEA [17].

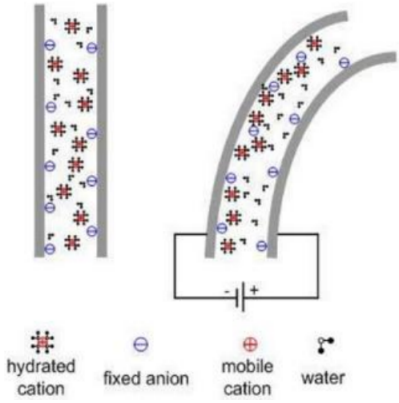

Figure 8: IPMC [14].

Magnetically responsive hydrogels are hydrogels which are actuated by a magnetic field. To actuate the hydrogel, magnetic particles are required to be incorporated into the material. This is mainly done by incorporating paramagnetic or ferromagnetic additives into the hydrogel [16]. These magnetic particles will transmit the received magnetic force of an external magnetic field onto the structure, which will change the material shape. The principle is provided in Figure 9.

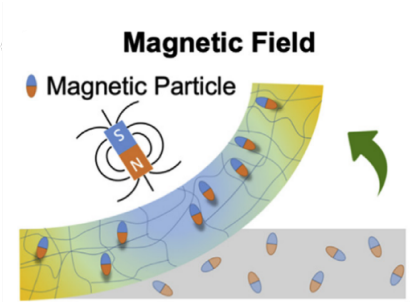

Figure 9: Magnetically responsive hydrogel [16].

Chemical responsive hydrogels are another type of hydrogels which can be used. This type of hydrogel is actuated by the chemical potential of the environment which can be converted to mechanical motion i.e. swelling or shrinking [17]. The two main types of chemical responsive hydrogels are solvent- and pH based. Solvent responsive hydrogels are actuated when there is a difference between the hydrophobicity of the solvent and the polymer network [20]. Due to this difference the hydrogel will swell or shrink. The smaller the difference in hydrophobicity between solvent and hydrogel, the more volumetric change will occur due to absorption of the solvent. Based on this principle hydrogels universally shrink in organic solvents and swell in water, as visible in Figure 10 of [17]. The second type of chemical responsive hydrogels is pH responsive hydrogels. As the pH responsive hydrogel is exposed to a variation in pH, the material can be actuated. This

is due to a difference in the osmotic pressure of the hydrogel network during pH variation [16]. Usually, this type of chemical responsive hydrogel is made from polyelectrolytes. Polyelectrolytes contains function groups. These functions groups can either be basic or acidic. By making use of these function groups, a ionic barrier can be formed. This barrier prevents ions of the same charge to be absorbed, while ions of the opposite charge can. This principle actuates the hydrogel to change it volume due to a ion localization, as presented in Figure 11.

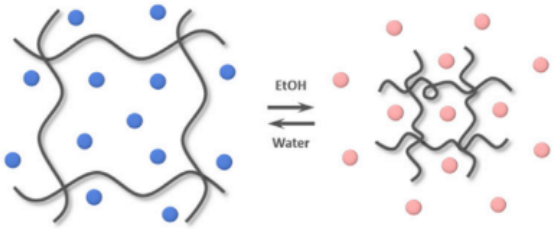

Figure 10: Solventreponsive hydrogel material behaviour [17].

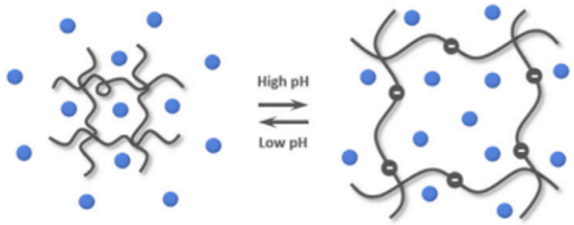

Figure 11: pH-responsive hydrogel material behaviour [17].

Light irradiation is used as stimulus for photoresponsive hydrogels. As a result, the hydrogel will change its volume or shape [17]. There are two main types of photoresponsive hydrogels. These two types are reversible cross-linking reaction and photothermal excitation. In the hydrogel are photoactive moieties required for as well reversible cross-linking as photothermal excitation [21]. Reversible cross-linking is done by making use of photoisomerization and photocleavage, while photothermal excitation is done by using reversible dyhadration-hydration [16].

4.2 Soft grippers

4.2.1 Electrical/magnetic actuators

One of the first types of DEAs was a so called self organized dielectric elastomer minimum energy structure (DEMES). One of the first structures of this type were introduced in the research of [22]. This DEMES is a structure where a flat piece of DEA is pre-stretched and attached to a flat frame in rest, which is very flexible. When there is no voltage applied to the DEA and therefore the structure is released, the structure will bend as the DEA is currently in a pre-stretched state attached to a flexible material. Therefore, the structure will result in a specific form, for example visible in Figure 12. Different initial shapes of the pre-stretched material result in different folded shapes. When there is a voltage applied to the DEA, the whole structure will unfold again as the initial flat situation. Based on this design, an improved version representing a tulip-shaped gripper was manufactured by [23] and is presented in Figure 13 and Figure 14. Another version of the DEMES which uses instead of a single DEA multiple DEAs to reconstruct a more finger based structure can be found in the research of [24] and [25] and are provided in respectively Figure 15 and Figure 16. Another types of grabbing objects, for example from the side by curling a flat surface around the object can be found in [26]. [27] provides an improved soft gripper with a varying stiffness dielectric elastomer by using electromatic chucking. [28] presented a soft gripper based on two DEAs, each representing a finger. These DEAs are pre stretched such that without applied voltage the fingers curls away from each other, visible in Figure 17 and Figure 18. After applying a voltage, the fingers will bend towards each other and the object can be grabbed. Besides, this fingers have a controllable adhesion for the shear holding force.

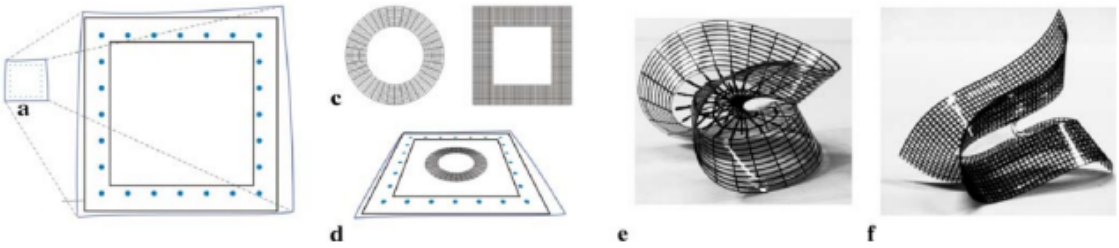

Figure 12: DEMES [22].

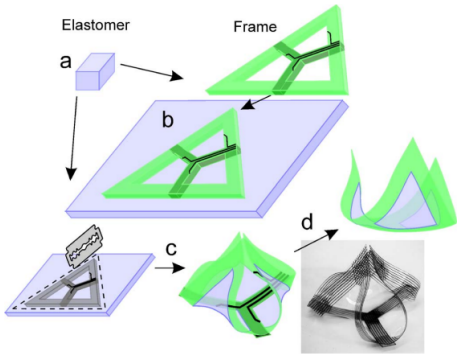

Figure 13: DEMES [23].

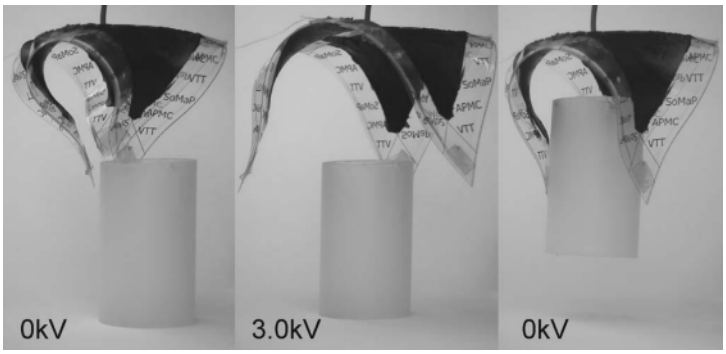

Figure 14: DEMES [23].

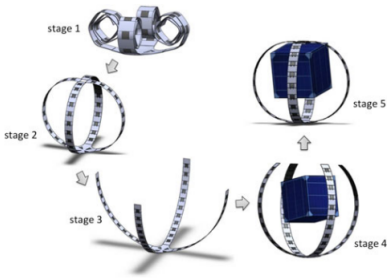

Figure 15: DEA [24].

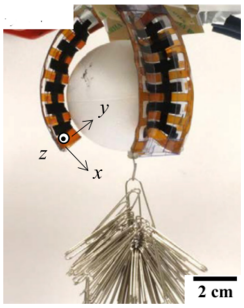

Figure 16: DEA [25].

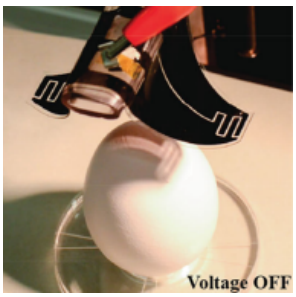

Figure 17: DEA [28].

Figure 18: DEA [28].

One of the first approaches for IPMCs as fingers is presented in the paper of [19]. However, this finger was a simple single IPMC. In the research of [29], a micro gripper is manufactured based on the use of two IPMCs, each representing a finger. [30] manufactured a gripper consisting out of three IPMCs. The four fingered gripper in Figure 19 and Figure 20 was fabricated by [31]. The previous grippers were all in the sizes of cm, while a benefit of IPMCs is that these also can me made in the range of mm. [32] have fabricated a micro gripper as visible in Figure 21.

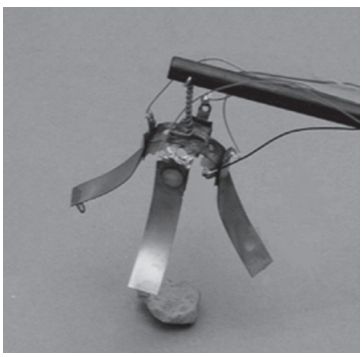

Figure 19: IPMC [31].

Figure 20: IPMC [31].

Figure 21: IPMC [32].

4.2.2 Fluidic actuators

Another type of actuator which can be used for soft grippers are fluidic actuators. Fluidic actuators based on activation using a medium, such as air or water. One of the first working principles of pneumatic actuators can be found in [33]. In this research, a simple circular structure containing three chambers along the z-axis is manufactured, as visible in Figure 22. Reinforcements were used in the circular(tangential) direction of the structure such that inflation only provides axial elongation, as can be seen in Figure 23. By making use of the 3 chambers, a difference in inflation between the chambers results in bending of the structure to a specific direction.

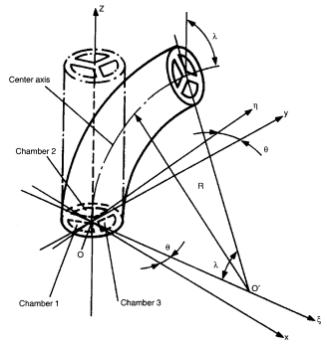

Figure 22: Bending of pneumatic actuator [33].

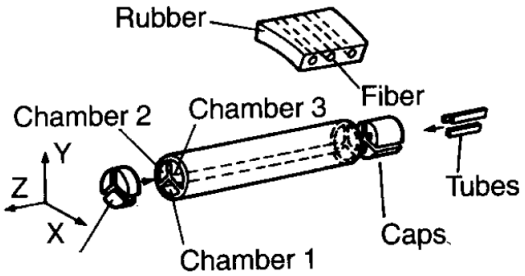

Figure 23: Pneumatic actuator parts [33].

The research of [34] provides soft fingers which consist of a rubbery material and contains a single chamber which can be inflated. However, this design makes use of a non-uniform wall thickness, resulting in a unsymmetrical stretching of the structure such that bending occurs.

[35] provided a structure consisting out of multiple fingers which are as well fiber reinforced as plastic sheet reinforced, as visible in Figure 25. The fibers prevent radial deformation of the finger, while the plastic sheet prevents axial deformation. Therefore, the finger structure will bend in the direction of the plastic sheet while inflated.

In [36] a pneumatic soft gripper, Figure 24, was manufactured which uses a multi-layered structure i.e. a top, middle and bottom layered structure consisting out of Ecoflex, PDMS and Ecoflex respectively. By using a multi-layered structure, the bending can be done in both directions. As a result, the structure was able to form a flat and as well a convex as a concave structure, as can be seen in Figure 26.

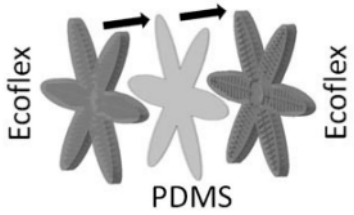

Figure 24: multi-layered pneumatic actuator [36].

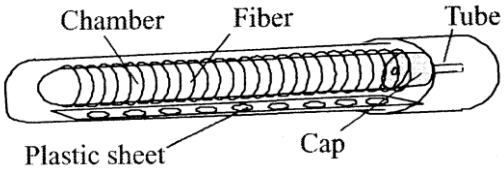

Figure 25: Reinforced pneumatic actuator [35].

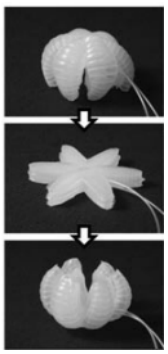

Figure 26: Multi-configurational pneumatic actuator [36].

[37] provided a research where the performance speed of pneumatic soft grippers were tested. Two different structures were tested, a fast and slow Pneu-net as visible in Figure 27 and Figure 28. It was found that pneumatic soft grippers can have a very small reaction time for a large amount

of bending. This research showed that a bending angle of around 300 degrees was possible in less than a second.

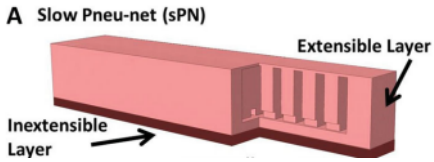

Figure 27: Slow Pneu-net [37].

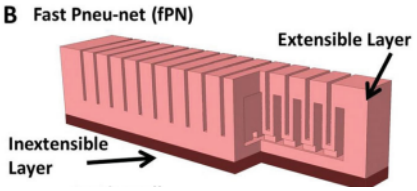

Figure 28: Fast Pneu-net [37].

[38] presented a novel principle for soft grippers, which is self healing. In this research a gripper is manufactured consisting out of three fingers, each oriented at 120 degrees from each other, out of polyaramid fibers. The structure of the fingers was based on an accordion attached on a strain limiting layer as visible in Figure 29. When the accordion inflates, the bending would be in the direction of the strain limiting layer. The structure was able to lift a wine glass by gripping from the outside (exterior surface pressure) or from the inside (interior surface pressure) while having the same configuration. This means that the exterior surface pressure was applied with friction between the strain limiting layer and the glass, while during interior surface pressure friction occurred between the accordion side and the glass, as presented in Figure 30. The novel principle included in this research is the self healing principle. It is shown that when the structure is punctured by a sharp object e.g. a needle, the actuator is still able to operate, even when the object of puncture is removed.

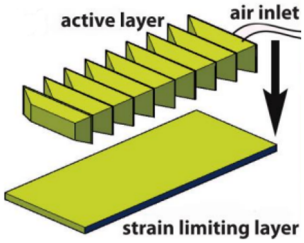

Figure 29: Accordion based pneumatic actuator [38].

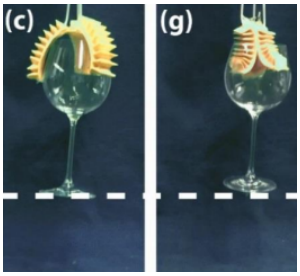

Figure 30: Accordion based pneumatic actuator grabbing a glass from outside and inside. [38].

[39] has provided a solution to apply the accordion based fingers, as presented by [38], in a water environment. The soft gripper manufactured in this research is able to handle vulnerable biological ecosystems, such as coral reefs, in deep seas.

In the research of [40], the performance of different angles of the top of the chamber during inflation is researched, as can be seen in Figure 31. Besides, structures were also tested in a amphibious environment. Additionally, 3 combinations of 2 different materials were considered for the upper and lower layer of a structure to determine the influence on the bending. At last, the influence of the width of the structures was varied.

The former mentioned soft grippers are all based on human body parts, as these can be considered to be based on a finger or a hand. However, there are also other living things where soft grippers are based on. One of these is the chameleon. A soft gripper is manufactured by [41] with the focus on the working principle of the tongue of the chameleon, as can be seen in Figure 32 and Figure 33. However, this gripper uses as well water as air. At first, the silicone cap is filled with water. When the silicone cap is surrounding the object, the water is retrieved from the cap. The force by the cap will be exerted pneumatically. Another form of nature as a basis for penumatic soft grippers are cephalopods, with a focus on the arms and/or tentacles of octopuses and squids. As can be seen in Figure 34, [42] manufactured a soft gripper "OCTARM" which can act like a tentacle.

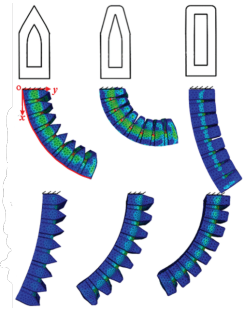

Figure 31: Different pneumatic actuator top shapes [40].

Figure 32: Chameleon's tongue for inspiration [41].

Figure 33: Gripper based on chameleon's tongue [41].

Figure 34: OCTARM holding a object [42].

A more improved version of the tentacle based soft gripper from [42] is presented in [43]. A tentacle consisting out of multiple segments and therefore multiple air chambers, such that the inflation time decreases, is provided in Figure 35. Besides, when there are multiple segments, each segment can be inflated such that the bending of that part can be in- or decreased, resulting in a structure which can have a very specific formation, to handle for example vulnerable objects as flowers, as visible in Figure 36.

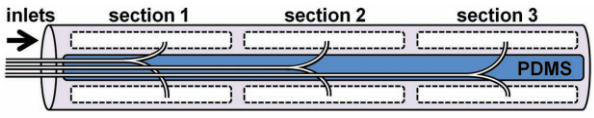

Figure 35: Pneumatic actuator conisting out of multiple chambers [43].

Figure 36: Tentacle shaped pneumatic actuator [43].

Additionally, an improved version for micro scale objects, even living thing as ants, is provided in the research of [44], as visible in Figure 40. As can be seen in Figure 37, this research showed that by applying a hump to the structure at the right location, the bending angle of the structure can be increased such that instead of a circle (Figure 38) a spiral (Figure 39) can be formed .

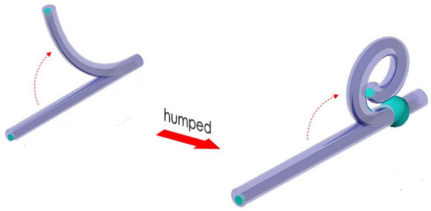

Figure 37: Influence of applying a hump [44].

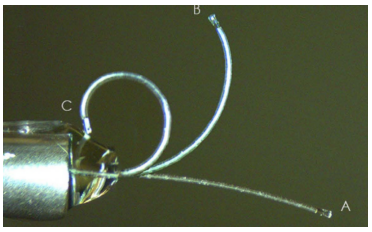

Figure 38: Circle forming without hump [44].

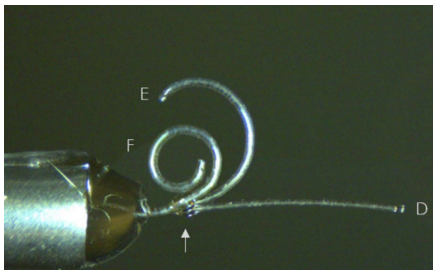

Figure 39: Spiral forming with hump [44].

Figure 40: Humped structure holding a ant [44].

4.2.3 Particle jamming actuators

Another possible actuation method is particle jamming. Particle jamming can be considered to be in two states, which is either soft or rigid. The soft state for particle jamming grippers can be seen as an enclosed space which contains particles. When the enclosed space is big enough such that the particles can move freely, the state can be considered soft. On the other hand, when the enclosed space is reduced, the particles will interlock with each other, resulting in an increased stiffness. This is considered to be the rigid state. As can be seen in Figure 41 from [45], particle jamming occurs when, for example, the air inside the enclosed space is removed, such that a vacuum occurs. This type of particle jamming is vacuum particle jamming. Due to the vacuum, the enclosed area decreases as there is a force generated on the membrane by vacuum pressure.

Another type of particle jamming is passive particle jamming, as visible in Figure 42. Instead of creating a vacuum in the whole structure, the enclosed area is now divided into loose particles and an air chamber. This elastic air chamber can be used as pneumatic actuator. By increasing the pressure and therefore the size of the the elastic air chamber i.e. actuator, a force will be exerted on the loose particles. As a result, particle jamming will occur. However, as the amount of bending increases, the reaction force of the particle pack on the actuator increases. Therefore, the bending range of the passive particle jamming actuator will be limited. As the bending angle and the stiffness of the passive particle jamming can not be adjusted independently, this can be seen as a disadvantage. In vacuum jamming, the particles are jammed due to a pressure on the chamber resulting from a pressure difference between the inside and outside of the chamber. Passive particle jamming occurs due to an external force on the elastic membrane between the air chamber and the particles, which is exerted by the elastic air chamber after inflation.

The last type of particle jamming is differential drive particle jamming. This structure consists out of two chambers, a particle chamber with loose particles and an elastic air chamber as visible in Figure 43. Additionally, a strain-limiting layer is included in the structure. As this structure includes a strain-limiting layer, inflation of the elastic air chamber will cause the structure to bend. By creating a higher pressure in the elastic chamber instead of the particle chamber, a pressure difference occurs and results in particle jamming. By comparing the differential drive particle jamming with vacuum jamming, a benefit is that now as well the amount of bending as the stiffness can be varied simultaneously. As well increasing as decreasing the enclosed area are typical done by varying the pressure. This principle can be used in soft grippers to increase the stiffness. According to [7], typical particles used are ground coffee, glass, plastic, beans and metallic beads.

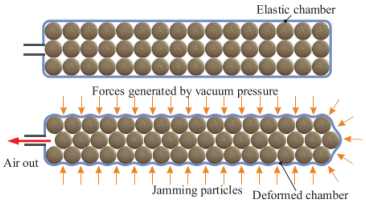

Figure 41: Vacuum particle jamming [45].

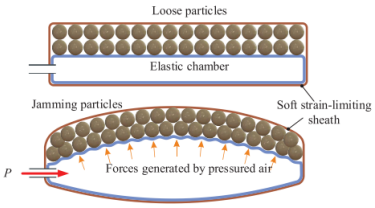

Figure 42: Passive particle jamming [45].

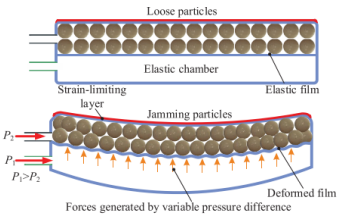

Figure 43: Differential drive particle jamming [45].

One of the first principles of particle jamming originates from the work of [46] and [47]. [46] and [47] considered to use particles instead of air inside rubbery pockets. In the research of [46], the construction of Figure 44 was used. The rubber pocket would deform under the load of grabbing the object, resulting in particle jamming. Therefore, the rubber pocket with particles become stiffer and can work as a deformable grip. Additionally, [48] provided a research which showed that particles in an enclosed area can adjust their orientation and rearrange themselves such that the enclosed area can cover an object entirely which makes grasping possible. Improving this principle led to a research by [49]. This research resulted in the Universal Soft Gripper (USG). Also a pocket with particles is considered, but instead of only making use of deformation due to grabbing an object, also the principle of evacuating the air from the pockets was applied, as visible in Figure 45. This research showed that the USG is able to grab many different objects varying from fragile objects as flashlight bulbs and raw eggs up to as well foam earplugs as solid heavier objects like hardware items and office supplies. A drawback of this gripper is that some object can not be grabbed due to their geometry (flat coins) or when the object is too deformable (cotton balls). In [50] an additional research is carried out as an extension to the previous research. In this research, the performance of an improved gripper was tested. A significant difference between the initial and improved gripper is that the initial gripper only uses negative pressure, while the new research considers also positive pressure. By making use of as well positive as negative pressure, the performance of the gripper was increased with 85% in reliability and 25% in error tolerance. Besides, another aspect of the improved gripper was that it is now even able to shoot objects by fast ejection. At last, the improved gripper was even able to grab and place multiple objects in a single grab while maintaining the relative position and orientation between these objects.

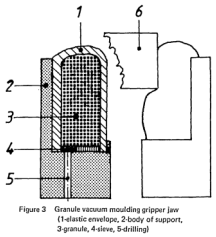

Figure 44: Rubbery pockets for particle jamming [46].

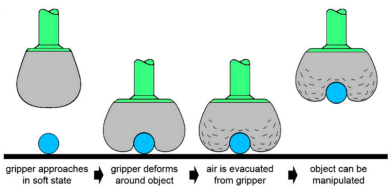

Figure 45: Universal Soft Gripper [49].

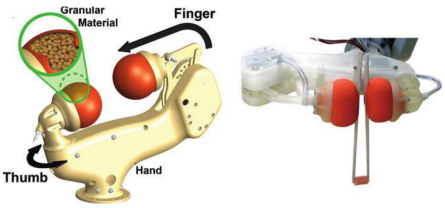

Figure 46: JamHand holding chopsticks [51].

The research of [52] provided a gripper which is able to be used in high pressure wet environments e.g. in deep sea waters at a depth of 1200m. The gripper which is used in this research is comparable with the USG by [49], as the gripper membrane is a latex balloon and the particles are glass beads. The fluid, on the other hand, is water instead of air. The benefit of using an incompressible liquid instead of a compressible gas is that the liquid can deliver and withstand more pressure. Besides, to achieve a high pressure with a gas, more and heavier equipment is required. [51] provided a research with another robot hand based structure, the JamHand. This structure can be seen as a hand consisting out of two fingers, where each of these fingers uses a particle jamming actuator. This soft gripper can be compared with the USG, but instead of 1 it has 2 fingers. It is shown that the JamHand is also very suitable for precision grasping such as handling chopsticks, as can be seen in Figure 46. An extension of particle jamming actuators can

be found in the research of [53]. In this research, a particle jamming actuator was used with a variable inner volume. As a results, the gripper has an increased adaptability to the object.

A different approach of using particle jamming can be found in the research of [54]. The particles in a finger structure are enclosing the move able skeleton, as visible in Figure 47. Instead of using particle jamming to increase the stiffness of the structure during force exertion with for example the USG from [49], particle jamming is now used to increase the stiffness of the structure for maintaining the current state of position. This means, that the particle jamming is used for maintaining posture control instead of force control. The benefit of this principle is that when a object is for example fragile or very deformable, the gripper can pick it up without having to apply a (high) force, as now the posture of the gripper remains constant.

In the research of [55], a pneumatic actuator is used to form a finger. However, particles are introduced in the structure as can be seen in Figure 48. As the finger is in rest, the particle are enclosed loosely in a chamber at one side of the finger. When the structure bends due to inflation, the chamber with loose particles will narrow, resulting in a thinner chamber where the particles will be squeezed against each other. This research concludes that within a small pressure range by including particles in the structure, the stiffness of the structure can be increased greatly. Besides, it is shown that large bending or deformation and a significant increase in stiffness can coexist. At last, this research showed that only a relatively small pneumatic pressure is required for activation of the gripper.

A research by [45] improved the principle of [55]. A more refined gripper is designed with the same principle. However, instead of using a soft strain limited sheath to form a single system from two independent chambers as in the research of [55], [45] forms a single structure consisting out of both of the chambers for as well the pneumatic actuation as the particles. Additionally, a fiber reinforcement is incorporated in the pneumatic chamber, where after a sheath is applied to embed the strain limiting layer and the fiber reinforcement to the structure as presented in Figure 49.

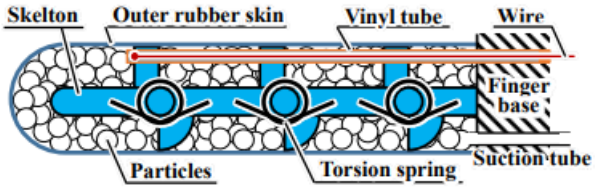

Figure 47: Particle jamming to maintain state of position [54].

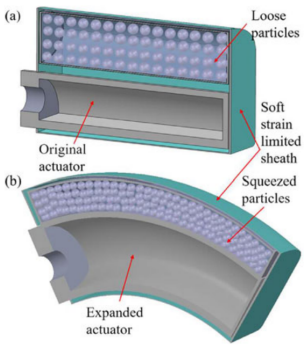

Figure 48: Particle jamming actuator [55].

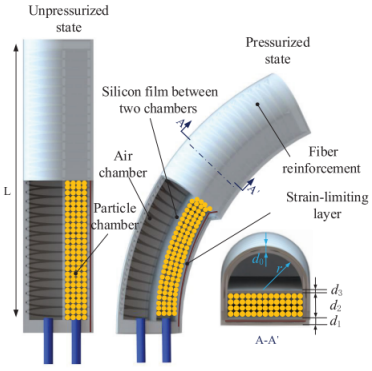

Figure 49: Particle jamming actuator with reinforcement [45].

4.2.4 Chemical reaction actuators

Another type of actuators are chemical reaction actuators i.e. combustion-powered grippers. An example of a chemical reaction actuator is provided by [56]. [56] has fabricated a tripedal soft robot which is combustion-powered by ignition of methane. As can be seen in Figure 50 and Figure 51, the robot consists out of three legs, each with an own combustion chamber. Due to combustion, the volume of the legs will increase significantly and will result in a high reaction force

on the fixed ground, resulting in a high acceleration and therefore in a jump. By adjusting the timing of the sparks and the fuel ignition, the direction and the height of the jump can be set as desired. Another actuator can be found in the research of [57]. In this research, a soft robot is manufactured which has a rigid core while the exterior remains soft. As can be seen in Figure 53, the robot is also able to make a jump and land on another location. The jump can be done by ignition of a mixture of oxygen and butane. Compared to the research of [56], there is only one ignition chamber. Therefore, the direction of jumping requires additional inflatable chambers in the legs. Dependent on the inflation of each leg, the direction for the jump can be set. A different concept is provided by [58]. In this paper, a soft robot - the octobot (Figure 52) - is manufactured. This robot represents a octopus, where eight arms are powered by the system. The power supply is done by including microfluidic logic. Microfluidic logic regulates the fluid flow in the system autonomously, leading to a decomposition of a mono propellant fuel, which results in actuation of the arms.

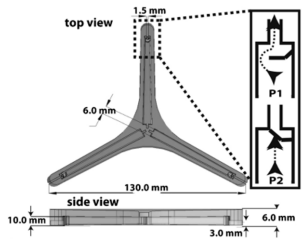

Figure 50: Chemical reaction actuator structure top and side view [56].

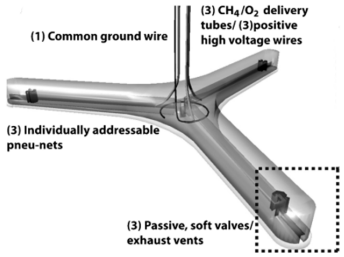

Figure 51: Chemical reaction actuator [56].

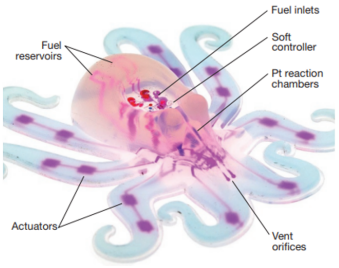

Figure 52: Jumping principle of inflated legs during ignition [58].

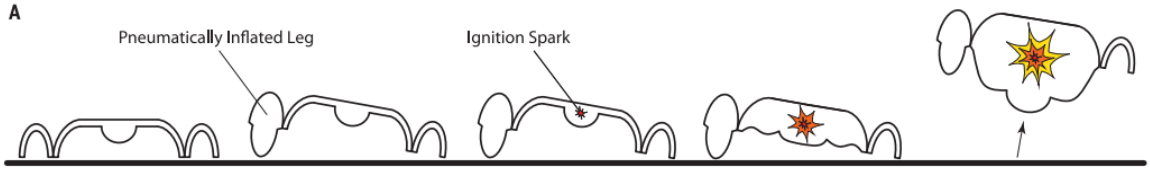

Figure 53: Octopus based microfluidic actuator [57].

4.2.5 Shape memory materials

An example of application of SMPs is provided in the research of [59]. The soft gripper manufactured in this research consists out of four fingers, as can be seen in Figure 54. Each finger consists out of a SMP. However, SMPs have the ability to deform after heating or reform back to the initial state after a deformed state. This means that there is only a one way use of this material. In other words, application of SMPs in soft grippers in the current situation is not very effective. It is only effective in specific situations. Therefore, this research adjusted SMP to a reversible, bidirectional shape memory effect (rbSME). The advantage of rbSMEs is provided below in Figure 55. As can be seen, there are three important temperatures T_{reset}, T_{high} and T_{low} respectively. When the temperature is T_{high}, the structure will be according to shape A. A temperature of T_{low} will result in shape B. When the temperature is increased to T_{reset}, reprogramming of the material occurs. This means that as well shape A as shape B will be erased. Now, at the temperature T_{reset}, new shapes A and B can be programmed by deforming the material, cooling it to T_{low} and heat again to T_{high}. Due to this principle, a cycle in temperatures can be established as presented in Figure 55. Making use of this application, the initial state of the soft gripper is when all four fingers are retracted, as visible in Figure 54. When the fingers are heated, the fingers will extend. When the fingers are cooled, the fingers will retract back to the initial state.

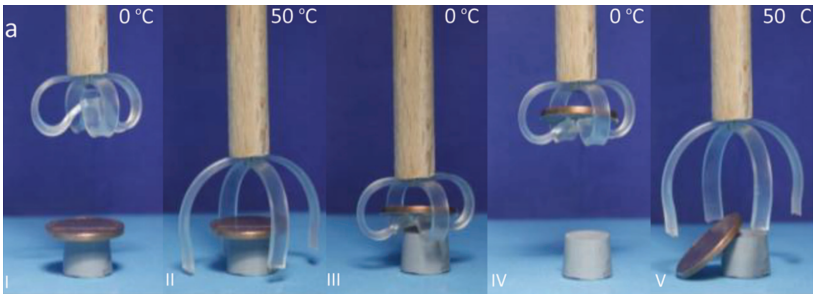

Figure 54: SMP soft gripper temperature cycle [59].

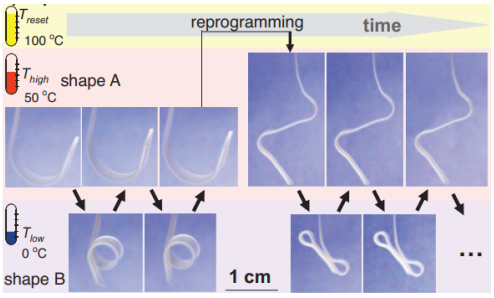

Figure 55: Working principle of SME with rbSME [59].

Another gripper based on SMPs is the four fingered gripper manufactured by [60]. The same approach is used as by [59], where an initial state and a programmed state are considered. However, there is no reset temperature for reconfiguration of the structure shape included in this material.

[61] manufactured a three fingered hand. Each finger has on the back and the front side of the finger SMA wires. These wires are used to ensure grasping. The SMA used in this research is a Ni-Ti alloy. When there are no stresses applied to the system and the temperature is approximately room temperature, there are two different martensitic phase fractions. When a force is applied leading to a tensile stress, one of the phases will be in favour, resulting in elongation as can be seen in Figure 56. When the temperature is increased, the phase transition occurs from martensitic to austenite (A phase). This phase change results in a decrease of length of the wire i.e. the wire works as the actuator.

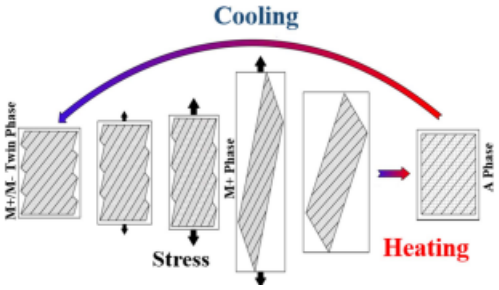

Figure 56: SMA material behaviour [61].

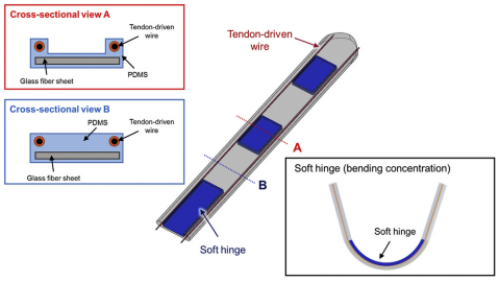

Figure 57: Finger with SMA wires [62].

[62] provided a gripper which is a five fingered hand (four fingers and a thumb). The actuator in these fingers are two tendon driven wires, as can be seen in Figure 57. When the wires are heated, bending of the wires and therefore bending of the structure occurs. This is due to the eccentricity of the SMA wires. When the wires are cooled, the hand will return to the initial state.

Another gripper based on SMA wires is manufactured during the research of [63]. However, this gripper included only two fingers. A benefit of this gripper it that it is very compact. The weight of the whole gripper module was less than 70 gram and was able to operate over three hours. Additionally, this gripper was able to manipulate smaller and more vulnerable objects such as flies.

4.2.6 Fabrication of soft grippers

There are many different fabrication techniques available for soft grippers. However, the type of fabrication depends on for example the application of the soft gripper and the size. Additionally, the type of actuation is relevant for fabricating a soft gripper. As an example, when a soft gripper with particles is required, generally moulding a single structure from multiple parts is required.

Fabrication of soft grippers can be divided in different category's. For example, Elastic Inflatable Actuators (EIA's) for soft grippers can be manufactured according to different production processes, as visible in Figure 58(A) [64]. As visible, 2D moulding covers a significant part of the surface. 3D moulding, additive manufacturing and full lithography covers smaller area's. Therefore, these manufacturing processes are more specific. In Figure 58(C),(B) and (D) the different mould

making techniques for respectively 2D moulding, 3D moulding and additive manufacturing are provided. As visible, there are significantly more techniques for 2D molding. However, Figure 58 is based on researches stated in [64], of which the report has a focus on EIA's for soft grippers. Therefore, Figure 58 only provides information based on EIA's soft grippers. Consequently, in this research a new simple overview is provided. An overview is provided in Table 3, where the category's *moulding*, *additive manufacturing* and *alternatives* provided. These category's indicate which production process is the most relevant production process of that research. In other words, a gripper can exist for example out of three rigid 3D printed parts, while the bending parts (for example the joints) are complex and moulded. As a result, the construction will still be assigned to the category moulding, as this is the complex and relevant/novel part. The first category is considered, as multiple soft grippers consists out of a material which generally is moulded, such as silicone. Besides, it provides the information that molds are required. There is made no difference between 2D or 3D moulding. Also fabrication processes as soft lithography are included in this category. The second category, additive manufacturing, provides the information that no molds are required, but it can for example be 3D printed with stereo lithography. The third category, alternatives, provides the information that other fabrication processes are required than moulding or additive manufacturing. This is for example relevant for the USG as presented in Figure 45 or when SMA wires are used for actuation. As visible, most of the soft grippers are either fabricated by a moulding process or by alternative processes. Only a couple of structures are fabricated with additive manufacturing.

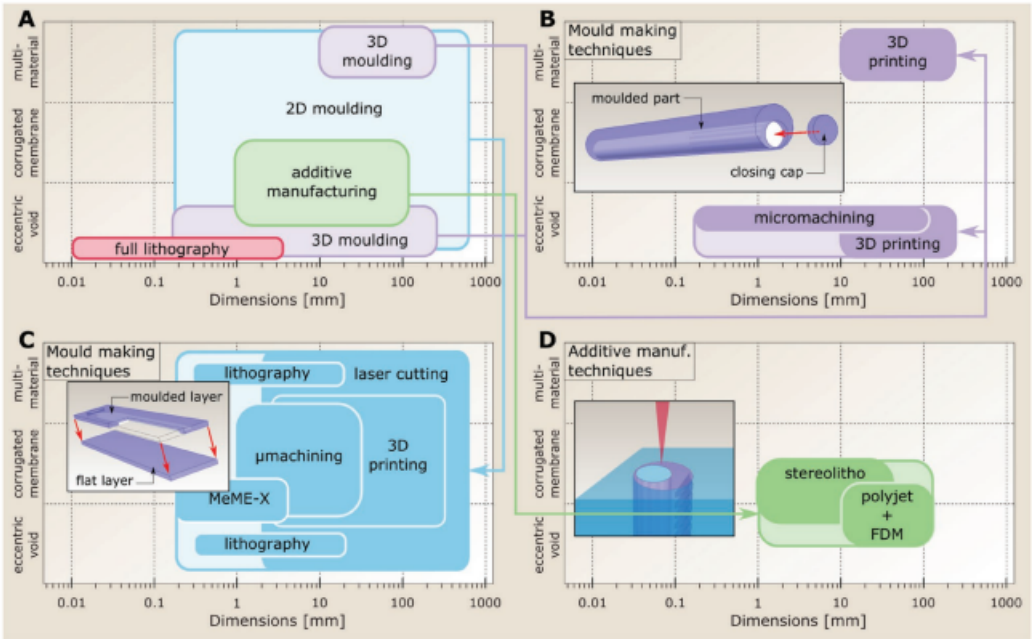

Figure 58: Fabrication techniques of elastic inflat- able actuators [64].

Category	References
Moulding	[24], [36], [37], [38], [39], [40], [43], [45], [55], [56], [58], [62], [65], [66], [67], [68]
Additive manufacturing	[54], [60], [69]
Alternatives	[19], [22], [25], [29], [31], [32], [34], [49], [50], [52], [51], [59], [63], [70], [23]

Table 3: Overview of production processes of relevant literature.

4.2.7 Testing of soft grippers

Testing of soft grippers can be done according to two main characteristics. These characteristics are the amount of bending and the force which can be exerted by the soft gripper. Additionally,

the soft grippers can be tested on for example the performance speed. However, these are often side performances. The focus of the performance of soft grippers is on the two main characteristics bending angle and force.

In [34], the bending performance was simply measured by the amount of tip displacement. In [65] a vision system is provided with a high speed camera. In their research, soft fingers were manufactured and fixed to a 3D printed fixture, as presented in Figure 59. To maintain the same location of the high speed camera with respect to the soft fingers, the camera is also fixed to the 3D printed frame. Therefore, the measurements of different soft fingers can be easily compared. The high speed camera has the capability to capture images of the soft gripper with a rate of 130 fps. Also, the high speed camera is in this research triggered by a micro controller which also controls the pneumatic actuator. Therefore, the captured images and the input information can be easily synchronized. The background behind the soft fingers is uniform dark black. Therefore, the soft finger can automatically be extracted from the picture. From this extraction, a lot of information about different aspects can be extracted. An automatic image processing program was developed to extract these aspects. As a result, the trajectory path, the maximum bending angle and the radial expansion can be determined, as visible in Figure 60. A pro of this measuring principle is that no other physical measurement devices are required which can affect the bending of the soft finger. The trajectory path and maximum bending angle can easily be determined by comparing for example the tip of the soft finger of all of the images taken during a single experiment. Due to the principle of controlling the pneumatic actuator and the high speed camera with a single micro controller, a calibration can be made between the cross section of the soft finger and the amount of pixels inside the soft finger on the images. [67] provides a finger bending test where the soft fingers are placed in front of a grid. As visible in Figure 61, after bending, the angle between the horizontal and the location of the finger tip can be measured. The origin is the inside of the base of the finger. In [69] the bending of the soft grippers is measured comparable with [67]. The origin is chosen at the center of the base of the soft gripper. As presented in Figure 62, the center at the tip of the soft gripper is the endpoint, which is used to determine the bending angle between the vertical, as the soft gripper is vertical in rest. The endpoint of the soft gripper is as well marked at rest as after bending on a coordinate paper background. With these markings, the bending angle can be measured manually. [68] measured the bending angle of the soft gripper from a side view with a black and white background, like a checkerboard as provided in Figure 63.

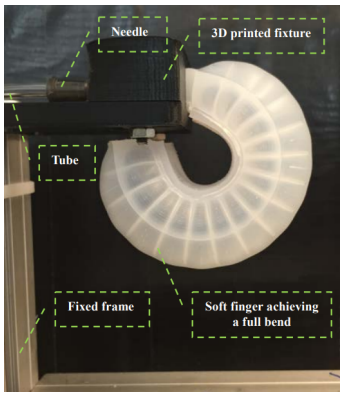

Figure 59: Measuring bending perforamnce with high speed camera [65].

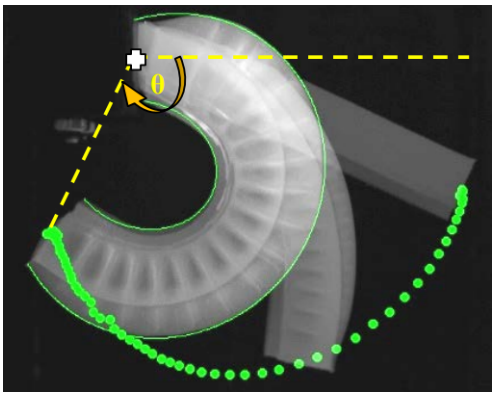

Figure 60: Retrieving data from high speed camera and reconstruct trajectory path [65].

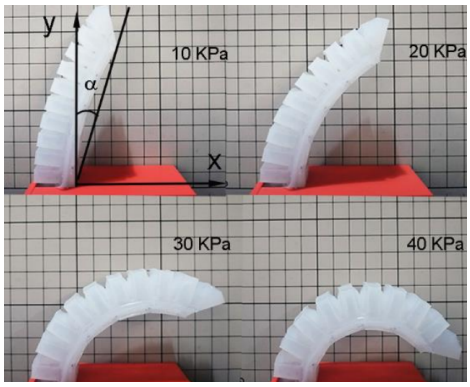

Figure 61: Measuring bending performance from origin on grid [67].

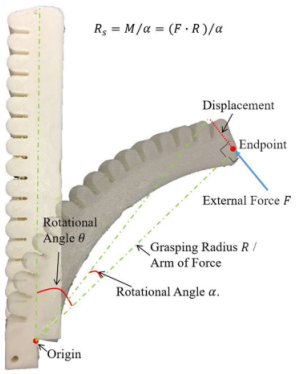

Figure 62: Measuring tip displacement [69].

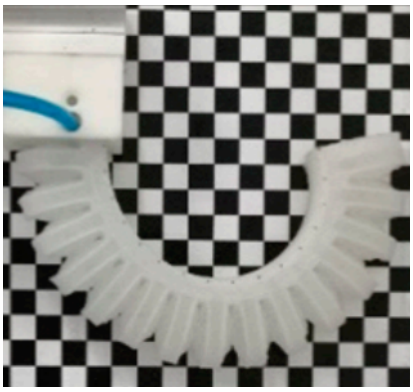

Figure 63: Measuring bending performance on "chessboard" grid [68].

In the research of [65] is not only the bending measured, but also the maximum contact force. To measure the contact force, a post was 3D printed which can be attached to the Schunk Mini45 sensor, which is able to measure force and torque. As already mentioned before with the high speed camera is this sensor also fixed to the fixture such that all of the tips of the soft fingers would end up with the tip acting a force on the 3D printed post, as visible in Figure 64. For measuring the force of the soft finger, [67] used a force sensor which is directly in contact with the finger tip while the base of the finger was fixed, see Figure 65. Also [68] presented in Figure 66 a measuring technique where the tip of the soft grippers presses against a force measuring button. Measuring the force of the soft grippers is done differently in the paper by [69]. The first test of Figure 67 is done on the tip of the finger to determine the rotational stiffness, while the second test was attached to the middle of the soft gripper with a cylinder to determine the pull-out force.

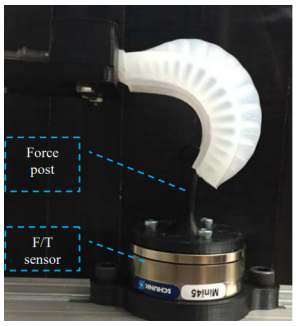

Figure 64: Measuring force with sensor [65].

Figure 65: Measuring force with sensor [67].

Figure 66: Measuring force with sensor [68].

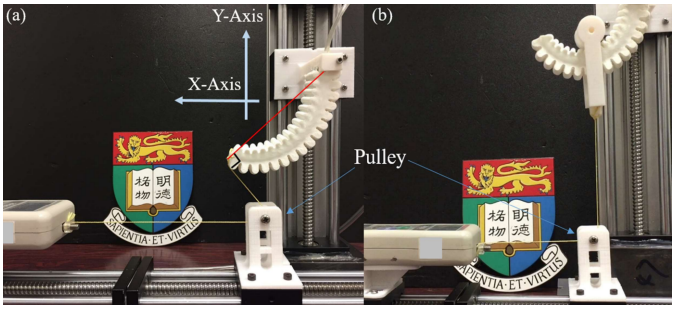

Figure 67: Measuring rotational stiffness and pull-out force [69].

In Table 4 a categorization is presented of multiple relevant papers in which the performance of soft grippers are measured. The first row represents that the amount of bending of the soft gripper in that research is measured according to the bending angle. The second row represents measuring the amount of bending, but instead of using the bending angle a curvature or tip displacement is considered. The third row provides the information whether the force exerted by the soft gripper is measured. The fourth row considers measuring additional characteristics, for example the speed of grabbing or the amount of strain.

Characteristics	Paper
Bending angle	[24],[25],[33],[62],[63],[55],[45],[65],[67],[68],[69],[71],[72]
Curvature or tip displacement	[19],[24],[25],[26],[27],[29],[30],[32],[43],[34],[35],[38],[40],[44],[63],[55],[69]
Force	[24],[25],[27],[28],[29],[30],[32],[35],[39],[44],[70],[49],[52],[63],[55],[45],[65] [67],[68],[69],[66],[73]
Additional characteristics	[19],[25],[27],[29],[30],[32],[43],[34],[35],[39],[40],[70],[49],[50],[59],[60],[62] [63],[55],[45],[65],[67],[69],[71]

Table 4: Overview of measured characteristics of relevant literature.

4.3 Limitations

Although there has already been a lot of research in the application of soft grippers, still they are not optimized. As soft grippers are made of soft materials, these often showed a lack of robustness. Besides, to increase the stiffness or to deliver a higher force, often larger power supplying machines are required. Additionally, even though many different types of smart materials are already used as actuator or as sensor, in soft grippers or not, this wide field of using different smart materials is still full of potential. Especially in the field of thermoresponsive smart materials, as common material classes are SMAs and pyroelectrics. Therefore, with a novel design by applying thermal sensitive hydrogels as actuators, an aim is done for adding a new potential field to the broad area of smart material actuated soft grippers.

5 Methodology

After an elaborate literature survey, the conceptual design can be provided of the novel actuator. Thereafter, the modelling approach for implementing thermoresponsive hydrogels in simulations is considered. The last part of this chapter describes the fabrication approach for the demos. Additionally, a comparison between the fabricated demo structures and simulations will be provided.

5.1 Conceptual design

For the novel actuator, a soft gripper actuated by thermoresponsive hydrogel particles is considered which must be adaptive to the environment i.e. to the object for grabbing. The novel actuator is showed in Figure 68 and Figure 69. Initially, a silicone structure is provided which includes multiple chambers. Each chamber includes a single identical thermoresponsive hydrogel particle at the initial temperature $T_{initial} > 273K$. By decreasing the temperature of all the particles to T_{low} with $0 < T_{low} < T_{initial}$, the hydrogel particles will swell. As a result stretching of the structure occurs. The benefit of using multiple chambers instead of a single large chamber is that the hydrogel particles are not able to move freely i.e. are fixed, which results in homogeneous amount of bending throughout the relevant parts of the structure due to homogeneous stretching of each chamber. Additionally, no bulges can occur. However, the stretching at the right side of the structure will be larger than the stretching at the left side of the structure, due to the difference in thickness of the layer. Therefore, the right side of the structure is the strain layer, as this is the side of the structure which will stretch the most. Due to this heterogeneous stretching, bending in the direction of the left side of the structure occurs. Consequently, this side, which is in the bending direction, will be identified as the strain limiting layer. This strain limiting layer is designed such that stretching is reduced at this side, for example and as in this case with an increased thickness. Besides these two layers the structure has also a top and bottom layer. However, as the top of the structure is often considered to be fixed to a rigid part, the thickness is often not very relevant. The bottom side is often free and the thickness can for example prevent stretching in this direction.

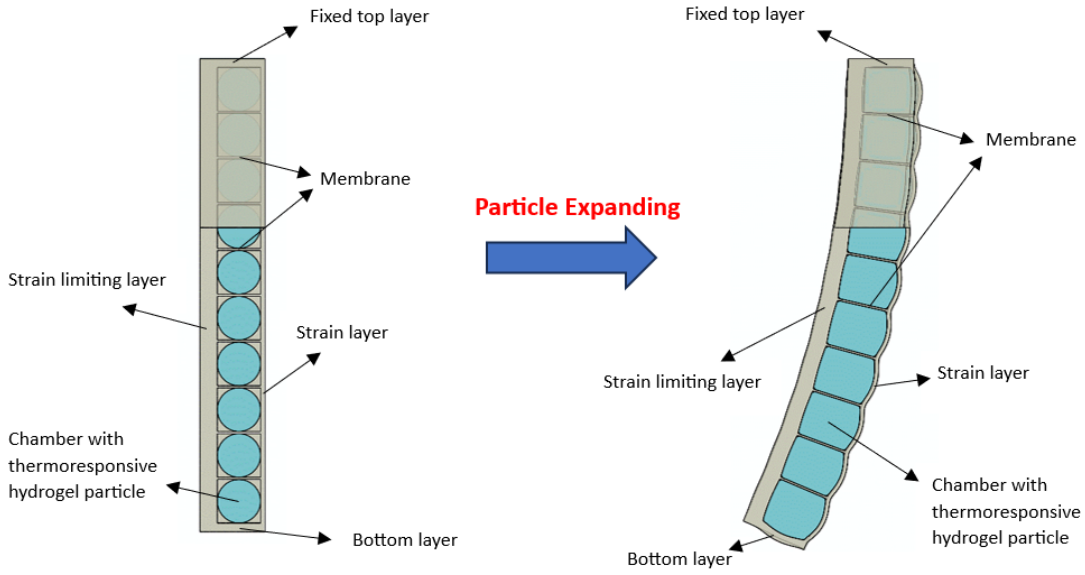

Figure 68: Conceptual design (2D)

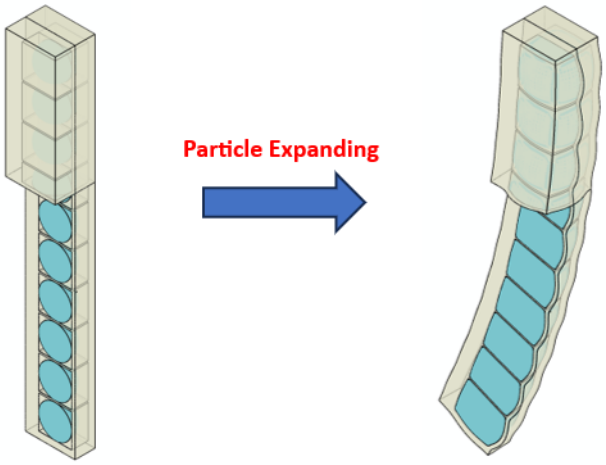

Figure 69: Conceptual design (3D)

Now that the working principle of this structure is clear, this actuator can be applied to form a completer soft gripper. Therefore, instead of considering the structure provided in Figure 68 as a soft gripper, this is considered as only a segment of a soft gripper. As a result, the conceptual design of an adaptive soft gripper is presented in Figure 70. This adaptive soft gripper consists out of three segments. Each segment is presented in Figure **??**, Figure 72 and Figure 73. Color coding is applied to represent parts of each segment in upcoming figures. The coupling section between segment 1 and 2 and the coupling part between segment 2 and 3 are presented in respectively Figure **??** and Figure 75. By mirroring specific segments, bending in both directions can be achieved with this novel actuator to achieve the required configuration, as presented in Figure **??**

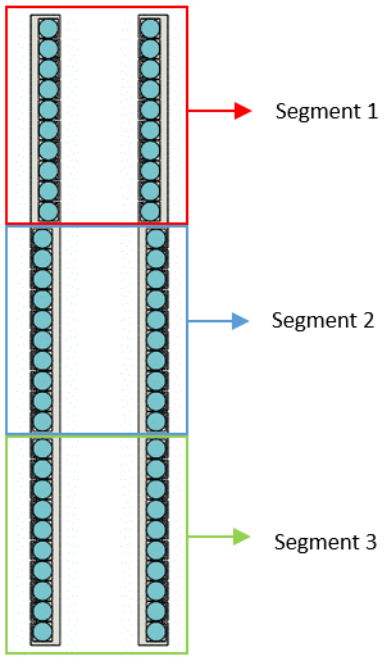

Figure 70: Adaptive soft gripper design divided in three segments.

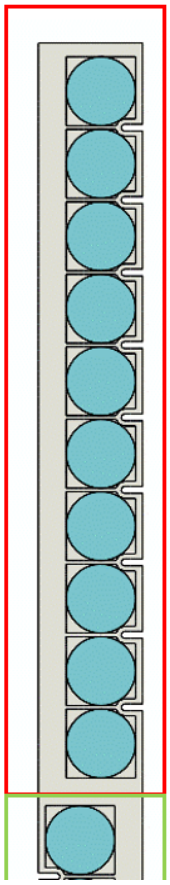

Figure 71: Segment 1 of the adaptive soft gripper.

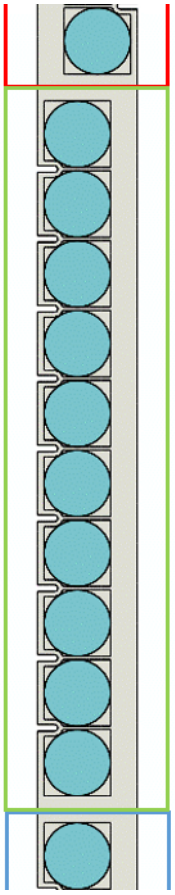

Figure 72: Segment 2 of the adaptive soft gripper.

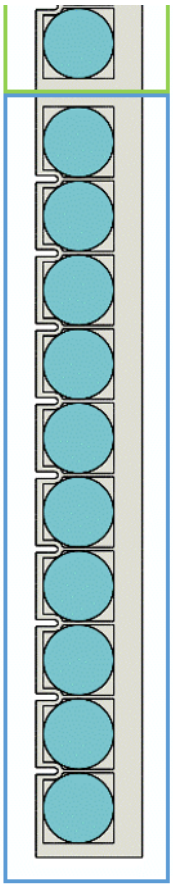

Figure 73: Segment 3 of the adaptive soft gripper.

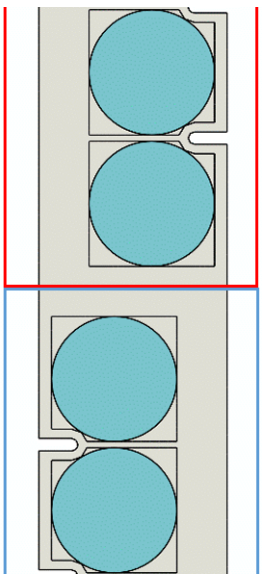

Figure 74: Coupling section between segment 1 and 2.

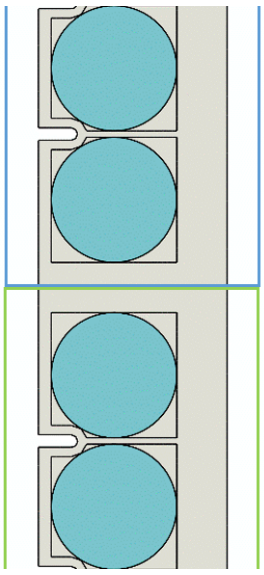

Figure 75: Coupling section between segment 2 and 3.

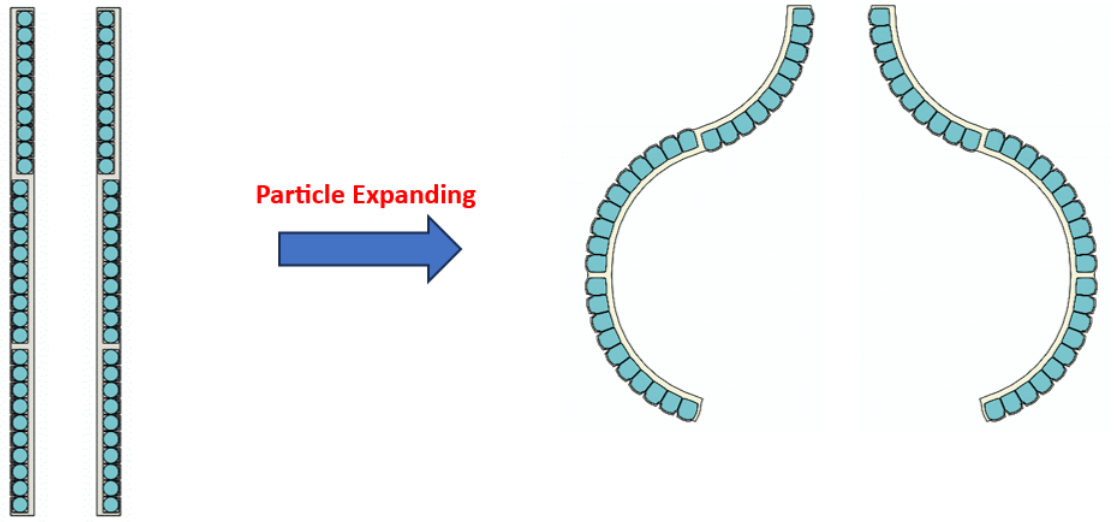

Figure 76: Actuated adaptive soft gripper design.

5.2 Modelling of the hydrogel

Before thermoresponsive hydrogels can be included in simulating software's, some formulas have to be determined to describe the behaviour of this material. However, establishing the complex mathematics behind thermoresponsive hydrogels is not in the scope of this research. Therefore, an overview is presented including relevant formulas. Additional information and to have an insight deeper in the complex mathematics behind the formulas provided in this research can be found in the papers of [74], [75], [76].

At first, some mathematics are required to determine the behaviour of polymers under influence of external loads in a solvent. As can be seen in Figure 77, a network of polymers in a solvent with chemical potential μ, under influence of a mechanical load P and a geometric constraint is considered. The free energy model for hydrogel can be described in the form of $W = W(\mathbf{F}, T, C)$, where $\mathbf{F}$ is the deformation gradient tensor, T is the temperature, C is the nominal concentration of solvent molecules and μ is the chemical potential of the solvent molecules. However, by considering that a chemical potential must be a constant at the equilibrium state, the formula $W = W(\mathbf{F}, T, C)$ can be changed via Legendre transform to Equation 1.

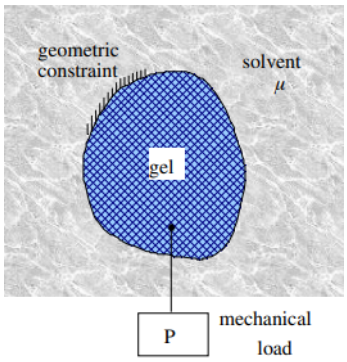

Figure 77: Polymer network in a solvent with chemical potential μ, under influence of a mechanical load P and a geometric constraint [74].

$$\hat{W} = W(\mathbf{F}, C) - \mu C \tag{1}$$

An additional relevant formula is required to represent the molecular incompressibility of the hydrogel. A characteristic of thermoresponsive hydrogels is that when water molecules are migrating out of the material, the network will contract. Due to this characteristic, the material decreases in volume without including any pores. Besides, when a mechanical load is applied, these can often be considered to be of the smaller size so that the chemical bonds of the hydrogel are undeformed. Additionally, absorbing (solvent) molecules is considered to have a significantly greater impact on volumetric change compared to physical association of the molecules. As a result, it can be considered that the volume of the hydrogel includes the volume of the dry network and the volume of the pure liquid solvent. Therefore, the volume of the hydrogel can be described with Equation 2, where υ represents the volume per solvent molecule.

$$1 + \upsilon C = \det \mathbf{F} \tag{2}$$

It can be considered that the behaviour of a hydrogel is mainly entropic. Swelling of the hydrogel is due to absorbing solvent molecules between the polymer chains. As the material is swelling, the configurational entropy of the polymer network decreases. On the other hand, the configurational entropy of the mixture of solvent molecules and polymer networks increases. As a result, there will be an equilibrium between the polymer network and the solvent. Consequently, Equation 3 can be used as a free energy function [77]. In this free energy function, N represents the number of chains per polymer volume and k represents the Boltzmann constant. A parameter χ, which is the Flory-Huggins interaction parameter, is included in this formula and measures the strength of pairwise interactions between the solvent molecules and the polymer network. When this parameter has a positive value, it represents that there is more interaction between solvent molecules themselves than between the solvent molecules and the polymer network.

$$W = \frac{1}{2}NkT[F_{iK}F_{iK} - 3 - 2\log(\det \mathbf{F})] - \frac{kT}{\upsilon}[\upsilon C \log(1 + \frac{1}{\upsilon C}) + \frac{\chi}{1 + \upsilon C}] \tag{3}$$

With some mathematics, Equation 1, Equation 2 and Equation 3 can be rewritten to Equation 4. In this formula, $I = F_{iK}F_{iK}$ and $J = \det \mathbf{F}$. However, instead of using the concentration of the solvent C as an independent variable, the chemical potential of the solvent μ is considered.

$$\hat{W}(\mathbf{F}, \mu) = \frac{1}{2}NkT(I - 3 - 2\log J) - \frac{kT}{\upsilon}[(J-1)\log\frac{J}{J-1} + \frac{\chi}{J}] - \frac{\mu}{\upsilon}(J-1) \tag{4}$$

Equation 4 can be combined with formula (13) presented in the research of [74], resulting in Equation 5. Using this formula, which is valid when a hydrogel is held at a constant chemical potential by solvent molecules, the stress (s_{iK}) of the hydrogel can be related to the deformation gradient.

$$\frac{s_{iK}}{kT/v} = Nv(F_{iK} - H_{iK}) + [J\log(1 - \frac{1}{J}) + 1 + \frac{\chi}{J} - \frac{\mu}{kT}J]H_{iK} \tag{5}$$

Equation 3 represents the free energy function. However, during calculation, a singularity can occur. To prevent singularity during the calculations, instead of considering a dry state where $\upsilon C = 0$ for the reference state, the condition $\upsilon C > 0$ is used. As a result, it is considered to use a reference state where the polymer network is in equilibrium with a solvent with chemical potential μ_0. Besides, during this reference state, free swelling is considered. Therefore, swelling is uniform in each direction i.e. $\lambda_x = \lambda_y = \lambda_z = \lambda_0$ with λ_x considering swelling in the x-direction, λ_y in the y-direction and λ_z in the z-direction. As the reference state is free swelling, it follows that the swelling ratio $J = \lambda_0^3$. Applying these conditions and some more complex mathematics, Equation 5 can be rewritten to Equation 6.

$$\frac{\mu_0}{kT} = \frac{N\upsilon}{\lambda_0^3}(\lambda_0^2 - 1) + \log(1 - \frac{1}{\lambda_0^3}) + \frac{1}{\lambda_0^3} + \frac{\chi}{\lambda_0^6} \tag{6}$$

By applying complex mathematics and the formulas (33), (34) and (35) of [76] to Equation 6, Equation 7 can be formulated. This equation will be used in subsubsection 5.2.1 to determine relevant parameters.

$$\frac{\mu_0}{kT} = \frac{Nv}{\lambda_0^3}(\lambda_0^2 - 1) + \log(1 - \frac{1}{\lambda_0^3}) + \frac{1}{\lambda_0^3} + \frac{(A_0 + B_0T) - (A_1 + B_1T)}{\lambda_0^6} + \frac{2(A_1 + B_1T)}{\lambda_0^9} \tag{7}$$

The free swelling $\mathbf{F}_0$ relative to the dry network is a simple diagonal matrix with the swelling ratio λ_0 on the diagonal as visible in Equation 8. However, for the reference state, the free swelling state is calculated with Equation 9. In this formula, **F'** represents the deformation gradient of the current state relative to the free swelling state while **F** is the deformation gradient of the current state relative to the dry network.

$$\mathbf{F}_0 = \begin{bmatrix} \lambda_0 & 0 & 0 \\ 0 & \lambda_0 & 0 \\ 0 & 0 & \lambda_0 \end{bmatrix} \tag{8}$$

$$\mathbf{F} = \mathbf{F}'\mathbf{F}_0 \tag{9}$$

Now that we consider instead of the dry state a free swelling state as reference state, a formula for the free energy density with a free swelling state as reference state can be formulated. This formula is presented in Equation 10. Now, for the final formula, Equation 4 and Equation 10 must be combined. The final formula is presented in Equation 11, in which $I' = F'_{iK}F'_{iK}$ and $J' = \det \mathbf{F}'$. This formula is the relevant formula which will be used for the subroutine UHYPER developed by [74] for ABAQUS, which is presented in Appendix A.

$$\hat{W}'(\mathbf{F}', \mu) = \lambda_0^{-3}\hat{W}(\mathbf{F}, \mu) \tag{10}$$

$$\begin{aligned} \hat{W}'(\mathbf{F}', \mu) = &\frac{\lambda_0^{-3}}{2} NkT[\lambda_0^2 I' - 3 - 2\log(\lambda_0^3 J')] \\ &- \frac{kT}{v}[(J' - \lambda_0^{-3})\log(\frac{J'}{\lambda_0^3 J' - 1}) + \frac{\chi}{\lambda_0^6 J'}] \\ &- \frac{\mu}{v}(J' - \lambda_0^{-3}) \end{aligned} \tag{11}$$

5.2.1 Validation of subroutine

For the simulations, some parameters have to be determined. Therefore, referring back to Equation 7, as this formula has the unknown variables μ_0, T, Nv and λ_0. In this formula, $A_0 = -12.947, A_1 = 17.92, B_0 = 0.04496$, and $B_1 = -0.0569$. However, some of these variables can be chosen so that only one of the variables is unknown and can be calculated.

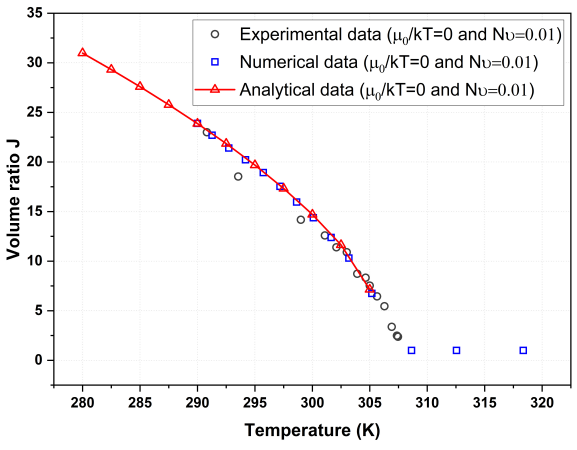

Figure 78: The volume ratio J of the free swelling hydrogel as a function of the temperature. The experimental and numerical data are retrieved from [78] and [79].

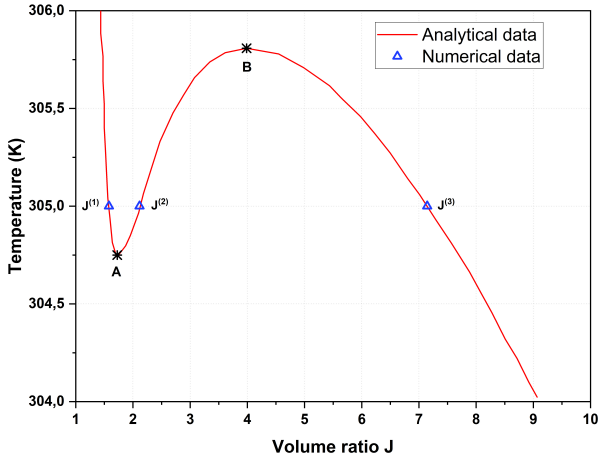

Figure 79: Volume ratio J that minimizes and maximizes the free energy at different temperatures [76].

Different values for Nv, μ and T are already calculated and tested by [76], [78] and [79]. Values for Nv are varying between 0.0035, 0.01 and 0.02 respectively, as visible in figure 3 presented in [76]. A value for $Nv = 0.01$ is considered with a varying value for μ_0, which are $0, -0.01$ and -0.02 to describe the volume ratio at different temperatures, as presented in figure 4 provided in [76]. Also, λ_0 can be extracted from this data, as $\lambda_0^3 = J \rightarrow \lambda_0 = J^{\frac{1}{3}}$. As can be seen from the provided data in Figure 78, a large volume ratio can be found for the values $Nv = 0.01$ and $\mu_0 = 0$. Starting from a temperature of T_0, the λ_0 can be calculated with Equation 7.

Solving the formula for $T = 305K$, $Nv = 0.01$ and $\mu_0 = 0$ results in three different values for λ_0, which are $\lambda_0^{(1)} = 1.164746$, $\lambda_0^{(2)} = 1.283580$ or $\lambda_0^{(3)} = 1.925984$, respectively. As $\lambda_0^3 = J$, the volume ratio can be calculated for each λ_0, resulting in $J^{(1)} = 1.580133$, $J^{(2)} = 2.114798$ and $J^{(3)} = 7.144273$. To determine which values are relevant for the simulations, a check is required. This check is presented in Figure 79. For the temperatures between point A and B, which are respectively $T_A \approx 304,75$ K and $T_B \approx 305,8$ K, the material can be in a stable or unstable state. According to the data in Figure 79, the values for the volume ratio J can be either at the left side of point A, between point A and B or at the right side of point B. When a point is considered at the left side of point A, the simulation will converge to A by decreasing the temperature. On the other hand, considering a point between A and B, the simulation will end in either point A or point B. However, the simulation can consider only a single stable state at a time. Therefore, one stable state can not jump to another stable state. When a point at the right side of point B is considered, the simulation will be terminated in point B after increasing the temperature and will not be terminated when the temperature is decreased. By looking at the values, $J^{(1)} = 1.580133$ will be at the left side of A, as presented in Figure 79. This means that during simulation, the volume ratio will end at point A and there will be no volume change anymore. $J^{(2)} = 2.114798$ on the other hand will be between point A and B and the simulation will end after reaching either one of those points. However, $J^{(3)} = 7.144273$ will not end as this is at the right side of part B, as the temperature will decrease. Therefore, the value $J^{(3)} = 7.144273$ i.e. $\lambda_0^{(3)} = \lambda_0 = 1.925984$ is relevant for the simulations.

The calculated value $J^{(3)} = 7.144273$ corresponds with the data provided in Figure 78. As the value complies with the literature, a validation can be done. At first, a hydrogel cube with a volume of $V_0 = 1 \times 1 \times 1 = 1\ mm^3$, see Figure 80, is programmed. The initial temperature of the cube is $T_0 = 305$ K. The temperature will we decreased until it reaches a temperature of $T_1 = 290$ K. As a result, the volume of the cube increased from V_0 to $V_1 = 1.49503 \times 1.49503 \times 1.49503 = 3.34156\ mm^3$, as visible in Figure 81. According to Figure 78, the volume ratio for a temperature of $T_0 = 305$ K is $J_0 \approx 7.15$ and for $T_1 = 290$ K is $J_1 \approx 24$. This means that $\Delta J = \frac{J_1}{J_0} \approx 3.35$. To validate the simulation results, ΔJ and ΔV must be compared. $\Delta V = \frac{V_1}{V_0} = 3.34146$. It can be concluded that $\Delta V = \Delta J$ and therefore the simulation can be considered as validated.

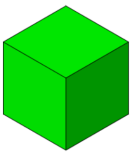

Figure 80: Hydrogel cube with a volume of $V_0 = 1\ mm^3$.

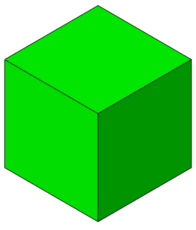

Figure 81: Hydrogel cube with a volume of $V_1 = 3.34156\ mm^3$.

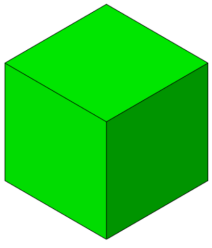

Figure 82: Hydrogel cube with a volume of $V_2 = 4.33601\ mm^3$.

As the data from Figure 78 is validated, the hydrogel can be used in simulations. However, to achieve some more bending, the temperature difference ΔT is increased, resulting in a simulation starting at a temperature of T_0 and ending at a temperature below T_1, which is T_2. According to the data of Figure 78, the volume of the hydrogel does not change above $T = 305$ K, as this is the dry state of the material. As water molecules are required to swell, a condition for T_2 is considered to be hold to maintain a working hydrogel. This condition is $273K < T_2 < T_0$. Therefore, to increase the volume ratio of the hydrogel, cooling to a temperature of $T_2 = 280$ K

is considered. The result is visible in Figure 82. The volume of the hydrogel cube increased even more to a value of $V_2 = 1.63066 \times 1.63066 \times 1.63066 = 4.33601\ mm^3$. As a result, the volume ratio $J_2 = \Delta J \cdot J_0 = 4.33601 \times 7.144273 = 30.97764$, which is presented in Figure 78.

5.3 Fabrication of demo structures and experiments setup

At first, the molds for the demos must be created. Designing the molds can be done in SolidWorks. As stated above in subsubsection 4.2.6, manufacturing the molds can be done with 3D printing. The novel actuator makes use of thermoresponsive particles inside the structure. Additionally, for this novel actuator, two molds are required as a membrane is used to divide a large chamber into multiple smaller chambers. Therefore, these molds are formed parallel to cutting plane 1 as presented in Figure 83. However, instead of cutting throughout the middle of the structure, the cutting plane is now moved to almost the side of the structure, resulting in for example the two molds as presented in Figure 84 and Figure 85. The molded parts of each mold can be glued together to a single structure after including a swelling particle in each chamber.

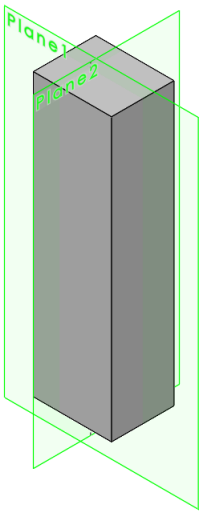

Figure 83: Cutting planes.

Figure 84: Mold for structure including chambers.

Figure 85: mold side structure

The different structures which will be manufactured are the the four geometry's straight, sharp, waved and cylinder. The material, length and reinforcement are for all of the structures similar, which are respectively Ecoflex 30, 10 particles (217 mm) and no reinforcement. The values for the thicknesses of the layers and membranes as presented in Figure 68 and the size of the chambers are for each structure similar, which will be clarified in subsubsection 5.3.1.

The molds are 3D printed with PLA (polylactic acid). As the molds are finished, the molding process can begin. For the silicone, Ecoflex 30 of Smooth-on will be used. At first, the Ecoflex 30 is prepared. This material has a pot life of 45 minutes and a cure time of four hours. Therefore, this material is suitable to use for the molding process. All of the printed molds are filled with the liquid Ecoflex 30. The molds are filled up to the top edge. After waiting for over 4 hours, the material was fully dry. All of the structures were extracted from the molds. The structures including the chamber were all placed at their closed side, such that the particles could be placed inside the chamber, as visible in Figure 86. However, instead of using thermoresponsive hydrogels, commercial swelling hydrogel particles i.e. super-absorbent polymer particles as sodium polyacrylate are used, which will swell when soaked in water. As a result, the particles will simulate the swelling principle of the thermoresponsive hydrogel with a simplified principle instead of decreasing the temperature of the particles inside the structure. Thereafter, the smaller molded parts i.e. the side layers to close the structure, have to be glued onto the larger structures. Glue these parts together is done

with Ecoflex 35, which has a pot life of 2.5 minutes and a cure time of five minutes. After waiting the cure time, the structures are complete. However, the initial state of the used particles are hard and very small when they are applied in the structure. Therefore, instead of considering this state as the initial state, water is injected with a needle inside the structures to soak the commercial particles. The particles will swell over time, resulting in a situation where the particles are approximately the same size as the chamber. This situation is considered to be the reference state, as visible in Figure 87. This will also be more efficient for a comparison with simulations in subsubsection 5.3.1 to reduce as well the calculation time as additional boundary conditions. As there is still water in the structures, the swelling will increase over time.

Figure 86: Molded structure including swelling particles.

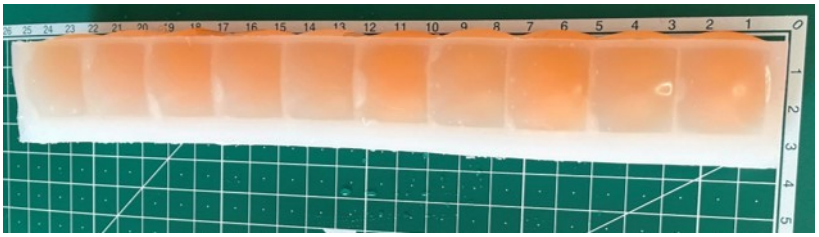

Figure 87: Straight demo structure on grid.

5.3.1 Comparison of the demos and simulations

As stated above, four different demos are manufactured. Simulations have to be compared with the demo structures to validate the novel actuator. The demos are four structures, each made out of Ecoflex 30 with a length of 10 particles without reinforcement. Therefore, these four structures are also simulated. A detailed view on the dimensions and parameters of each structure, which are exactly similar to the demos, is provided in subsection (1) of Appendix B. The full structures can be reconstructed by combining the relevant top parts (which is also a bottom) with the middle parts. As an example, to form the straight structure comparable with the red demo structure of Figure 92, for the top and the bottom Figure 88 is used, while for the middle Figure 89 is used. The dimensions in 3D are presented in Figure 90. However, in this figure the structure is waved, but the values are similar for a straight structure. For the behaviour of the hydrogel, the parameters as described in subsubsection 5.2.1 are used. For the structure materials, which are silicon's, a Neo-Hookean model is used to predict the hyperelastic material behaviour. As for the demos not the similar particles can be used as during simulation, only a comparison is made by determining the trend between all of the structures. The initial situation of the simulations, as presented in Figure 91, are comparable to the initial situation as the demos, as visible in Figure 87.

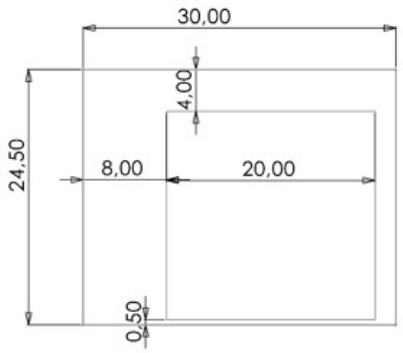

Figure 88: straight top.

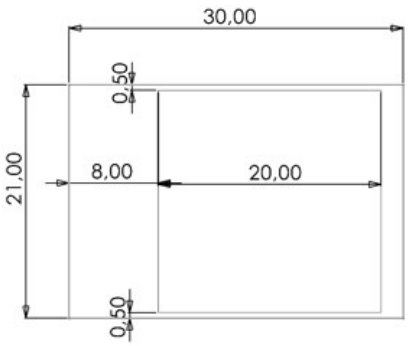

Figure 89: straight mid.

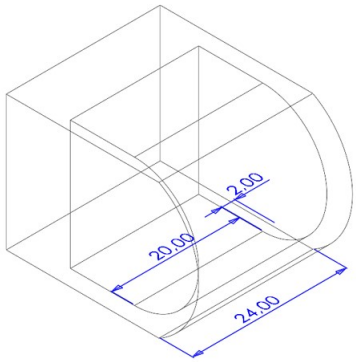

Figure 90: 3D no reinforcement.

The result of the structures after a couple of days of swelling is provided in Figure 92. As can be seen, the bending angle increases from left to right. Therefore, the trend of these geometry's from least to most bending is straight, waved, sharp and cylinder. More detailed figures of the structures on a grid can be found in Appendix D.

Figure 91: Initial situation of simulation.

Figure 92: From left to right: straight, waved, sharp, cylinder.

The results of the simulations of the demo structures are provided in Figure 93. The colors are associating the structures to the demo's presented in Figure 92. Comparing the demo structures with the simulations, a similar pattern is found. Despite the fact that other type of particle material, which swell in water and are temperature independent, were used for the hydrogel particles, a similar trend was found. Besides, as visible, the bending angle of each structure simulation are in the same order of the demo structures. The best performing structure is the cylinder shape, followed by a sharp and waved structure. Again, the straight structure was outperformed. Therefore, the novel actuator and the simulations are validated.

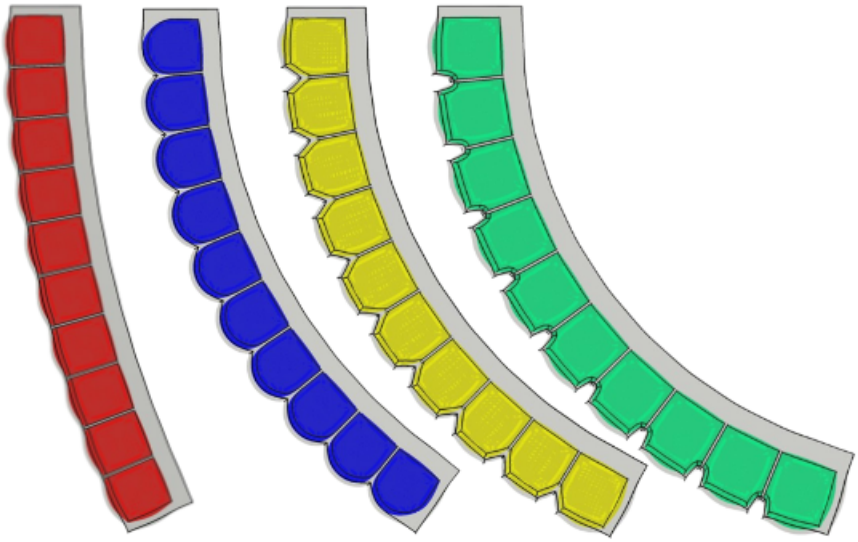

Figure 93: Simulation comparison of the bending performance (in degrees) of the demo structures. From left to right: straight (24.590), waved (54.415), sharp (62.172) and cylinder (71.806).

A more detailed view on this comparison is provided in Figure 94. The displacement relative to the origin in the horizontal and vertical direction is measured for 8 locations along the strain limiting layer of each structure for as well the demo structures as the simulations.

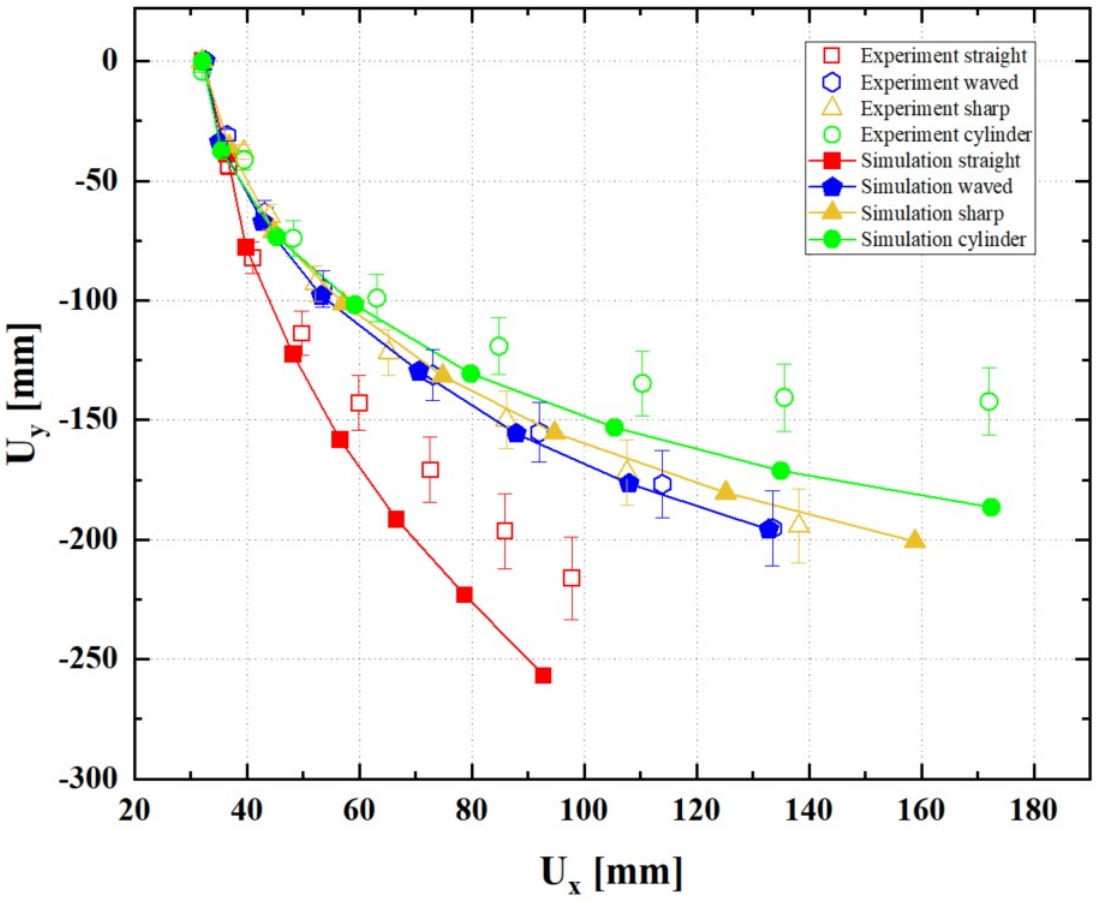

Figure 94: Comparison between simulations and experiments.

6 Design of the actuator

At first, many different relevant parameters of a soft gripper are considered. Additionally, a calibration is done to verify the expected behaviour of the simulations. From the relevant parameters, a selection of specific parameters will be selected and normalized to determine the parameters for the Design of Experience, which will be presented in section 7.

6.1 Potential influncial parameters

This subsection determines the factors which influences the bending performance. The bending performance of soft grippers can vary, as there are many different aspects which can influence this. Examples of relevant aspects are the length of the structure and the material. Therefore, a difference is made between two types of aspects which can affect the bending performance, which are structural parameters and material parameters.

6.1.1 Structural parameters

At first, a categorization can be made to define the difference between structures and their effect. The three different kind of categorizations in this report are *structural dimensions*, *structural geometry* and *structural properties*. The structural dimensions include the geometrical aspects such as the thickness of the strain limiting layer, the strain layer and the top and bottom of the structure. The second category is the structural geometry. The structure can have different shapes at the strain layer, for example straight or waved. Besides, the gap size is also included, which is the deepness of the gaps. The last category is the structural properties. This includes the effect of the amount of particles on the structure performance. These structural parameters can be as well dependent as independent on each other. As an example, when the length increases, the amount of particle increases. However, the amount of particles can be increased without increasing the length by instead of one large hydrogel ball multiple balls are considered. The overall categorization can be found in Table 5.

Category's		
Structural dimensions	Structural geometry	Structural properties
Strain layer	Shape	Particle layer
Strain limiting layer	Gap size	
Top layer		
Bottom layer		
Length		

Table 5: Structural parameter categorization.

After defining the relevant category's, a convenient way of application of these categorization on the structure can be determined. Therefore, Figure 95 is provided below to show the separation of the full structure into part A and B.

Part A represents the front part of the structure, which consists out of the strain limiting layer, the side layers and the top and bottom layer. This part can be considered to be relevant for only the structural dimensions. Part B can be considered as the back of the structure and is relevant for as well the structural dimensions as the structural geometry. In Figure 95 part B is shown as a simple straight shape. In Figure 99 - Figure 102 other shapes will be provided. The structure formed by part A and B combined will be considered to be relevant for the category structural properties, as now the particle layer can be defined.

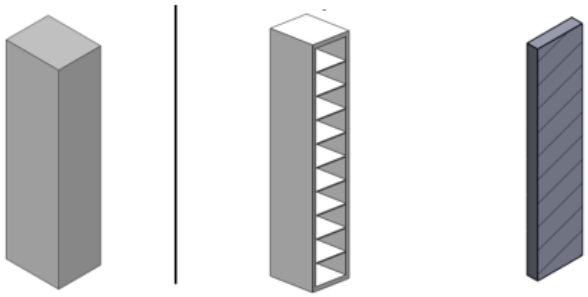

Figure 95: Part splitting in front and back part.

(1) Structural dimensions

The structural dimensions define the structure regarding wall thicknesses and lengths of the structure. For simplicity, in Figure 97 and Figure 98, the structural dimensions for a straight structure are presented. The structure can be cut in two different directions to obtain the relevant sectional views. The first cut can be done according to cutting plane 1 of Figure 96 resulting in Figure 97. As can be seen, the relevant parameters provided are the length (l), height (h), chamber height (c) and the thicknesses of the membrane (t_m), top (t_{top}), bottom (t_{bottom}), strain (t_s) and strain limiting (t_{sl}) layers. Besides this sectional view, Figure 98 can be provided by cutting the full structure according to plane 2 in Figure 96. In this view, the relevant dimensions provided are the length, width (w), chamber height (c) and the thicknesses of the membrane, top, bottom and side (t_{side}) layers.

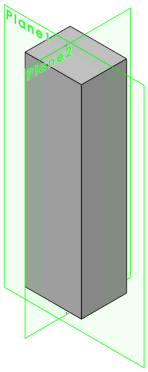

Figure 96: Cutting planes.

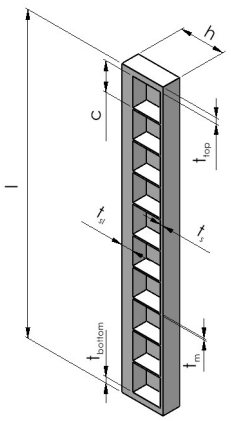

Figure 97: Sectional view 1 (cutting plane 1).

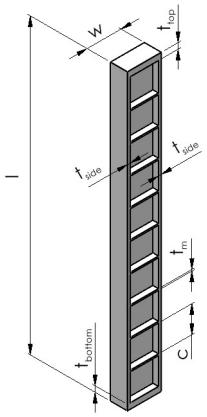

Figure 98: Sectional view (cutting plane 2).

(2) Structural geometry

The structural geometry is very important for the bending performance of soft grippers. At first, the shape of the structure is relevant. As can be seen in section 4, literature survey, many structures are either straight or waved. Logically can be expected that waved shapes structures can bend more, while straight structures will be more rigid. Different shapes are provided in Figure 99 - Figure 102. One important parameter is the gap size represented with the deepness of the gap (d_{gap}). An example can be found in Figure 103, where the gap size is indicated of a sharp structure as presented in Figure 101.

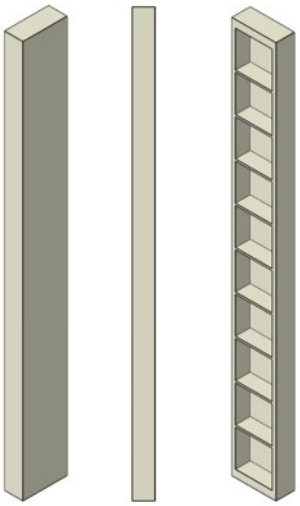

Figure 99: Straight geometry.

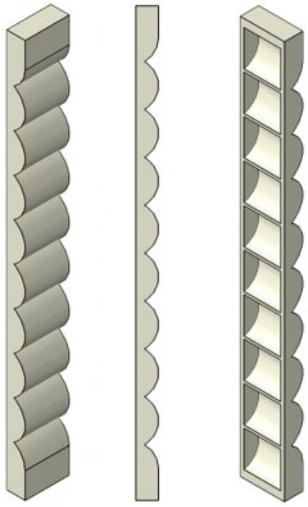

Figure 100: Waved geometry.

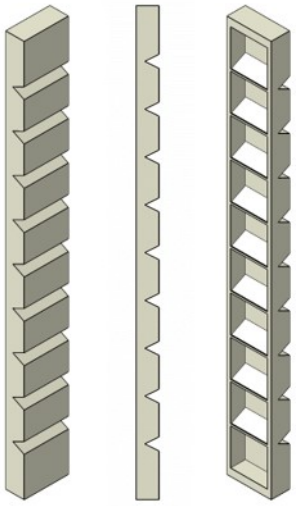

Figure 101: Sharp geometry.

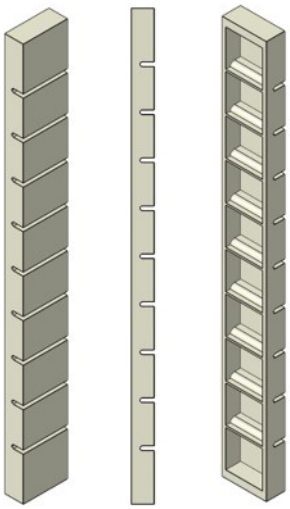

Figure 102: Cylinder geometry.

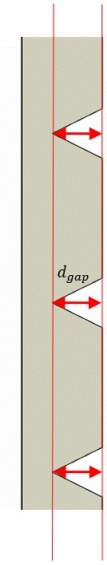

Figure 103: Deepness of the gap (gap size) indicated with d_{gap}.

(3) Structural properties

The structural properties can be represented with the particle layer. The particle layer can be adjusted, for example with the amount of particles. One can consider that each layer consists of only one particle. However, there is also an option to include more smaller particles instead of a single particle, as visible in Figure 104. A difference between these two options is, for example, that the structure of the soft gripper can be simplified when only one layer of particles is considered. In this situation, a structure can be made which easily encloses the single particle layer. However, when using only a single particle layer in a simple structure, there is a possibility that the corners are not filled by the particle. However, by decreasing the size of the particle and increasing the amount of particles, a more filled structure can be found. Besides, there is even a possibility to have a variety in particles properties or sizes.

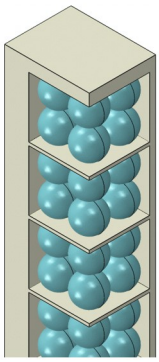

Figure 104: Chamber including multiple small particles instead of one large particle.

6.1.2 Material parameters

Besides the structural parameters, also material parameters are relevant. These material parameters influence the bending performance by the category's material properties and reinforcement.

Category's	
Material properties	Reinforcement
Structure material	External
Hydrogel material	Internal

Table 6: Categorization for material parameters.

(1) Material properties

The material of the structure is very important for fabricating a soft gripper. When the material is very stiff, the amount of bending will be small. On the other hand, the structure will be able to deliver a greater force. The material is not only relevant for the stiffness while designing a soft gripper. Also other considerations must be taken into account to find the right material. An example is that some materials are not suitable during some specific working conditions. Specific soft grippers can be applied in a hot/cold or dry/wet environment such as underwater for grabbing organisms, while other soft grippers have to be sterile in a medical environment as during operations. Dependent on the application, a specific material must be chosen.

Also the specifications of the hydrogel material are very important for the bending performance of soft grippers. There are multiple types of material which can be used, each having their own pros and cons. At first, the swelling/shrinking process has a certain ratio for each type of material. Dependent on for example the amount of bending, some specific materials can be used. For the same amount of particles, a higher swelling ratio will result in a higher amount of bending of the structure. However, also the stiffness of the hydrogel is important. For some applications of soft grippers more force is required. Therefore, if the hydrogel is stiffer, more force can be exerted by the structure. Another aspect of the material can be the temperature dependency. Some materials work at different temperature areas, which can be more suitable for specific working conditions.

(2) Structure reinforcements

The structure of the soft gripper can be enhanced, such that application during specific conditions is possible. An example can be given when the stiffness of the structure must be increased, such that the gripper can exert more force. To increase the stiffness, a reinforced material can be used. There can be made a difference between two types of reinforcement, which are external and internal reinforcements. An example of external reinforcement is cables of a stiffer material, like fibers, are applied around a pneumatic structure. As a result, material stretching in the radial direction will be reduced significantly or is even negligible. Therefore, more stretch will occur in the extension of the structure. Also internal reinforcement is possible. In this case, reinforcement of the strain

limiting layer is done with integration of a much stiffer layer i.e. a more rigid plate in the material. As a result, the strain limiting layer will stretch less. Dependent on the material of reinforcement, different configurations can occur. For example, by reinforcement of the strain limiting layer with paper which is flexible but does not stretch compared to the structure material, more bending can occur without much variation in stiffness. However, another example as when the reinforcement is a rigid plastic material, less bending can occur and the material can become significant stiffer. Another option is to make use of a stiffer material in the membrane between the hydrogel particles. However, there is not yet much known about this, therefore this has some potential for research. Dependent on the type of reinforcement, the bending performance can be influenced.

6.1.3 Calibration

As the relevant factors which influence the bending performance of soft grippers as stated above are many, a consideration must be made which factors are included in this research. At first, a couple of simulations are required for calibration of the initial simulations. Besides, some initial simulations are required to determine which and how certain factors will be tested. Additionally, after determination of the relevant factors, a normalization is required of this factors.

An initial set of simulations is done, to verify previous assumptions as above. The first simulation is to verify that a decreased thickness of the strain limiting layer decreases the amount of bending. In Figure 105, three different structures are provided. The red structure can be seen as a straight demo structure with a strain limiting layer thickness of 8 mm and a strain layer thickness of 2 mm. The blue structure is slightly different, as the thickness of the strain limiting layer is reduced. The thickness of the strain layer is the same as for the demo structure. Reducing the thickness of the strain limiting layer results in a decreased amount of bending. The third structure which is represented with the color pink has a strain limiting layer similar to the demo structure. However, the strain layer is in this case reduced. The result is an increase of the bending angle, as there will be more stretching at this side of the structure. The dimensions are provided in table Table 7.

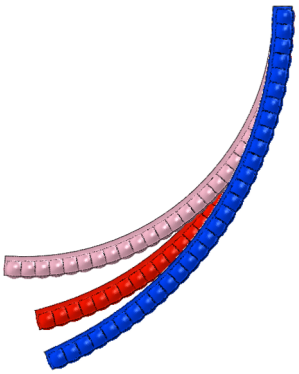

Figure 105: Comparison of different thicknesses of strain limiting layer and strain layer.

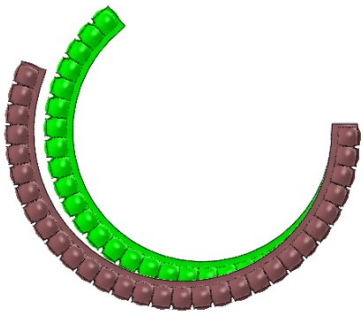

Figure 106: Comparison of different gap width's.

Structure color	Strain limiting layer [mm]	Strain layer [mm]
Red	8	2
Blue	6	2
Pink	8	1.5

Table 7: Overview relevant values for comparison of strain limiting layer and strain layer.

Additionally, a simulation was performed to compare a difference in gap width while maintaining the similar deepness of the gap. A comparison between the influence of the gap size of the cylinder shape is used for calibration. As visible in Table 8, a brown and green structure are

provided. The green structure is a demo structure, of which the gap size is provided in Table 8. The brown structure has a smaller gap width, resulting in a significant decrease in bending. This is as expected. Therefore, the simulations are calibrated according to expectation.

Structure color	Gap width [mm]
Brown	1
Green	2

Table 8: Overview of values of different gap width's for comparison.

6.2 Normalization

There are many factors which can influence the bending performance of the soft gripper. However, this research will be limited to determine the influence of length, material, reinforcement and geometry on the bending performance of soft grippers. At first, multiple sets of simulations are required to determine upper and lower bounds for the effect on the bending performance of soft grippers. These simulations will be used as the normalization for the DoE.

The first set of simulations normalizes the parameter length. A set of six simulations consisting out of the lengths 217, 427, 637, 847, 1057 and 1267 mm are considered. These length correspondents to a structure with respectively 10,20,30,40,50 and 60 hydrogel particles. The material (Ecoflex 30), reinforcement (none) and geometry (straight) were similar for each simulation, as can be seen in Table 10. The relevant parts which are used for these structures can be found in subsection (1) of Appendix B.

Secondly, the normalization of the material is determined by a simulation set of seven simulations. The used materials are Ecoflex 30, Ecoflex 50, Dragon Skin 10 Medium (hereafter known as Dragon Skin 10), Soloplast 150318, Mold Star 20T, Dragon Skin 20, Dragon Skin 30 and RTV 615. These materials are tested as these represent a wide variety of Neo-Hookean values, as visible in Table 9. As visible in Table 10 the length (10), reinforcement (none) and geometry (straight) of the structure were held constant for each simulation. The relevant parts which are used for these structures can be found in subsection (1) of Appendix B.

Material	Neo-Hookean
Ecoflex 30	$\mu = 0.03245$
Ecoflex 50	$\mu = 0.048176$
Dragon Skin 10	$\mu = 0.07888$
Soloplast 150318	$\mu = 0.12323$
Mold Star 20T	$\mu = 0.16984$
Dragon Skin 20	$\mu = 0.207047$
Dragon Skin 30	$\mu = 0.24203$
RTV 615	$\mu = 0.33861$

Table 9: Constitutive model parameters (expressed in MPa).

Thirdly, the reinforcement of the structure is normalized by using the options none, small or large for a set of three simulations. With reinforcement, the use of stiffer material between the particles is considered, as there is not yet any research done about this consideration by knowledge. As the reinforcement is none, the material between the particles is similar as the structure material. However, when a small or large reinforcement is considered, a small or large part of the material layer between the particles is made of the stiffer material. A material which is a factor of approximately 9245 stiffer is used for reinforcement. The differences can be seen in Figure 107, Figure 108 and Figure 109. As can be seen, the green part in the structures is the reinforcement. In Figure 107, no reinforcement is applied. In the second structure, Figure 108, a small reinforcement is applied. This is from the inside of the strain limiting layer up to half of the membrane between the particles. The third structure, Figure 109, includes the large reinforcement. This reinforcement is from the outside of the strain limiting layer up to half of the membrane between the particles. For these set of simulations, the length (10), the material (Ecoflex 30) and

the geometry (straight) are held constant, as presented in Table 10. The relevant parts which are used for these structures can be found in subsection (1), (2) and (3) of Appendix B.

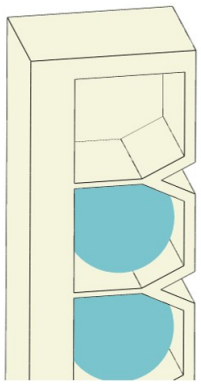

Figure 107: Sharp structure without reinforcement.

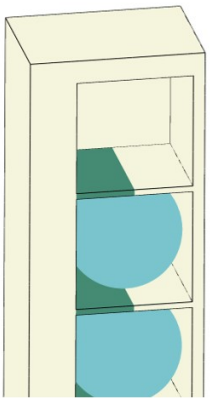

Figure 108: Straight structure with small reinforcement.

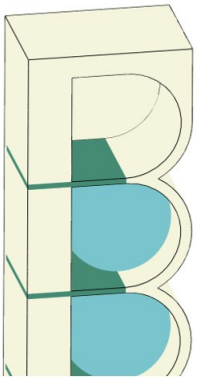

Figure 109: Waved structure with large reinforcement.

At last, for the shape of the structure the options straight, sharp, waved and cylinder, as presented in Figure 99 - Figure 102, are considered for a set of four simulations. The gap size of all of the structures is held constant at a certain distance of 6.20 mm. For the waved structure, the gap size is 6,19 mm. This difference can be neglected, as this is only 0.01 mm. As presented in Table 10 the length (10), material (Ecoflex 30) and reinforcement (none) are held constant. The relevant parts which are used for these structures can be found in subsection (1) of Appendix B. In Table 10, the full overview of simulations for the normalization is presented.

Length (hydrogel particles)	Material	Reinforcement	Geometry
10	Ecoflex 30	none	straight
20	Ecoflex 30	none	straight
30	Ecoflex 30	none	straight
40	Ecoflex 30	none	straight
50	Ecoflex 30	none	straight
60	Ecoflex 30	none	straight
10	Ecoflex 30	none	straight
10	Ecoflex 50	none	straight
10	Dragon Skin 10	none	straight
10	Soloplast 150318	none	straight
10	Mold Star 20T	none	straight
10	Dragon Skin 20	none	straight
10	Dragon Skin 30	none	straight
10	RTV 615	none	straight
10	Ecoflex 30	none	straight
10	Ecoflex 30	small	straight
10	Ecoflex 30	large	straight
10	Ecoflex 30	none	straight
10	Ecoflex 30	none	sharp
10	Ecoflex 30	none	waved
10	Ecoflex 30	none	cylinder

Table 10: Overview of simulations for normalization.

6.3 Results and discussion

After determination of the relevant parameters, simulations are done to normalize these parameters for the Design of Experiments. At first, the results of the normalization of the length are provided in Figure 110. As can be seen, increasing the length will result in more bending. Increasing the length from 10 to 20 particles result in a bending angle increasement of $\frac{50}{25} = 2$. However, the increasement of the bending angle is reducing as the amount of particles increases. For a increasement in length from 50 to 60 particles, the bending angle increases only by $\frac{152}{126} = 1.206$.

For the material, the results of the normalization are provided in Figure 111. The bending angle for the Ecoflex 30 and Ecoflex 50 are significantly different compared to the other materials. Consequently, all of the materials except for Ecoflex 30 and Ecoflex 50 are in the range of bending angle of 20.99 ± 0.33 degrees.

Reinforcement effects are provided in Figure 112. The bending angle of the structure has a minor difference between reinforcement or not. A maximum difference of 0.44 degrees can be found between no reinforcement and a large reinforcement.

The results of the normalization of the geometry's are provided in Figure 113. As visible, the most amount of bending can be achieved with a cylinder structure. After the cylinder structure, respectively the sharp and waved structures perform well. At last, the straight structure perform significantly less than the other structure shapes.

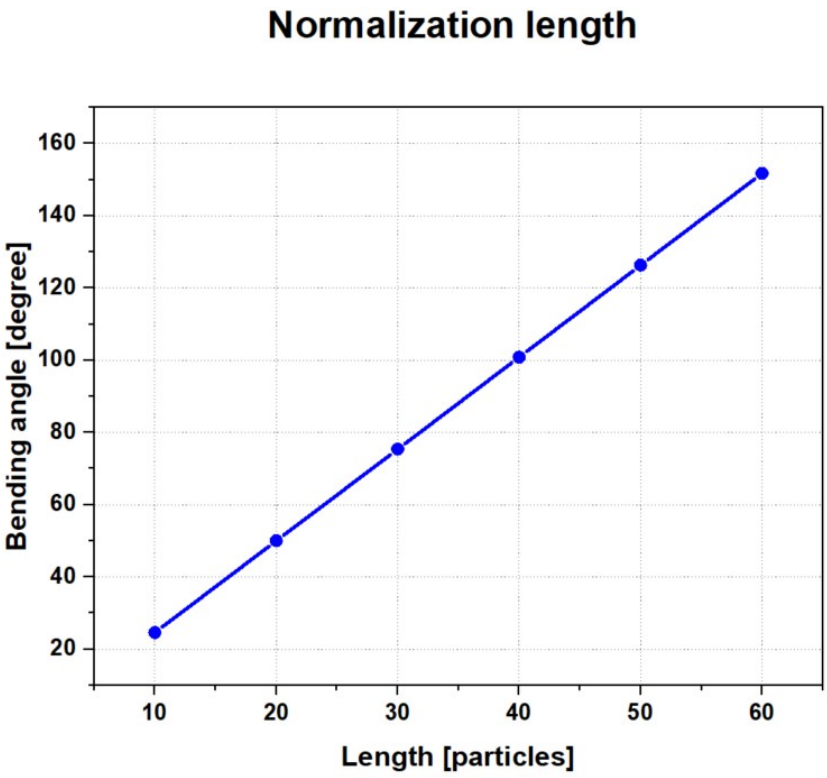

Figure 110: Normalization results for parameter length.

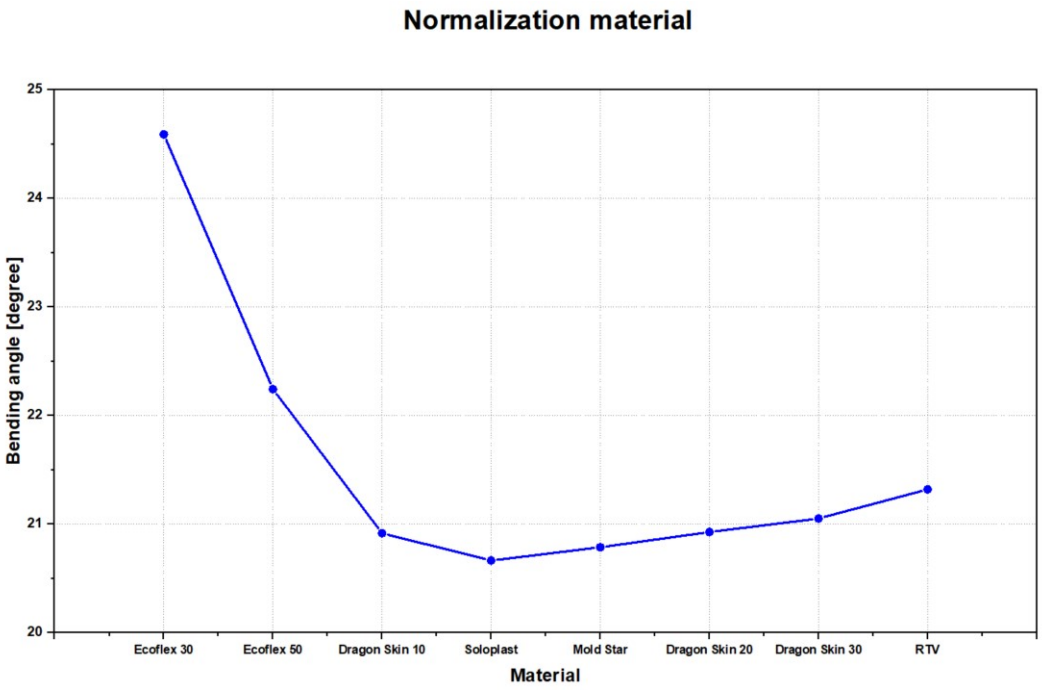

Figure 111: Normalization results for parameter material.

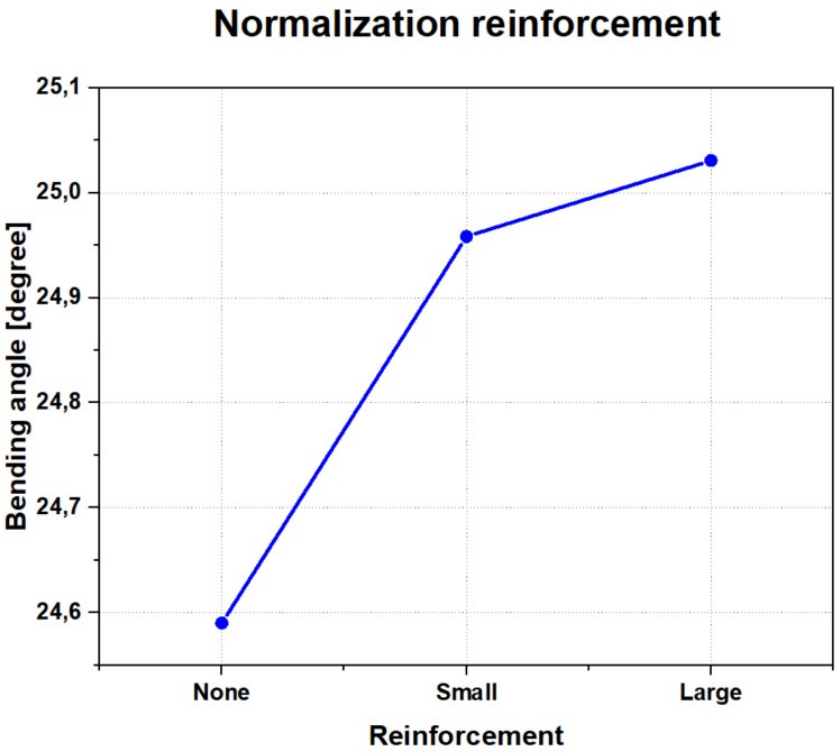

Figure 112: Normalization results for parameter reinforcement.

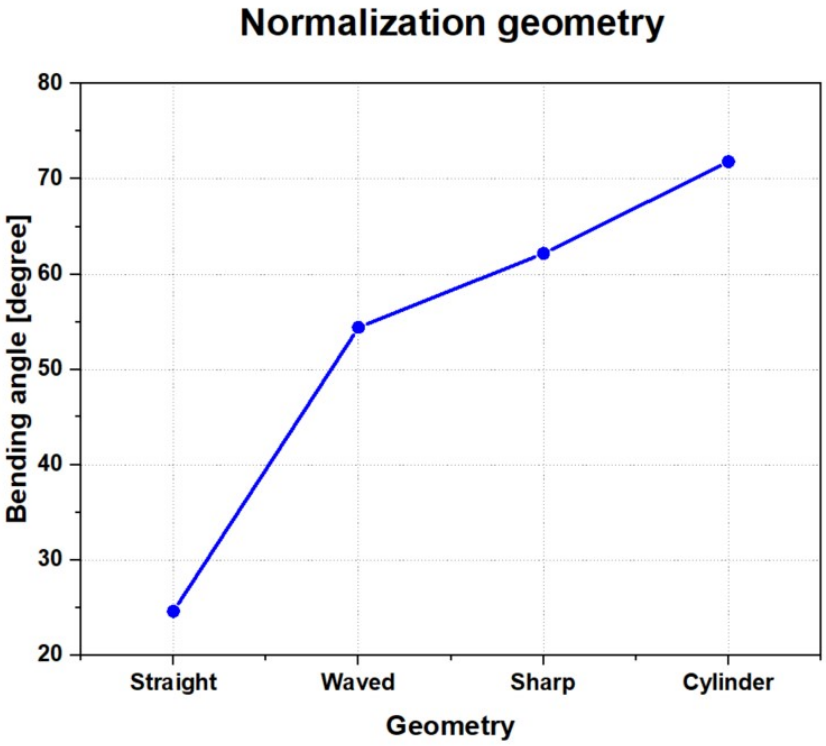

Figure 113: Normalization results for parameter geometry.

6.4 Conclusion

This chapter provides the relevant parameters for soft gripper structures. The relevant parameters investigated in this research are the length, shape, material and reinforcement of the membrane of the structures. At first, a normalization was done to determine the lower and upper bounds of the parameters. Increasing the length, result in an increased bending angle. For the geometry, the most amount of bending is achieved by the cylinder shape, followed by sharp, waved and straight respectively. However, the straight shape is significantly outperformed by the other structure shapes. For the material, Ecoflex 30 has the most amount of bending, followed by the Ecoflex 50. The other materials used were all of the same order. A small difference in the bending angle is found by applying a reinforcement in the membrane between the particles. However, according to the results, a large reinforcement increases the bending angle slightly.

After normalization, a full factorial DoE will be carried out. Therefore, specific values for the parameters must be selected. The values for the DoE of the parameter length will be 10, 30 and 50 particles. The bending angle for these values are significant difference of each other. For the material, Ecoflex 30, Ecoflex 50 and Dragon Skin 10 are considered, as the bending angle is relatively different of each other. Also, the bending angle of Dragon Skin 10 is in the order of the other used materials. Additionally, these materials are common for soft grippers and easy of use for fabrication. The parameter of reinforcement showed a minor effect on the bending performance. However, for larger structures the effect may be increased. As the difference in bending between small and large reinforcement is almost negligible, only no and large reinforcements will be included in the DoE. The geometry's selected for the DoE are straight, waved and cylinder. straight is considered to be a reference case. Waved and sharp are not significantly different in amount of bending, while cylinder outperforms all off the structures.

7 Design of Experiments

In this chapter, a full factorial DoE will be done to determine the influence of each individual parameter on the bending performance. The aim is to find the optimal structure configuration to obtain the maximum amount of bending. Therefore, obtaining an insight in the main effects and the interaction between multiple parameters can be very useful. At last, a simulation of a potential soft gripper will be provided to present a working concept for further research.

7.1 Design of Experiments

After normalizing the relevant factors for this research, a DoE can be presented. As visible in Figure 112, there is not much difference in bending angle between small and large reinforcement. However, for the other parameters, there is significance difference. Therefore, a full factorial design is proposed consisting out of 4 factors with 3 levels, except for the reinforcement which has 2 levels. This results in a total of $3 \times 3 \times 2 \times 3 = 54$ simulations. The levels of each parameter are provided in Table 11, where level 1 is the lower level, 2 the middle level and 3 the upper level.

Level	Parameter			
	Length	Material	Reinforcement	Geometry
1	10	Ecoflex 30	none	straight
2	30	Ecoflex 50	large	waved
3	50	Dragon Skin 10		cylinder

Table 11: Overview DoE parameters and levels.

From Table 11, the total list of DoE can be constructed and is presented in Table 12. The total amount of simulations are divided in sets of 3. The differences between each set is a single factor at a time, except for the geometry, of which each level is included in each set. As a result, the sets consisting of each geometry vary in length, material and reinforcement. Therefore, a total of $3 \times 3 \times 2 = 18$ sets are considered. The sets and simulations are named according to their properties. Therefore, the name is according to the principle *length-material-reinforcement-geometry*. For the first simulation, the name 10-eco30-0-straight represents a structure consisting out of respectively length 10, the material Ecoflex 30, no reinforcement and a straight geometry. The relevant parts which are used for these structures can be found in subsection (1) and (3) of Appendix B.

Set	Simulation	Length	Material	Reinforcement	Geometry
10-eco30-none-s/w/c	10-eco30-0-straight	10	Ecoflex 30	0	straight
	10-eco30-0-waved	10	Ecoflex 30	0	waved
	10-eco30-0-cylinder	10	Ecoflex 30	0	cylinder
10-eco30-1-s/w/c	10-eco30-1-straight	10	Ecoflex 30	large	straight
	10-eco30-1-waved	10	Ecoflex 30	large	waved
	10-eco30-1-cylinder	10	Ecoflex 30	large	cylinder
10-eco50-none-s/w/c	10-eco50-0-straight	10	Ecoflex 50	0	straight
	10-eco50-0-waved	10	Ecoflex 50	0	waved
	10-eco50-0-cylinder	10	Ecoflex 50	0	cylinder
10-eco50-1-s/w/c	10-eco50-1-straight	10	Ecoflex 50	large	straight
	10-eco50-1-waved	10	Ecoflex 50	large	waved
	10-eco50-1-cylinder	10	Ecoflex 50	large	cylinder
10-dragon10-none-s/w/c	10-dragon10-0-straight	10	Dragon Skin 10	0	straight
	10-dragon10-0-waved	10	Dragon Skin 10	0	waved
	10-dragon10-0-cylinder	10	Dragon Skin 10	0	cylinder
10-dragon10-1-s/w/c	10-dragon10-1-straight	10	Dragon Skin 10	large	straight
	10-dragon10-1-waved	10	Dragon Skin 10	large	waved
	10-dragon10-1-cylinder	10	Dragon Skin 10	large	cylinder
30-eco30-none-s/w/c	30-eco30-0-straight	30	Ecoflex 30	0	straight
	30-eco30-0-waved	30	Ecoflex 30	0	waved
	30-eco30-0-cylinder	30	Ecoflex 30	0	cylinder
30-eco30-1-s/w/c	30-eco30-1-straight	30	Ecoflex 30	large	straight
	30-eco30-1-waved	30	Ecoflex 30	large	waved
	30-eco30-1-cylinder	30	Ecoflex 30	large	cylinder
30-eco50-none-s/w/c	30-eco50-0-straight	30	Ecoflex 50	0	straight
	30-eco50-0-waved	30	Ecoflex 50	0	waved
	30-eco50-0-cylinder	30	Ecoflex 50	0	cylinder
30-eco50-1-s/w/c	30-eco50-1-straight	30	Ecoflex 50	large	straight
	30-eco50-1-waved	30	Ecoflex 50	large	waved
	30-eco50-1-cylinder	30	Ecoflex 50	large	cylinder
30-dragon10-none-s/w/c	30-dragon10-0-straight	30	Dragon Skin 10	0	straight
	30-dragon10-0-waved	30	Dragon Skin 10	0	waved
	30-dragon10-0-cylinder	30	Dragon Skin 10	0	cylinder
30-dragon10-1-s/w/c	30-dragon10-1-straight	30	Dragon Skin 10	large	straight
	30-dragon10-1-waved	30	Dragon Skin 10	large	waved
	30-dragon10-1-cylinder	30	Dragon Skin 10	large	cylinder
50-eco30-none-s/w/c	50-eco30-0-straight	50	Ecoflex 30	0	straight
	50-eco30-0-waved	50	Ecoflex 30	0	waved
	50-eco30-0-cylinder	50	Ecoflex 30	0	cylinder
50-eco30-1-s/w/c	50-eco30-1-straight	50	Ecoflex 30	large	straight
	50-eco30-1-waved	50	Ecoflex 30	large	waved
	50-eco30-1-cylinder	50	Ecoflex 30	large	cylinder
50-eco50-none-s/w/c	50-eco50-0-straight	50	Ecoflex 50	0	straight
	50-eco50-0-waved	50	Ecoflex 50	0	waved
	50-eco50-0-cylinder	50	Ecoflex 50	0	cylinder
50-eco50-1-s/w/c	50-eco50-1-straight	50	Ecoflex 50	large	straight
	50-eco50-1-waved	50	Ecoflex 50	large	waved
	50-eco50-1-cylinder	50	Ecoflex 50	large	cylinder
50-dragon10-none-s/w/c	50-dragon10-0-straight	50	Dragon Skin 10	0	straight
	50-dragon10-0-waved	50	Dragon Skin 10	0	waved
	50-dragon10-0-cylinder	50	Dragon Skin 10	0	cylinder
50-dragon10-1-s/w/c	50-dragon10-1-straight	50	Dragon Skin 10	large	straight
	50-dragon10-1-waved	50	Dragon Skin 10	large	waved
	50-dragon10-1-cylinder	50	Dragon Skin 10	large	cylinder

Table 12: Overview simulations for Design of Experiments.

7.2 Results and discussion

The results of the simulations carried out from the DoE are provided below in Table 13. In the third column, the bending angle is presented. The bending angle is measured as the clockwise rotation of the normal to the bottom layer between the initial position and the end position, as visible in Figure 114.

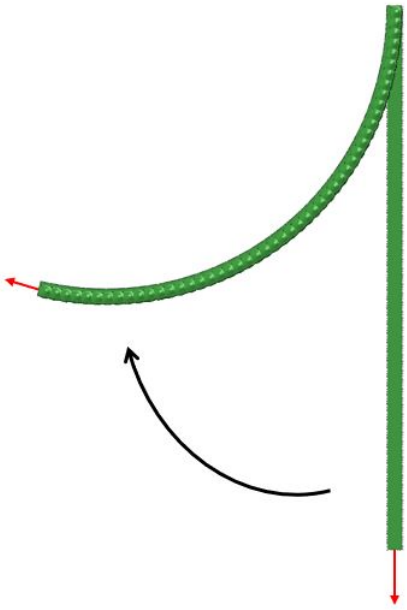

Figure 114: Measuring the bending performance.

Set	Name	Bending angle
10-eco30-none-s/w/c	10-eco30-0-straight	24,590227
	10-eco30-0-waved	54,415198
	10-eco30-0-cylinder	71,805963
10-eco30-1-s/w/c	10-eco30-1-straight	25,030588
	10-eco30-1-waved	53,413724
	10-eco30-1-cylinder	70,824654
10-eco50-none-s/w/c	10-eco50-0-straight	22,243343
	10-eco50-0-waved	47,527014
	10-eco50-0-cylinder	62,171501
10-eco50-1-s/w/c	10-eco50-1-straight	21,783724
	10-eco50-1-waved	44,674087
	10-eco50-1-cylinder	59,679622
10-dragon10-none-s/w/c	10-dragon10-0-straight	20,916308
	10-dragon10-0-waved	41,218892
	10-dragon10-0-cylinder	52,97471
10-dragon10-1-s/w/c	10-dragon10-1-straight	19,418981
	10-dragon10-1-waved	36,408795
	10-dragon10-1-cylinder	48,633833
30-eco30-none-s/w/c	30-eco30-0-straight	75,400270
	30-eco30-0-waved	169,199584
	30-eco30-0-cylinder	225,913391
30-eco30-1-s/w/c	30-eco30-1-straight	76,331071
	30-eco30-1-waved	167,018152
	30-eco30-1-cylinder	223,821837
30-eco50-none-s/w/c	30-eco50-0-straight	68,169068
	30-eco50-0-waved	147,98532
	30-eco50-0-cylinder	195,474216
30-eco50-1-s/w/c	30-eco50-1-straight	66,018543
	30-eco50-1-waved	139,715721
	30-eco50-1-cylinder	188,324634
30-dragon10-none-s/w/c	30-dragon10-0-straight	63,999223
	30-dragon10-0-waved	128,486605
	30-dragon10-0-cylinder	166,264222
30-dragon10-1-s/w/c	30-dragon10-1-straight	58,341711
	30-dragon10-1-waved	113,764473
	30-dragon10-1-cylinder	152,919778
50-eco30-none-s/w/c	50-eco30-0-straight	126,329756
	50-eco30-0-waved	284,042098
	50-eco30-0-cylinder	360
50-eco30-1-s/w/c	50-eco30-1-straight	129,40068
	50-eco30-1-waved	280,606295
	50-eco30-1-cylinder	359,676015
50-eco50-none-s/w/c	50-eco50-0-straight	109,692024
	50-eco50-0-waved	248,469669
	50-eco50-0-cylinder	329,040467
50-eco50-1-s/w/c	50-eco50-1-straight	112,476887
	50-eco50-1-waved	234,709771
	50-eco50-1-cylinder	316,854033
50-dragon10-none-s/w/c	50-dragon10-0-straight	102,510859
	50-dragon10-0-waved	215,757199
	50-dragon10-0-cylinder	279,785363
50-dragon10-1-s/w/c	50-dragon10-1-straight	99,86966
	50-dragon10-1-waved	191,043037
	50-dragon10-1-cylinder	257,127161

Table 13: Overview Design of Experiments results.

In Figure 115,Figure 116 and Figure 117 a comparison is provided for the bending angle between all of the structures of the same length, respectively for lengths 10, 30 and 50. The results are presented by the different materials and geometry's, with and without reinforcement.

Firstly, there is a significant difference in the resulting bending angle between the different geometry's. In all of the figures, the largest bending angle for each material is achieved with a cylindrical geometry, followed by the waved structure and with the smallest bending angle the straight geometry.

Secondly, the largest bending angle for each structure can be reached with Ecoflex 30. By looking at the slope, a variation of the material has the most influence on the cylindrical geometry's. The variation of material has less effect on the waved geometry's and an even smaller effect on the straight structures.

Thirdly, what is noticeable, is that for Ecoflex 30 all of the geometry's the amount of bending is comparable between with and without reinforcement. However, for the straight structures, by applying reinforcement the amount of bending increases in contrast to the waved and cylinder structures. For Ecoflex 50 the bending angle decreases with reinforcement for all of the structures of each length, except for the straight structure with a length of 50 particles. For this situation, the bending angle increases slightly. For Dragon Skin 10, the reinforcement decreases the bending angle for all of the structures.

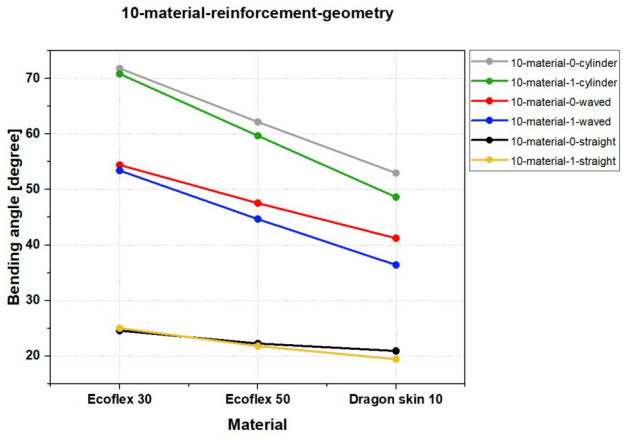

Figure 115: Visualization results of Design of Experiments for structures of length 10.

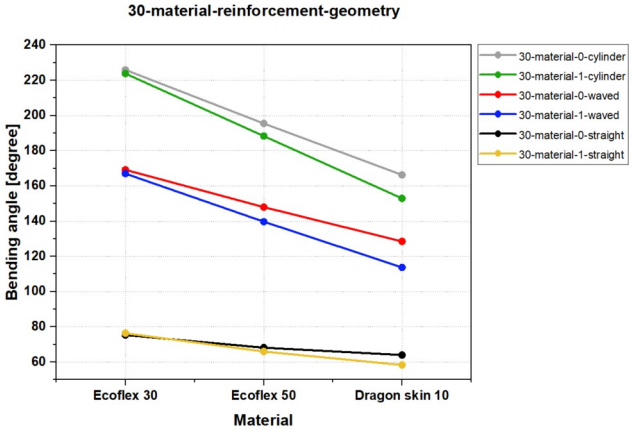

Figure 116: Visualization results of Design of Experiments for structures of length 30.

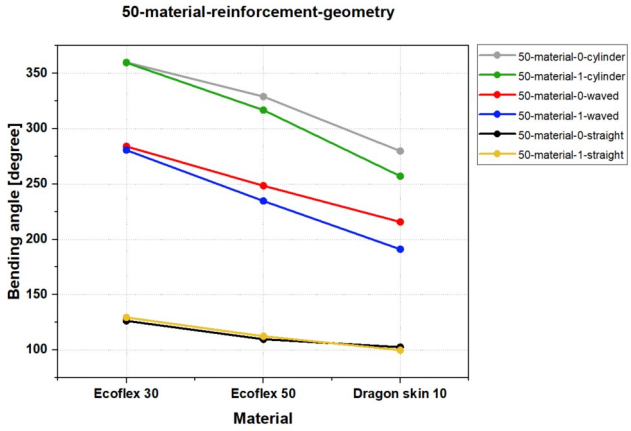

Figure 117: Visualization results of Design of Experiments for structures of length 50.

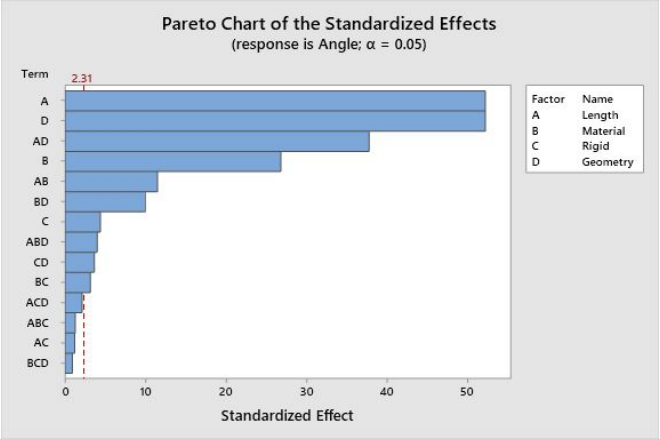

Figure 118: Pareto chart.

Another visual representation is a Pareto chart of the standardized effects, see Figure 118. In

this chart, the influence of the parameters on the bending angle are presented. As visible, the parameters length, material and geometry have the most influence on the bending angle, followed by the interaction of length and geometry. Material has a smaller effect, but still noticeable. The other parameters and interactions have less effect on the bending angle.

Besides a Pareto chart, a main effect plot, see Figure 119, is provided. This plot provides the information of which factor has the most influence on the bending angle of the structures. In this figure, the mean of the bending angle is plotted against each level of the factors length, material, reinforcement and geometry. The larger the slope, the more influence a parameter has on the result. Therefore, the factor length has the largest effect on the bending angle of the structures. However, the geometry has a significant effect too. The material has a smaller effect, and the effect of the reinforcement is minor and almost negligible.

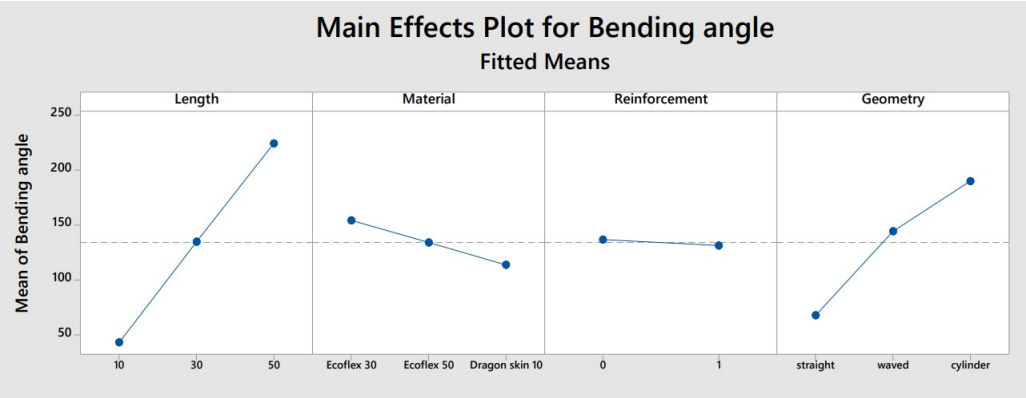

Figure 119: Main effect plot for parameters length, material, reinforcement and geometry.

Additionally, an interaction plot is presented in Figure 120. From this figure, it can be seen that the most interaction occurs between *length and geometry*, as the angle between the lines is the largest. There is less interaction between *length and material* and *material and geometry*. The interaction between *length and reinforcement*, *material and reinforcement* and *reinforcement and geometry* can be considered as minor or no interaction.

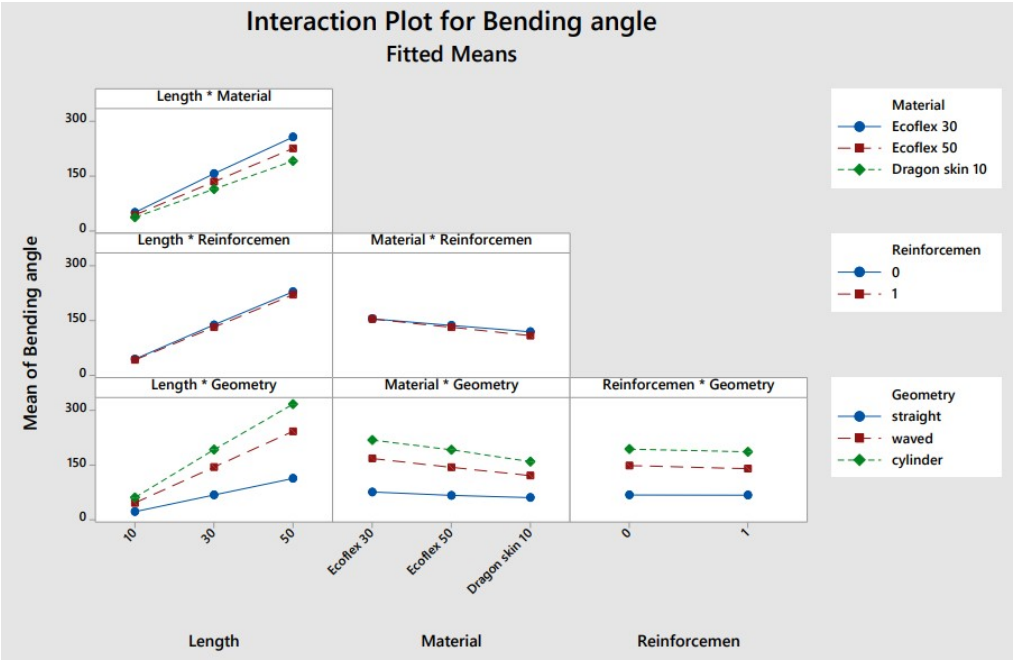

Figure 120: Interaction plot for parameters length, material, reinforcement and geometry.

7.3 Potential application

As this research is only a small contribution to the large field of soft grippers, a potential application is provided. According to the results, a promising structure for a relative large amount of bending for a small temperature difference consists out of a Ecoflex 30 cylindrical geometry without reinforcement. This structure has relatively the most amount of bending per Kelvin. Therefore, this structure would be suitable for further research on an improved structure of the novel actuator provided in this research: a multi segmented soft gripper. A multi segmented gripper would be very beneficial for, for example, objects with a varying shape. As there can be object with an odd shape, for example the object in Figure 121, multi segmented soft grippers are able to handle these objects. The principal of multi segmented grippers is based on segments which can perform independently and therefore the whole structure can adapt itself to a required configuration to grab odd shaped objects. Additionally, by using multi segmented soft grippers, a difference in material can be used for specific segments. For example, the material of the last segment can be different as this part needs less bending and more stiffness.

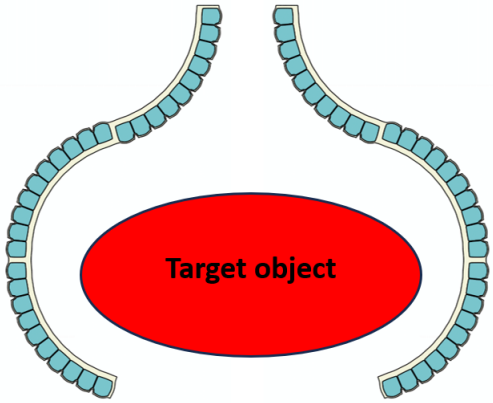

Figure 121: Adaptive soft gripper based on multiple segments.

A simulation is provided in different steps in Figure 122 - Figure 125. The figures are in 2D to simplify the working principle. In Figure 122, the initial position of the structure is provided. The structure consists out of two structures, each having a length of 30 particles i.e. 651 mm. The material used is Ecoflex 30. The structures are both divided into three segments, which are characterized with a thick layer of 8 mm between each segment. All of the three segments have a cylinder geometry as presented in this report. The orientation of the first segment (upper) is the opposite of the second (middle) and third (lower) segments. Each segment contains 10 thermoresponsive hydrogel particles. The properties of the hydrogel particles are similar as the properties used in this research, see subsubsection 5.2.1. As can be seen, the structure is initially at rest and perfectly vertical. By decreasing the temperature of the first segment from 305 K to 280 K, the structures will bend outwards by swelling of the hydrogel particles, presented in green particles in Figure 123. Now, the gripper can approach the object and the grippers will be on each side of the object. The second step of the simulation is provided in Figure 124, where the temperature of the second segment is reduced. The hydrogel particles in the second segment will swell, resulting in a bending toward the object. The grippers are now alongside the object. At last, the final step is presented in Figure 125 where grabbing the object is done by decreasing the temperature of the last segment, resulting in swelling of the particles in this segment. The gripper is now able to grab the odd shaped target object. Reconfiguration of the segments will result in other grabbing shapes. Therefore, in Figure 126(a), Figure 126(b) and Figure 126(c) are different combinations of segments provided.

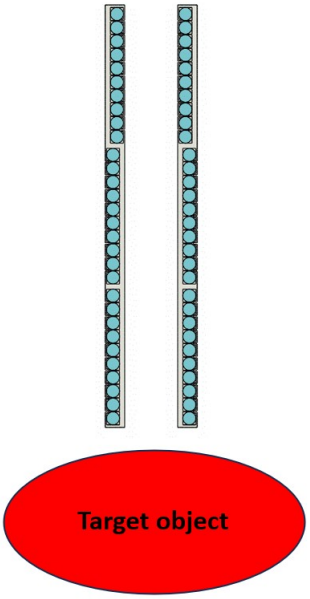

Figure 122: Initial position: gripper is in rest. No segments are actuated.

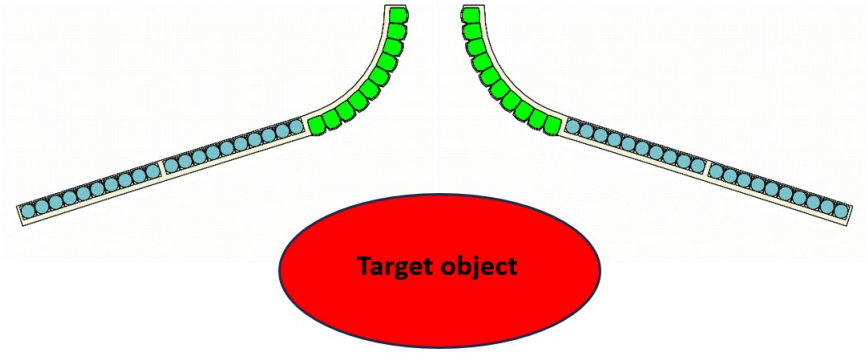

Figure 123: Step 1: gripper opens and approaches target object. Segment 1 is actuated.

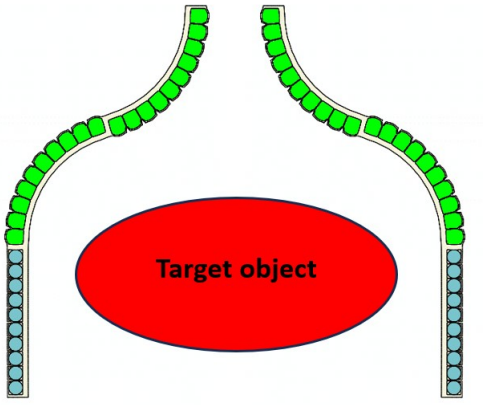

Figure 124: Step 2: gripper bends towards the target object. Segment 2 is actuated.

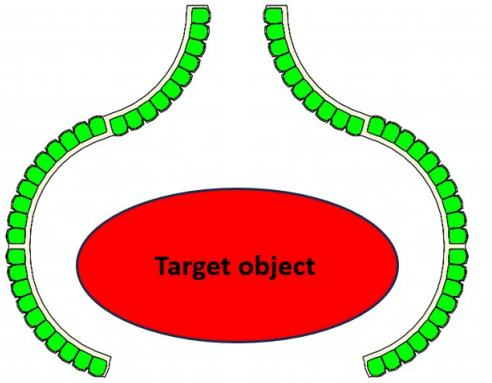

Figure 125: Step 3: gripper encloses target object. Segment 3 is actuated.

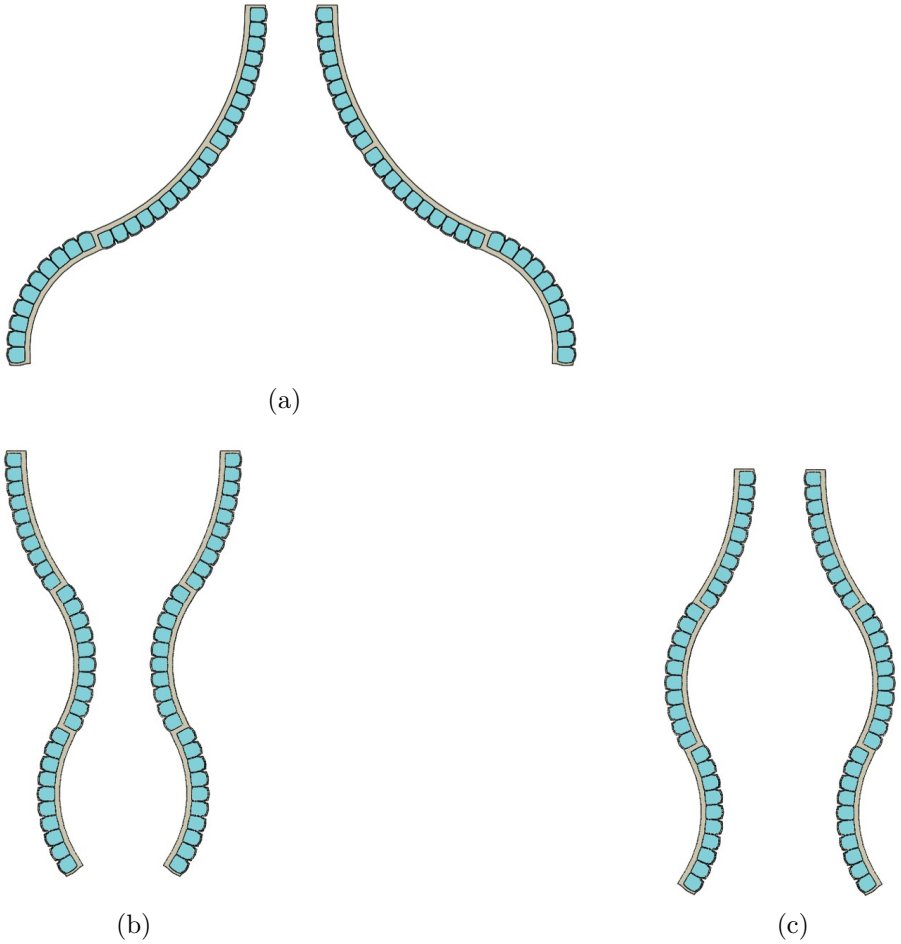

Figure 126: Different configurations as multi segmented adaptive soft gripper. (a) outward-outward-inward, (b) inward-outward-inward and (c) outward-inward-outward.

7.4 Conclusion

In this chapter, a full factorial Design of Experiments is provided. In total, 54 simulations are performed. The amount of tested influential parameters is four, which are length, material, reinforcement and geometry. From these parameters, length, material and geometry are considered to have 3 levels, while reinforcement has only two levels. As a result, 18 sets of three simulations are formed. Each set is based on a specific length, material and reinforcement of the structures, with a variation in the geometry. A table with all of the results of the sets are provided. Plots of the results are presented and analysed. For each length (10/30/50), a similar pattern can be found. The best performing combination is an Ecoflex 30 structure of 50 particles with a cylinder geometry without reinforcements. This structure can form a full circle with the smallest temperature difference. In general, structures without reinforcement outperform structures with reinforcement. Additionally, mainly the cylinder shaped geometry's are outperforming the other structures. However, waved structures of Ecoflex 30 can be considered to perform as well as the worst performed cylinder structure, which is made of Dragon Skin 10.

A Pareto chart and the main effect plots are provided, which presents that the parameters length and geometry have the most influence on the bending performance. Following these parameters, the next most influence is exerted by the interaction effect of length and geometry. The main effect of material and reinforcement are respectively small and minor i.e. negligible. The interaction plots confirms that most of the interaction is between the parameters length and geometry and therefore have a significant effect on the bending performance.

A potential application is provided, where a soft gripper is presented consisting out of two

structures. Both of the structures have the cylinder geometry, as these can provide the most bending. Dividing the structures in multiple segments means that specific segments, in this research the first, can be mirrored, resulting in that as well bending inwards as outwards is achieved. As a result, the soft gripper is now able to bend outwards at first by decreasing the temperature of the hydrogel particles in the first segment to approach the object. Thereafter, the gripper can use the other segments to enclose the object and grab it. Due to these segments, the gripper can be configured to the required shape.

8 Conclusion and future work

At the beginning of this report in section 3, the main and sub research questions are provided. The main research question is ***How to develop a simulation to determine the effect of specific parameters on the bending performance of soft grippers actuated by thermoresponsive hydrogel?***. Therefore, at first sub research question *What is the state of the art of smart materials and soft grippers?* is answered by section 4, where an extensive literature research is done. The focus of this literature research was on smart materials and soft grippers. However, smart materials is narrowed down to shape memory materials and hydrogels, as shape memory materials and electroactive polymers, which can also be applied as hydrogel, are the most used smart materials. Hydrogels is considered as this is part of the novel actuator. A gap resulting from the literature survey showed that soft gripper actuation by thermoresponsive hydrogels is a minor field and this research can contribute to this potential field.

In section 5 the novel actuator is presented to answer the sub research question *What is the novel design for soft grippers actuated by thermoresponsive hydrogel?*. A conceptual design is provided including a structure filled with thermoresponsive hydrogel particles. By decreasing the temperature, the hydrogel particles will swell and the structure will bend due to heterogeneous stretching of the structure. Additionally, to answer the sub research question *How to simulate thermoresponsive hydrogel?*, a research is done on the mathematics to implement thermoresponsive hydrogel in simulations. A subroutine file is used to represent the behaviour of thermoresponsive hydrogel. A validation with the literature is done, which confirms that the designed simulation performs as expected. Additionally, demos are fabricated and compared with simulations of similar structures. The demos consists out of four similar structures, regarding material, length and reinforcement, with only a variation in the geometry shape. The comparison between the demos and the simulations presented the same pattern. The pattern shows that cylinder shape has the best bending performance, followed by sharp and waved. The straight structure has the least amount of bending.

section 5 and section 6 answers the sub research questions *what are the relevant parameters and what is their effect on the bending performance of soft grippers?* and *How can the novel design be applied as a soft gripper?*. At first the relevant parameters for soft grippers is determined. A calibration is done to determine whether the simulations behave as expected. From the relevant parameters, a selection is made for this research of which the influence will be determined. These parameters are length, material, geometry and reinforcement of the structure. A normalization is done to determine the lower and upper bounds for the Design of Experiments. The Design of Experiments can be formed from the normalization. For the length, the values 10,30 and 50 particles are considered. The material used is Ecoflex 30, Ecoflex 50 or Dragon Skin 10. The geometry of the structures are straight, cylinder or waved. Either a large reinforcement is included or no reinforcement at all. As shown in the results in section 7, the structure with the most amount of bending is a structure of 50 particles made of Ecoflex 30 with a cylinder geometry without any reinforcement. This structure can form a full circle. In general, structures without reinforcement outperform structures with reinforcement. Additionally, mainly the cylinder shaped geometry's are outperforming the other structures. However, waved structures of Ecoflex 30 can be considered to perform as well as the worst performed cylinder structure, which is made of Dragon Skin 10. A Pareto chart and main effect plots provides which parameter has the main effect on the structure. The main effects on the bending performance are exerted by the length and the geometry. The material has a less effect, while the reinforcement has a minor effect. The interaction plots provided that interaction between the length and the geometry is the highest.

Additionally, a potential application of a soft gripper is presented to answer the sub research question *How can the novel principle be applied as a soft gripper?*. A soft gripper formed by two structures consisting out of multiple (mirrored) segments results in a gripper which can bend as well outwards as inwards. Therefore, this soft gripper is able to open by actuating specific segments to approach the target object and enclose the object by actuating other specific segments. Different steps of a simulation is provided to give a visible representation of this soft gripper's performance.

For future work, when a simulation of a potential soft gripper is finished, the soft grippers must be made and tested. Testing of the structures is important, as in these simulations external forces e.g. gravity are neglected. Besides, the structures are only simulated to see the difference in the amount of bending and not to determine the force which can be exerted. As stated in chapter subsubsection 4.2.7, the main characteristics are the amount of bending and the force exerted by the gripper. Therefore, the focus is on measuring these properties. The top of the structure can be fixed to a rigid plate. A camera can be used from the side, similar to the measurements as in Figure 59. By including a dark black background, the structures can easily be extracted from the pictures. From this extraction, the bending angle can be measured with a simple software. The exerted force of the structures can be measured with an accurate force sensors, similar as for example in Figure 64. The structures are fixed to a rigid plate. Then, by decreasing the temperature, the hydrogel particles will increase in diameter, resulting in bending and therefore exerting force on the sensor. Additionally, the test as presented in Figure 67 can be executed to determine the rotational stiffness.

All in all, the main research question ***How to develop a simulation to determine the effect of specific parameters on the bending performance of soft grippers actuated by thermoresponsive hydrogel?*** is now answered by answering the sub research questions. It is shown which factors are considered and how these affects the bending performance. Additionally, demos are compared to validate the simulations. The most influence on the bending performance is acted out by the length, followed by the geometry. Therefore, longer structures with a cylinder geometry are suitable for a large bending angle with a smaller temperature difference. Also, it is shown that reinforcement of a membrane between particles has a negligible contribution to the bending performance.

This research has ended with a simulation which provides the novel actuator design as a basis for the working principle of soft grippers actuated with thermoresponsive particles. By considering the demo structures, the stiffness of the system does not seem to be high enough for grabbing objects. Also, the simulation did not take any forces into account to see the pure influence on the bending performance. Additionally, in simulations the temperature of the hydrogel particles can be adjusted manually. A method is required to adjust the hydrogel temperature in real structures. Therefore, it can be stated that still a lot of research is required before this novel potential approach can be applied as a fully working soft gripper.

References

[1] Kevin Tai, Abdul-Rahman El-Sayed, Mohammadali Shahriari, Mohammad Biglarbegian, and Shohel Mahmud. "State of the Art Robotic Grippers and Applications". In: *Robotics* 5.2 (2016), p. 11. DOI: 10.3390/robotics5020011.

[2] B. Siciliano and O. Khatib. In: *Springer Handbook of Robotics* (2008). DOI: 10.1007/978-3-540-30301-5.

[3] Gareth J. Monkman, Stefan Hesse, Ralf Steinmann, and Henrik Schunk. In: *Robot grippers* (2006). DOI: 10.1002/9783527610280.

[4] J. Krüger, T.K. Lien, and A. Verl. "Cooperation of human and machines in Assembly Lines". In: *CIRP Annals* 58.2 (2009), pp. 628–646. DOI: 10.1016/j.cirp.2009.09.009.

[5] Sangbae Kim, Cecilia Laschi, and Barry Trimmer. "Soft robotics: A bioinspired evolution in Robotics". In: *Trends in Biotechnology* 31.5 (2013), pp. 287–294. DOI: 10.1016/j.tibtech.2013.03.002.

[6] Surya Nurzaman, Fuyima Lida, and Cecilia Laschi. "Soft robotics [TC spotlight]". In: *IEEE Robotics amp;amp; Automation Magazine* 20.3 (2013), pp. 24–95. DOI: 10.1109/mra.2013.2279342.

[7] Jun Shintake, Vito Cacucciolo, Dario Floreano, and Herbert Shea. "Soft robotic grippers". In: *Advanced Materials* 30.29 (2018), p. 1707035. DOI: 10.1002/adma.201707035.

[8] Junfeng Li, Lei Zu, Guoliang Zhong, Mingchang He, Haibin Yin, and Yuegang Tan. "Stiffness characteristics of soft finger with embedded SMA fibers". In: *Composite Structures* 160 (2017), pp. 758–764. DOI: 10.1016/j.compstruct.2016.10.045.

[9] Guanjun Bao, Hui Fang, Lingfeng Chen, Yuehua Wan, Fang Xu, Qinghua Yang, and Libin Zhang. "Soft robotics: Academic insights and perspectives through Bibliometric analysis". In: *Soft Robotics* 5.3 (2018), pp. 229–241. DOI: 10.1089/soro.2017.0135.

[10] A.M. Okamura, N. Smaby, and M.R. Cutkosky. "An overview of dexterous manipulation". In: *Proceedings 2000 ICRA. Millennium Conference. IEEE International Conference on Robotics and Automation. Symposia Proceedings (Cat. No.00CH37065)* (). DOI: 10.1109/robot.2000.844067.

[11] James Walker, Thomas Zidek, Cory Harbel, Sanghyun Yoon, F. Sterling Strickland, Srinivas Kumar, and Minchul Shin. "Soft robotics: A review of recent developments of pneumatic soft actuators". In: *Actuators* 9.1 (2020), p. 3. DOI: 10.3390/act9010003.

[12] Mariangela Manti, Taimoor Hassan, Giovanni Passetti, Nicolò D'Elia, Cecilia Laschi, and Matteo Cianchetti. "A bioinspired soft robotic gripper for adaptable and effective grasping". In: *Soft Robotics* 2.3 (2015), pp. 107–116. DOI: 10.1089/soro.2015.0009.

[13] Ghareeb N and Farhat M. "Smart Materials and Structures: State of the art and applications". In: *Nano Research amp; Applications* 04.02 (2018). DOI: 10.21767/2471-9838.100034.

[14] Paola Andrea Castiblanco, José Luis Ramirez, and Astrid Rubiano. "Smart materials and their application in robotic hand systems: A state of the art". In: *Indonesian Journal of Science and Technology* 6.2 (2021), pp. 401–426. DOI: 10.17509/ijost.v6i2.35630.

[15] Heather Holman, Minoo Naozer Kavarana, and Taufiek Konrad Rajab. "Smart materials in cardiovascular implants: Shape memory alloys and shape memory polymers". In: *Artificial Organs* 45.5 (2020), pp. 454–463. DOI: 10.1111/aor.13851.

[16] M. Ding, L. Jing, H. Yang, C.E. Machnicki, X. Fu, K. Li, I.Y. Wong, and P.-Y. Chen. "Multifunctional soft machines based on stimuli-responsive hydrogels: From freestanding hydrogels to Smart Integrated Systems". In: *Materials Today Advances* 8 (2020), p. 100088. DOI: 10.1016/j.mtadv.2020.100088.

[17] Y. Lee, W.J. Song, and J.-Y. Sun. "Hydrogel Soft Robotics". In: *Materials Today Physics* 15 (2020), p. 100258. DOI: 10.1016/j.mtphys.2020.100258.

[18] Qiang Shi, Hao Liu, Deding Tang, Yuhui Li, XiuJun Li, and Feng Xu. "Bioactuators based on stimulus-responsive hydrogels and their emerging biomedical applications". In: *NPG Asia Materials* 11.1 (2019). DOI: 10.1038/s41427-019-0165-3.

[19] Sia Nemat-Nasser and Yongxian Wu. "Comparative experimental study of ionic polymer–metal composites with different backbone ionomers and in various cation forms". In: *Journal of Applied Physics* 93.9 (2003), pp. 5255–5267. DOI: 10.1063/1.1563300.

[20] Etienne Palleau, Daniel Morales, Michael D. Dickey, and Orlin D. Velev. "Reversible patterning and actuation of hydrogels by electrically assisted ionoprinting". In: *Nature Communications* 4.1 (2013). DOI: 10.1038/ncomms3257.

[21] Lei Li, Johannes M. Scheiger, and Pavel A. Levkin. "Design and applications of photoresponsive hydrogels". In: *Advanced Materials* 31.26 (2019), p. 1807333. DOI: 10.1002/adma.201807333.

[22] G. Kofod, M. Paajanen, and S. Bauer. "Self-organized minimum-energy structures for dielectric elastomer actuators". In: *Applied Physics A* 85.2 (2006), pp. 141–143. DOI: 10.1007/s00339-006-3680-3.

[23] Guggi Kofod, Werner Wirges, Mika Paajanen, and Siegfried Bauer. "Energy minimization for self-organized structure formation and actuation". In: *Applied Physics Letters* 90.8 (2007), p. 081916. DOI: 10.1063/1.2695785.

[24] Oluwaseun A. Araromi, Irina Gavrilovich, Jun Shintake, Samuel Rosset, Muriel Richard, Volker Gass, and Herbert R. Shea. "Rollable multisegment dielectric elastomer minimum energy structures for a deployable microsatellite gripper". In: *IEEE/ASME Transactions on Mechatronics* 20.1 (2015), pp. 438–446. DOI: 10.1109/tmech.2014.2329367.

[25] Gih-Keong Lau, Kim-Rui Heng, Anansa S. Ahmed, and Milan Shrestha. "Dielectric elastomer fingers for versatile grasping and nimble pinching". In: *Applied Physics Letters* 110.18 (2017), p. 182906. DOI: 10.1063/1.4983036.

[26] Samuel Shian, Katia Bertoldi, and David R. Clarke. "Dielectric Elastomer based "grippers" for Soft Robotics". In: *Advanced Materials* 27.43 (2015), pp. 6814–6819. DOI: 10.1002/adma.201503078.

[27] Hiroya Imamura, Kevin Kadooka, and Minoru Taya. "A variable stiffness dielectric elastomer actuator based on electrostatic chucking". In: *Soft Matter* 13.18 (2017), pp. 3440–3448. DOI: 10.1039/c7sm00546f.

[28] Jun Shintake, Samuel Rosset, Bryan Schubert, Dario Floreano, and Herbert Shea. "Polymer actuators: Versatile soft grippers with intrinsic electroadhesion based on multifunctional polymer actuators (adv. mater. 2/2016)". In: *Advanced Materials* 28.2 (2016), pp. 205–205. DOI: 10.1002/adma.201670008.

[29] R K Jain, S Datta, S Majumder, and A Dutta. "Two IPMC Fingers Based Micro Gripper for handling". In: *International Journal of Advanced Robotic Systems* 8.1 (2011), p. 13. DOI: 10.5772/10523.

[30] R.C. Richardson, M.C. Levesley, M.D. Brown, J.A. Hawkes, K. Watterson, and P.G. Walker. "Control of Ionic polymer metal composites". In: *IEEE/ASME Transactions on Mechatronics* 8.2 (2003), pp. 245–253. DOI: 10.1109/tmech.2003.812835.

[31] Y. Bar-Cohen, V.F. Cardoso, C. Ribeiro, and S. Lanceros-Méndez. "Electroactive polymers as actuators". In: *Advanced Piezoelectric Materials* (2017), pp. 319–352. DOI: 10.1016/b978-0-08-102135-4.00008-4.

[32] Ujwal Deole, Ron Lumia, Mohsen Shahinpoor, and Michael Bermudez. "Design and test of IPMC artificial muscle microgripper". In: *Journal of Micro-Nano Mechatronics* 4.3 (2008), pp. 95–102. DOI: 10.1007/s12213-008-0004-z.

[33] Koichi Suzumori, Shoichi Likura, and Hisoshisa Tanaka. "Applying a flexible microactuator to robotic mechanisms". In: *IEEE Control Systems* 12.1 (1992), pp. 21–27. DOI: 10.1109/37.120448.

[34] Ahmed Abo-Ismail. "On the development of a new pneumatic versatile gripper". In: *Proceedings of the JFPS International Symposium on Fluid Power* 1993.2 (1993), pp. 701–706. DOI: 10.5739/isfp.1993.701.

[35] Shujiro DOHTA, Takashi SHINOHARA, and Hisashi MATSUSHITA. "Development of a pneumatic rubber hand". In: *Proceedings of the JFPS International Symposium on Fluid Power* 2002.5–1 (2002), pp. 49–54. DOI: 10.5739/isfp.2002.49.

[36] Filip Ilievski, Aaron D. Mazzeo, Robert F. Shepherd, Xin Chen, and George M. Whitesides. "Soft Robotics for chemists". In: *Angewandte Chemie International Edition* 50.8 (2011), pp. 1890–1895. DOI: 10.1002/anie.201006464.

[37] Bobak Mosadegh, Panagiotis Polygerinos, Christoph Keplinger, Sophia Wennstedt, Robert F. Shepherd, Unmukt Gupta, Jongmin Shim, Katia Bertoldi, Conor J. Walsh, and George M. Whitesides. "Pneumatic networks for soft robotics that actuate rapidly". In: *Advanced Functional Materials* 24.15 (2014), pp. 2163–2170. DOI: 10.1002/adfm.201303288.

[38] Robert F. Shepherd, Adam A. Stokes, Rui M. Nunes, and George M. Whitesides. "Soft machines that are resistant to puncture and that self seal". In: *Advanced Materials* 25.46 (2013), pp. 6709–6713. DOI: 10.1002/adma.201303175.

[39] Kevin C. Galloway, Kaitlyn P. Becker, Brennan Phillips, Jordan Kirby, Stephen Licht, Dan Tchernov, Robert J. Wood, and David F. Gruber. "Soft Robotic grippers for biological sampling on Deep Reefs". In: *Soft Robotics* 3.1 (2016), pp. 23–33. DOI: 10.1089/soro.2015.0019.

[40] Yufei Hao, Tianmiao Wang, Ziyu Ren, Zheyuan Gong, Hui Wang, Xingbang Yang, Shaoya Guan, and Li Wen. "Modeling and experiments of a soft robotic gripper in amphibious environments". In: *International Journal of Advanced Robotic Systems* 14.3 (2017), p. 172988141770714. DOI: 10.1177/1729881417707148.

[41] Festo. *FlexShapeGripper - Gripping modelled on a chameleon's tongue.* URL: https://www.festo.com/net/SupportPortal/Files/367915/Festo_FlexShapeGripper_en.pdf.

[42] Ian D. Walker, Darren M. Dawson, Tamar Flash, Frank W. Grasso, Roger T. Hanlon, Binyamin Hochner, William M. Kier, Christopher C. Pagano, Christopher D. Rahn, and Qiming M. Zhang. "Continuum robot arms inspired by cephalopods". In: *SPIE Proceedings* (2005). DOI: 10.1117/12.606201.

[43] Ramses V. Martinez, Jamie L. Branch, Carina R. Fish, Lihua Jin, Robert F. Shepherd, Rui M. Nunes, Zhigang Suo, and George M. Whitesides. "Robotic tentacles with three-dimensional mobility based on flexible elastomers". In: *Advanced Materials* 25.2 (2012), pp. 205–212. DOI: 10.1002/adma.201203002.

[44] Jungwook Paek, Inho Cho, and Jaeyoun Kim. "Microrobotic tentacles with spiral bending capability based on shape-engineered elastomeric microtubes". In: *Scientific Reports* 5.1 (2015). DOI: 10.1038/srep10768.

[45] Pei Jiang, Yandong Yang, Michael Z Chen, and Yonghua Chen. "A variable stiffness gripper based on differential drive particle jamming". In: *Bioinspiration amp; Biomimetics* 14.3 (2019), p. 036009. DOI: 10.1088/1748-3190/ab04d1.

[46] I. Schmidt. "Flexible moulding jaws for grippers". In: *Industrial Robot: An International Journal* 5.1 (1978), pp. 24–26. DOI: 10.1108/eb004491.

[47] Perovskii. In: *Russian Engng* (1980).

[48] T. Rienmüller and H. Weissmantel. In: *18th Int. Symp. Ind. Rob.* (1988).

[49] Eric Brown, Nicholas Rodenberg, John Amend, Annan Mozeika, Erik Steltz, Mitchell R. Zakin, Hod Lipson, and Heinrich M. Jaeger. "Universal robotic gripper based on the jamming of granular material". In: *Proceedings of the National Academy of Sciences* 107.44 (2010), pp. 18809–18814. DOI: 10.1073/pnas.1003250107.

[50] John R. Amend, Eric Brown, Nicholas Rodenberg, Heinrich M. Jaeger, and Hod Lipson. "A positive pressure universal gripper based on the jamming of granular material". In: *IEEE Transactions on Robotics* 28.2 (2012), pp. 341–350. DOI: 10.1109/tro.2011.2171093.

[51] John Amend and Hod Lipson. "The jamhand: Dexterous manipulation with minimal actuation". In: *Soft Robotics* 4.1 (2017), pp. 70–80. DOI: 10.1089/soro.2016.0037.

[52] Stephen Licht, Everett Collins, Manuel Lopes Mendes, and Christopher Baxter. "Stronger at depth: Jamming grippers as deep sea sampling tools". In: *Soft Robotics* 4.4 (2017), pp. 305–316. DOI: 10.1089/soro.2017.0028.

[53] Masahiro Fujita, Kenjiro Tadakuma, Eri Takane, Tomoya Ichimura, Hirone Komatsu, Akito Nomura, Masashi Konyo, and Satoshi Tadokoro. "Variable inner volume mechanism for soft and robust gripping — improvement of gripping performance for large-object gripping". In: *2016 IEEE International Symposium on Safety, Security, and Rescue Robotics (SSRR)* (2016). DOI: 10.1109/ssrr.2016.7784332.

[54] Kaori Mizushima, Takumi Oku, Yosuke Suzuki, Tokuo Tsuji, and Tetsuyou Watanabe. "Multi-fingered robotic hand based on hybrid mechanism of tendon-driven and jamming transition". In: *2018 IEEE International Conference on Soft Robotics (RoboSoft)* (2018). DOI: 10.1109/robosoft.2018.8404948.

[55] Yingtian Li, Yonghua Chen, Yang Yang, and Ying Wei. "Passive particle jamming and its stiffening of soft robotic grippers". In: *IEEE Transactions on Robotics* 33.2 (2017), pp. 446–455. DOI: 10.1109/tro.2016.2636899.

[56] Robert F. Shepherd, Adam A. Stokes, Jacob Freake, Jabulani Barber, Phillip W. Snyder, Aaron D. Mazzeo, Ludovico Cademartiri, Stephen A. Morin, and George M. Whitesides. "Using explosions to power a soft robot". In: *Angewandte Chemie International Edition* 52.10 (2013), pp. 2892–2896. DOI: 10.1002/anie.201209540.

[57] Nicholas W. Bartlett, Michael T. Tolley, Johannes T. Overvelde, James C. Weaver, Bobak Mosadegh, Katia Bertoldi, George M. Whitesides, and Robert J. Wood. "A 3D-printed, functionally graded soft robot powered by combustion". In: *Science* 349.6244 (2015), pp. 161–165. DOI: 10.1126/science.aab0129.

[58] Michael Wehner, Ryan L. Truby, Daniel J. Fitzgerald, Bobak Mosadegh, George M. Whitesides, Jennifer A. Lewis, and Robert J. Wood. "An integrated design and fabrication strategy for entirely soft, autonomous robots". In: *Nature* 536.7617 (2016), pp. 451–455. DOI: 10.1038/nature19100.

[59] Marc Behl, Karl Kratz, Jörg Zotzmann, Ulrich Nöchel, and Andreas Lendlein. "Reversible bidirectional shape-memory polymers". In: *Advanced Materials* 25.32 (2013), pp. 4466–4469. DOI: 10.1002/adma.201300880.

[60] Qi Ge, Amir Hosein Sakhaei, Howon Lee, Conner K. Dunn, Nicholas X. Fang, and Martin L. Dunn. "Multimaterial 4D printing with tailorable shape memory polymers". In: *Scientific Reports* 6.1 (2016). DOI: 10.1038/srep31110.

[61] F Simone, G Rizzello, and S Seelecke. "Metal muscles and nerves—a self-sensing SMA-actuated hand concept". In: *Smart Materials and Structures* 26.9 (2017), p. 095007. DOI: 10.1088/1361-665x/aa7ad5.

[62] Hyung-Il Kim, Min-Woo Han, Sung-Hyuk Song, and Sung-Hoon Ahn. "Soft morphing hand driven by SMA Tendon Wire". In: *Composites Part B: Engineering* 105 (2016), pp. 138–148. DOI: 10.1016/j.compositesb.2016.09.004.

[63] Chao-Chieh Lan, Che-Min Lin, and Chen-Hsien Fan. "A self-sensing Microgripper module with wide handling ranges". In: *IEEE/ASME Transactions on Mechatronics* 16.1 (2011), pp. 141–150. DOI: 10.1109/tmech.2009.2037495.

[64] Benjamin Gorissen, Dominiek Reynaerts, Satoshi Konishi, Kazuhiro Yoshida, Joon-Wan Kim, and Michael De Volder. "Elastic inflatable actuators for soft robotic applications". In: *Advanced Materials* 29.43 (2017), p. 1604977. DOI: 10.1002/adma.201604977.

[65] Khaled Elgeneidy, Niels Lohse, and Michael Jackson. "Experimental analysis of the bending response of soft gripper fingers". In: *Volume 5B: 40th Mechanisms and Robotics Conference* (2016). DOI: 10.1115/detc2016-59630.

[66] Matteo Cianchetti, Tommaso Ranzani, Giada Gerboni, Iris De Falco, Cecilia Laschi, and Arianna Menciassi. "Stiff-flop surgical manipulator: Mechanical design and experimental characterization of the single module". In: *2013 IEEE/RSJ International Conference on Intelligent Robots and Systems* (2013). DOI: 10.1109/iros.2013.6696866.

[67] Hongjun Li, Dengyu Xie, and Yeping Xie. "A soft pneumatic gripper with endoskeletons resisting out-of-plane bending". In: *Actuators* 11.9 (2022), p. 246. DOI: 10.3390/act11090246.

[68] Hongjie Zhang, Wenwen Liu, Ming Yu, and Yanyan Hou. "Design, fabrication, and performance test of a new type of soft-robotic gripper for grasping". In: *Sensors* 22.14 (2022), p. 5221. DOI: 10.3390/s22145221.

[69] Yingtian Li, Yonghua Chen, and Yunquan Li. "Distributed design of passive particle jamming based soft grippers". In: *2018 IEEE International Conference on Soft Robotics (RoboSoft)* (2018). DOI: 10.1109/robosoft.2018.8405383.

[70] Ho Choi and Muammer Koç. "Design and feasibility tests of a flexible gripper based on inflatable rubber pockets". In: *International Journal of Machine Tools and Manufacture* 46.12–13 (2006), pp. 1350–1361. DOI: 10.1016/j.ijmachtools.2005.10.009.

[71] Yu Miao, Wei Dong, and Zhijiang Du. "Design of a soft robot with multiple motion patterns using soft pneumatic actuators". In: *IOP Conference Series: Materials Science and Engineering* 269 (2017), p. 012013. DOI: 10.1088/1757-899x/269/1/012013.

[72] Jianying Hu, Nan Jiang, and Jianke Du. "Thermally controlled large deformation in temperature-sensitive hydrogels bilayers". In: *International Journal of Smart and Nano Materials* 12.4 (2021), pp. 450–471. DOI: 10.1080/19475411.2021.1958091.

[73] Harold-Rodrigo Valenzuela-Coloma, Yi-sheng Lau-Cortes, Ricardo-Enrique Fuentes-Romero, Juan Cristobal Zagal, and Ricardo-Franco Mendoza-Garcia. "Mentaca: An universal jamming gripper on Wheels". In: *2015 CHILEAN Conference on Electrical, Electronics Engineering, Information and Communication Technologies (CHILECON)* (2015). DOI: 10.1109/chilecon.2015.7404666.

[74] Wei Hong, Zishun Liu, and Zhigang Suo. "Inhomogeneous swelling of a gel in equilibrium with a solvent and mechanical load". In: *International Journal of Solids and Structures* 46.17 (2009), pp. 3282–3289. DOI: 10.1016/j.ijsolstr.2009.04.022.

[75] Zhiwei Ding, William Toh, Jianying Hu, Zishun Liu, and Teng Yong Ng. "A simplified coupled thermo-mechanical model for the transient analysis of temperature-sensitive hydrogels". In: *Mechanics of Materials* 97 (2016), pp. 212–227. DOI: 10.1016/j.mechmat.2016.02.018.

[76] Zhiwei Ding, Zishun Liu, Jianying Hu, Somsak Swaddiwudhipong, and Zhengzhi Yang. "Inhomogeneous large deformation study of temperature-sensitive hydrogel". In: *International Journal of Solids and Structures* 50.16–17 (2013), pp. 2610–2619. DOI: 10.1016/j.ijsolstr.2013.04.011.

[77] Paul J. Flory and John Rehner. "Statistical mechanics of cross-linked Polymer Networks II. swelling". In: *The Journal of Chemical Physics* 11.11 (1943), pp. 521–526. DOI: 10.1063/1.1723792.

[78] Kwang Suk Oh, Jeong Seok Oh, Hyun Seok Choi, and Young Chan Bae. "Effect of cross-linking density on swelling behavior of nipa gel particles". In: *Macromolecules* 31.21 (1998), pp. 7328–7335. DOI: 10.1021/ma971554y.

[79] A. Suzuki and T. Ishii. "Phase coexistence of neutral polymer gels under mechanical constraint". In: *The Journal of Chemical Physics* 110.4 (1999), pp. 2289–2296. DOI: 10.1063/1.477882.

[80] Luc Marechal, Pascale Balland, Lukas Lindenroth, Fotis Petrou, Christos Kontovounisios, and Fernando Bello. "Toward a common framework and database of materials for Soft Robotics". In: *Soft Robotics* 8.3 (2021), pp. 284–297. DOI: 10.1089/soro.2019.0115.

Appendices

A Subroutine file

```
                SUBROUTINE UHYPER(BI1,BI2,AJ,U,UI1,UI2,UI3,TEMP,NOEL,
     1 CMNAME,INCMPFLAG,NUMSTATEV,STATEV,NUMFIELDV,FIELDV,
     2 FIELDVINC,NUMPROPS,PROPS)
C=================================================================
C       User defined hyperelastic material subroutine
C          for gel with Flory-Rehner free-energy function
C          to be used in Abaqus Standard
C       Fomulated and written by Wei Hong, April 20, 2008
C-----------------------------------------------------------------
C       Material properties to be passed to the subroutine:
C          PROPS(1) - Nv
C          PROPS(2) - mu/kT
C          PROPS(3) - lambda_0 initial swelling
C       State variable:
C          TEMP - wendu
C          The initial value of chemical potential should agree
C             with the initial swelling, given as follows:
C          mu_0/kT = Nv*(1/lambda_0-1/detF0) + ln(1-1/detF0)
C                          + 1/detF0+ chi0/detF0^2+2*chi1/detF0^3
C          where detF0 = lambda_0^3
C       Output
C          Free-energy function U(I, J) and its derivatives
C          All free-energy density and stress given by the
C             calculation are normalized by kT/v
C           chi=A0+B0*wendu+(A1+B1*wendu)/AJ/detF0
C=================================================================
C
       INCLUDE 'ABA_PARAM.INC'
C
       CHARACTER*80 CMNAME
       DIMENSION U(2),UI1(3),UI2(6),UI3(6),STATEV(*),FIELDV(*),
     1 FIELDVINC(*),PROPS(*)
       REAL(8) Nv, chi, lambda0, detF0, mu_kT, wendu, chi1
       Nv = PROPS(1)
       mu_kT = PROPS(2)
       lambda0 = PROPS(3)
       detF0 = lambda0**3
       A0=-12.947
       A1=17.92
       B0=0.0449
       B1=-0.0569
       wendu = TEMP ! TEMP is used to represent chemical potential
       chi1=A1+B1*wendu
       chi0=A0+B0*wendu


          U(1) = Nv/2 * ( 1/lambda0*BI1*AJ**(2.0/3.0) - 3/detF0
     & - 2/detF0*(3*LOG(lambda0) + LOG(AJ)) )
     & - chi0/detF0**2/AJ-chi1/detF0**3/AJ**2
     & - (AJ-1/detF0)*LOG(AJ/(AJ-1/detF0)) - mu_kT*(AJ-1/detF0)
     & + chi0/detF0+chi1/detF0**2/AJ
```

```
      U(2) = 0
      UI1(1) = Nv/2/lambda0*AJ**(2.0/3.0)
      UI1(2) = 0
      UI1(3) = Nv/3/lambda0*BI1*AJ**(-1.0/3.0)
& + (1-Nv)/AJ/detF0 - LOG(AJ/(AJ-1/detF0)) - mu_kT
& + chi0/(detF0*AJ)**2+2*chi1/(detF0*AJ)**3
& - chi1/detF0**2/AJ**2
      UI2 = 0
      UI2(3) = -Nv/9/lambda0*BI1*AJ**(-4.0/3.0) -(1-Nv)/AJ**2/detF0
& + 1/AJ/(AJ-1/detF0)/detF0 - 2*chi0/detF0**2/AJ**3
& - 6*chi1/detF0**3/AJ**4
& + 2*chi1/detF0**2/AJ**3
   UI2(5) = Nv/3/lambda0 * AJ**(-1.0/3.0)
      UI3 = 0
      UI3(4) = -Nv/9/lambda0 * AJ**(-4.0/3.0)
      UI3(6) = 4*Nv/27/lambda0*BI1*AJ**(-7.0/3.0) + 2*(1-Nv)/AJ**3/detF0
& - (2*AJ-1/detF0)/(AJ*(AJ-1/detF0))**2/detF0
& + 6*chi0/detF0**2/AJ**4+24*chi1/detF0**3/AJ**5
& - 6*chi1/detF0**2/AJ**4
 RETURN
 END
```

B Detailed information of structures

(1) No reinforcement

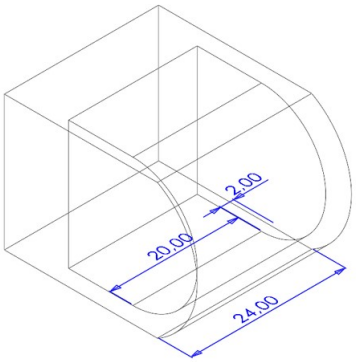

Figure 127: 3D no reinforcement.

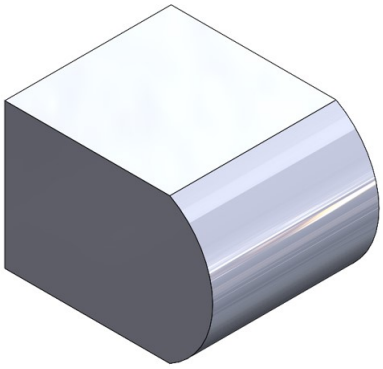

Figure 128: 3D no reinforcement 2.

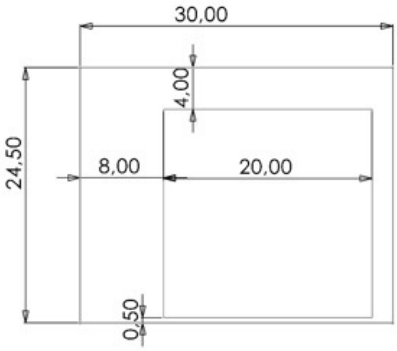

Figure 129: straight top.

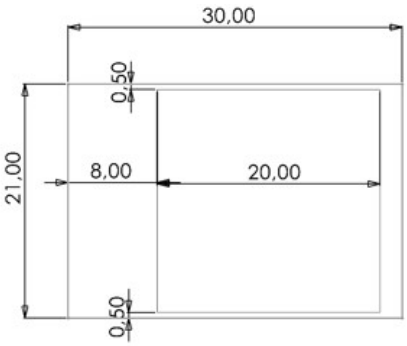

Figure 130: straight mid.

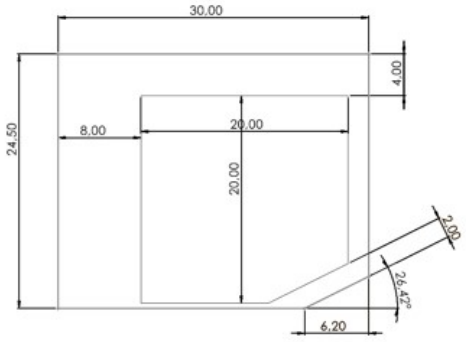

Figure 131: sharp top.

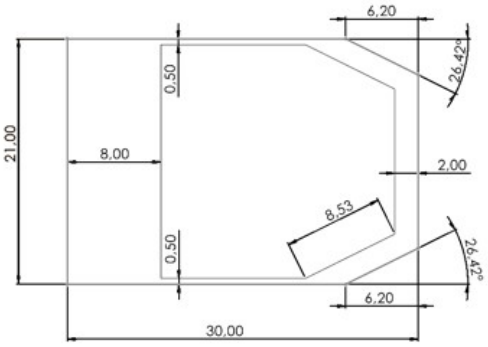

Figure 132: sharp mid.

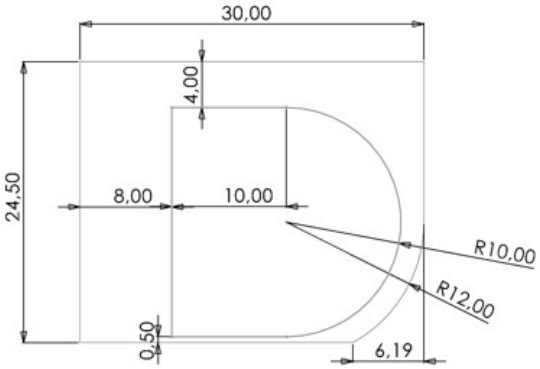

Figure 133: waved top.

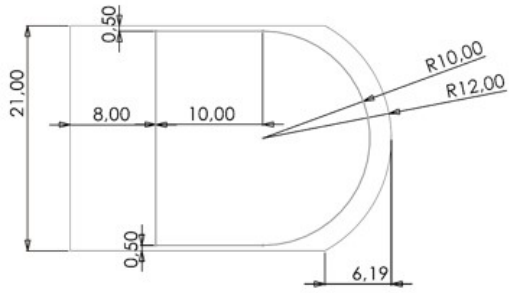

Figure 134: waved mid.

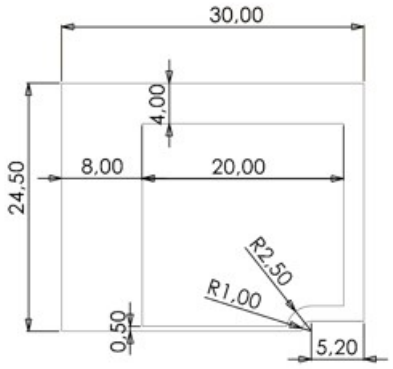

Figure 135: cylinder top.

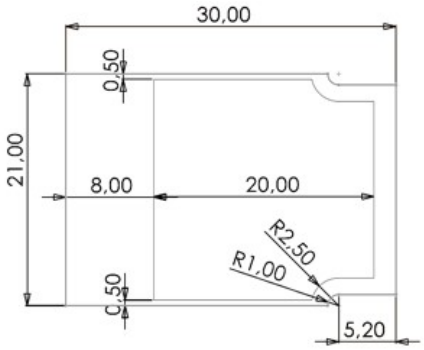

Figure 136: cylinder mid.

(2) Small reinforcement

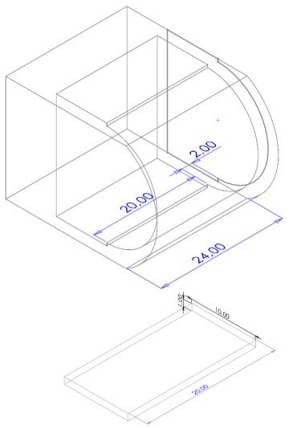

Figure 137: 3D small reinforcement.

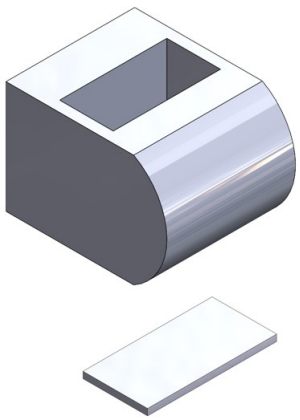

Figure 138: 3D small reinforcement 2.

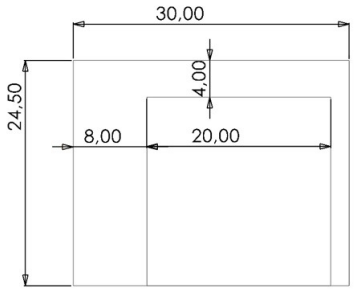

Figure 139: straight top small.

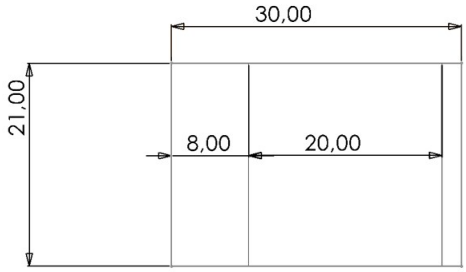

Figure 140: straight mid small.

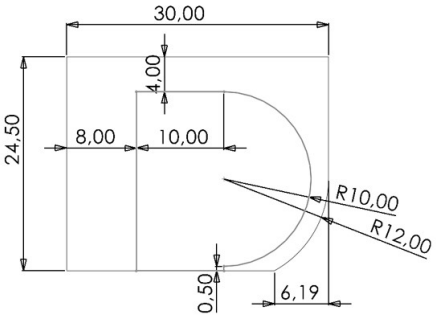

Figure 141: waved top small.

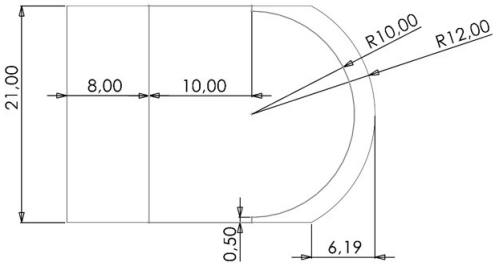

Figure 142: waved mid small.

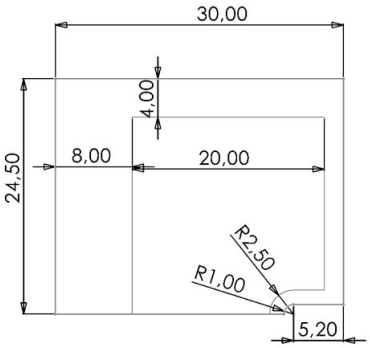

Figure 143: cylinder top small.

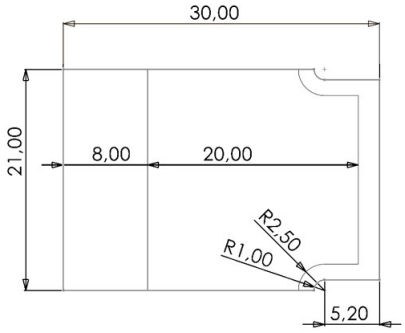

Figure 144: cylinder mid small.

(3) Large reinforcement

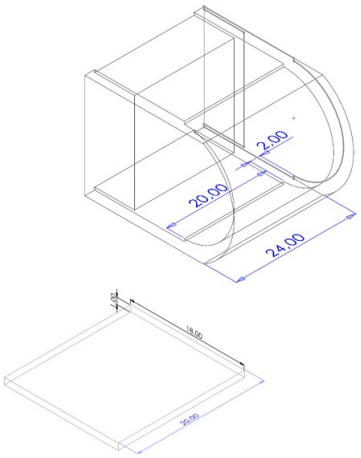

Figure 145: 3D large reinforcement.

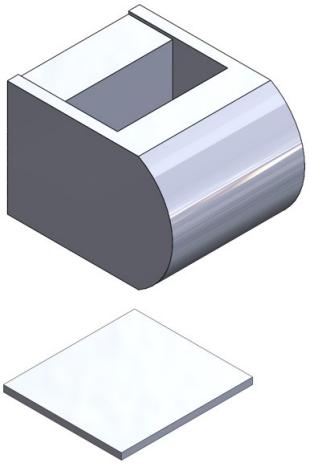

Figure 146: 3D large reinforcement 2.

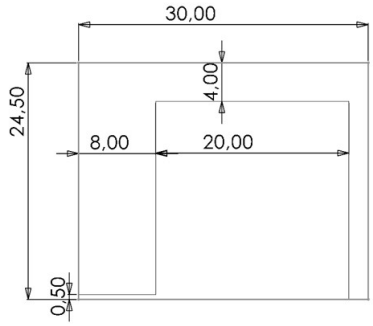

Figure 147: straight top large.

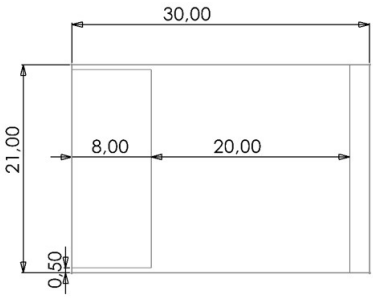

Figure 148: straight mid large

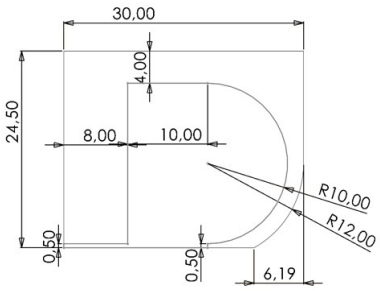

Figure 149: waved top large.

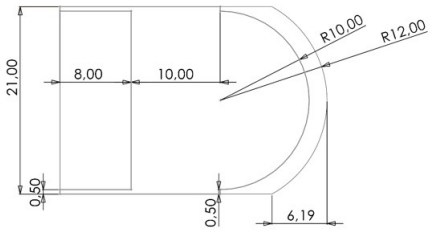

Figure 150: waved mid large.

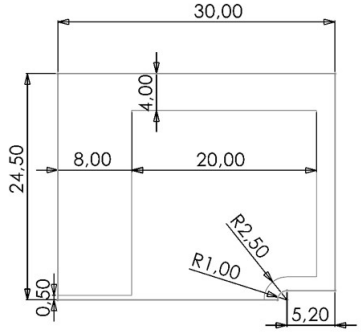

Figure 151: cylinder top large.

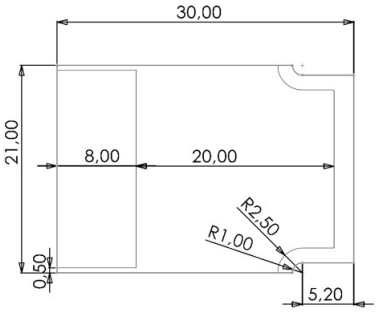

Figure 152: cylinder mid large.

C ABAQUS MODULE INPUT

Abaqus module's There are multiple different available modules in ABAQUS. In each module, different aspects of the simulation can be set. Therefore, in this chapter, a description for the relevant modules are provided to describe how the simulations are implemented in ABAQUS. When certain options in the modules are not addressed, they can be assumed to be on default. The different modules in ABAQUS are: part, property, assembly, step, interaction, load, mesh, optimization, job, visualization and sketch. The Optimization and Sketch module are not used in this research.

The **Part module** is relevant for creating/editing the relevant parts. For each different structure, a middle and top part are created in SolidWorks. Both parts are exported from SolidWorks as a SAT file and imported to ABAQUS. These parts will be used to form the structure of the soft gripper. Additionally, a sphere is created in ABAQUS which will be used as a hydrogel particle. The sphere is divided into 8 parts as visible in Figure 153, which is beneficial later in the simulation for establishing the mesh. Additionally, to determine the results at the end of a simulation, an output database file (.ODB) can be imported as a part at a specific time step. By taking the final time step, the result can be extracted by making use of datum planes. These datum planes are at the fixed top surface and at the end of the structure, as presented in Figure 154. The angle between these datum planes can be extracted easily with a measuring tool in ABAQUS.

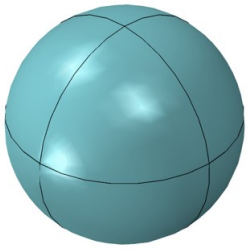

Figure 153: Hydrogel particle in simulation.

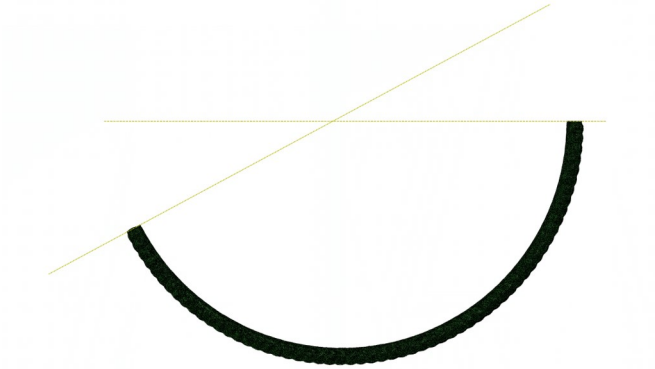

Figure 154: Measuring the bending angle of a structure.

In the **property module** are the materials defined of each part. In the material manager, two materials are defined, which are the hydrogel and silicone. The material behaviors used for both materials are a *Density*, *Depvar* and *Hyperelastic*. For the *Density* behavior, both the materials are considered to be 9E-12. As we have no density relative loads, this is unimportant. However, a density was required in the simulation. The *Depvar* behavior are both applied with the same values for the option *Number of solution-dependent state variables* and *Variable number controlling element deletion*, which are respectively 3 and 0. This behavior is applied so that the materials are coupled with a used subroutine. At last, there is a difference in the *Hyperelastic* behavior. For the hydrogel, the material type is considered to be isotropic. A user-defined strain energy potential is used. The input source are coefficients and the moduli time scale (for viscoelasticity) is instantaneous. Compressibility is included. The number of property values is 3. These values are for the factors 1, 2 and 3, which are respectively 0.01, 0 and 1.925984. These factors 1, 2 and 3 represent the values for the UHYPER, which are respectively PROPS (1), PROPS (2) and PROPS (3) i.e. Nv, $\frac{\mu}{kT}$ and λ_0. For the *Hyperelastic* behavior of silicone is the material type also isotropic. However, for the strain energy potential is Neo Hooke considered. The input source is also coefficients with a long-term for moduli time scale (for viscoelasticity). The strain energy potential order is 1. The data is not temperature dependent. The values for the factors C10 and D1 are respectively 0.03245 and 30. C10 represents the Neo-Hookean value μ of [80]. D1 represents the elasticity of the material. Silicone is in this module assigned to the middle and top parts, while

the hydrogel is assigned to the spherical particles.

In the **Assembly module**, the parts are implemented together to form a full structure. At first, a top part is selected. To the bottom of this top part, multiple middle parts are attached, with at the bottom again a top part. Dependent on the required length of the structure, more or less middle parts can be implemented. In each middle and top part is a spherical particle implemented. At last, all of the middle and top parts are merged into a single structure part. This is as well more representative for the real world approach as well as that this is more beneficial by establishing the mesh. Two different kind of sets are generated in this module, which are the *top surface structure* and *hydrogel particles*. The set for the top surface of the structure will be used for the boundary condition and the hydrogel particles set is used for the temperature gradient, which will both be clarified in the load module.

In the **Step module**, an initial step followed by six different steps are generated. The time period for each step is 1 and the nonlinear geometric effects are on. The automatic stabilization is none and the adiabatic heating effects are not included. A automatic incrementation is considered with 5000 as a maximum number of increments. The initial increment size is 0.01, with a minimum and maximum of respectively 1E-08 and 1. Everything on the "other" tab is at default. The first field output request of the field output request manager has as output variables the pre-selected defaults. Additionally, a field output request which included the thermal output variables was included. Both the field output request started from step 1 and are propagated. At last, a history output request was generated which included all of the energy output variables.

The **Interaction module** is used to form an interaction between the parts. A single interaction was created, which was a general contact (standard) starting from the initial step and propagated. From the surface pairs, the option All* with self is selected. A global property assignment was generated. In this contact property, *Tangential* behavior, *Normal* behavior and *Geometric properties* were included. For the tangential behavior, a penalty was selected for the friction formulation. Isotropic directionality was selected. The friction coefficient is 0.01. Without applying a minor friction coefficient, errors could occur. A hard contact with allowable separation after contact was considered for the normal behavior. For the geometric properties, the out-of-plane surface thickness or cross-sectional area (standard) was 1.

The **Load module** determines the boundary conditions and the loads during the simulation. For the boundary condition, the set top surface structure was used, as presented in Figure 155. This surface is considered to be fixed, such that there is no displacement and/or rotation in any direction at this surface. This boundary condition is applied in the initial step and is propagated. As a load, a temperature is applied to the set hydrogel particles. In the initial step the temperature is set to 305 K. From step 1 to 6, the temperature decreases with 5 K per step, resulting in step 6 a temperature of 280 K. Therefore, 7 loads are required. Each load is considered to be static, general. The distribution is direct specification and the section variations is constant through region. The magnitude represents the temperature. The amplitude selected is ramp.

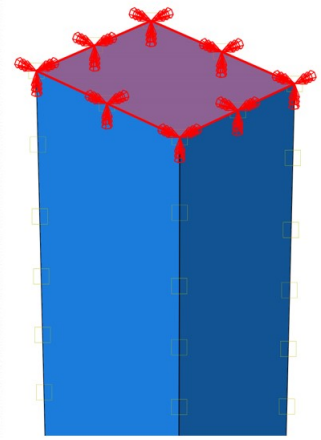

Figure 155: Top boundary condition represents fixed surface.

In the **Mesh module**, the meshes are defined for each part. For the spherical particles, each simulations has the same size. The approximate global size is 1. For the element type, the element library is standard. The geometric order is linear. A hex mesh is applied with a hybrid formulation, resulting in a C3D8H mesh: 8-node linear brick, hybrid, constant pressure. For the structures, a small variation can be found in the approximate global size. However, the mainly used size is 1.5. Also for the structures is the element library standard and the geometric order linear. However, instead of using a hex mesh, a tet mesh is considered. Using a hex mesh often resulted in errors. Additionally, the calculation time increased significantly. A hybrid formulation is used, resulting in a C3D4H mesh: 4-node linear tetrahedron, hybrid, linear pressure. The other options are all left on default.

The **Job module** is used to run the simulation and to include the subroutine file. While creating a job, all of the options are held on default, except for the tab general where the subroutine file UHYPER of [74] can be included. The **visualization module** is only used at the end of a simulation to check whether a simulation is completed or not. If not, the message files including the errors can be checked here.

D Demo structure measurements

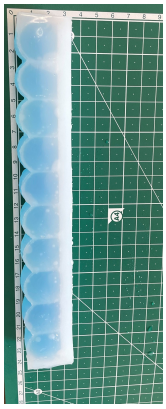

Figure 156: Picture of waved demo without bending.

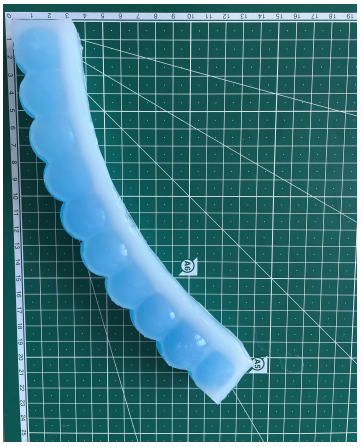

Figure 157: Picture of waved demo with bending.

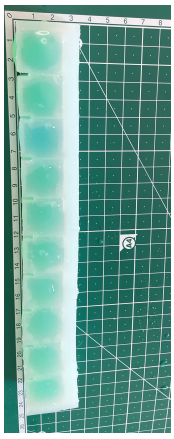

Figure 158: Picture of cylinder demo without bending.

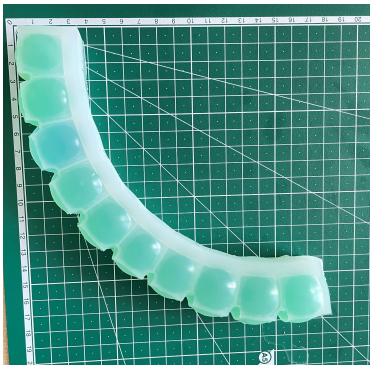

Figure 159: Picture of cylinder demo with bending.

Figure 160: Picture of straight demo without bending.

Figure 161: Picture of straight demo with bending.

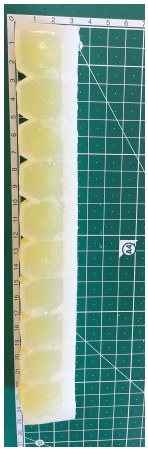

Figure 162: Picture of sharp demo without bending.

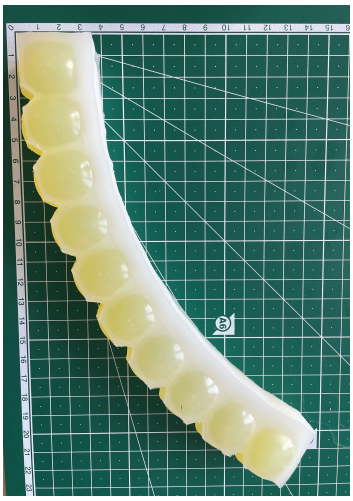

Figure 163: Picture of sharp demo with bending.

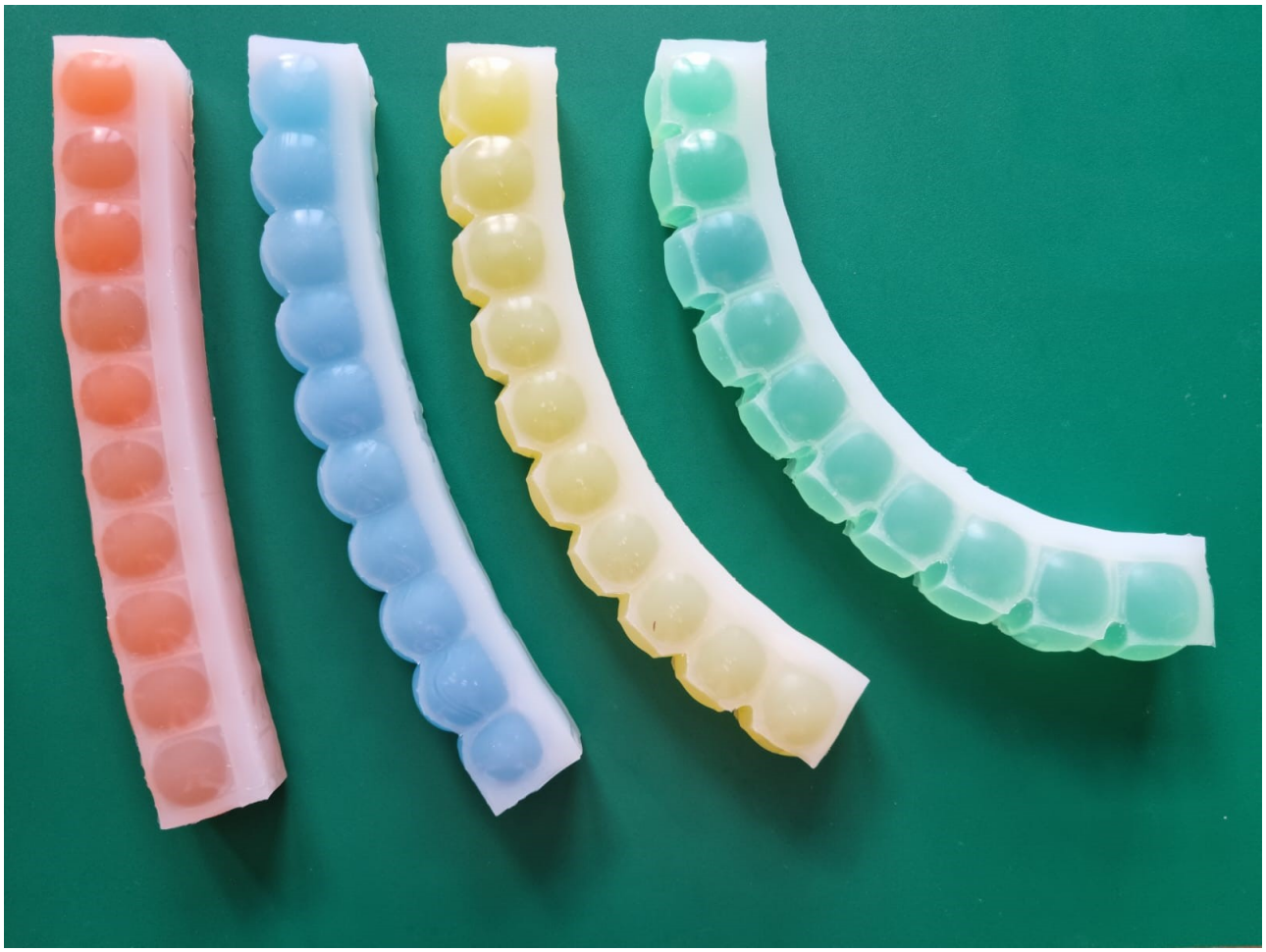

Figure 164: Picture of all demo structures next to each other. From left to right: straight, waved, sharp and cylinder.